ETH zürich

Bedretto Lab



BedrettoLab

Science Report

November 2024

D EAPS

Contents

The Bedretto Underground Laboratory for Geosciences and Geoenergies **4**
Brief history of the Bedretto tunnel 4
Research at the BedrettoLab 5

Geothermal testbed **7**
ARTEMIS: Awareness and Resilience Through European Multi-Sensor System 9
Recent publications 10

Earthquake Physics testbed **18**
FEAR: Fault Activation and Earthquake Rupture 20
PRECODE: Progressive Excavation Damage Zone Evolution During and Post Mine-By Tunneling 63
SPINE: Stress Profiling in Enhanced Geothermal Systems 64

Deep Life Observatory (DELOS) **67**
PHATES: Microbial responses to rapid physical-chemical changes in the continental subsurface 69
C-FIX: Carbon fixation in deep crystalline rock 69
ILLUME: Investigations into the diversity of cell-cell associations and non-standard life using metagenomics and cryogenic electron microscopy 69

Characterizing and understanding Enhanced Geothermal Systems (EGS) - novel tools and applications in a deep underground laboratory **71**
Investigation of seismic anisotropy in the BedrettoLab 71
Geomechanical modeling of induced seismicity in EGS 72
Quantifying Fracture Geometry and Heterogeneity in Rock Reservoirs Using GPR . . 73
Seismicity analysis during hydraulic stimulations 74
Illuminating hydraulic stimulation processes by advanced seismic techniques 77

Publications 2023-2024 **78**

References **80**

The Bedretto Underground Laboratory for Geosciences and Geoenergies

The Bedretto Underground Laboratory for Geosciences and Geoenergies ("BedrettoLab") was established in 2018 in the existing Bedretto tunnel in the Swiss Central Alps, near the Gotthard pass region (Ma et al 2022). The Bedretto tunnel is 5'200 m long and connects the Furka Base tunnel in the northwest with the Bedretto valley in the southeast (Keller and Schneider 1982). Situated in crystalline rock with an overburden of up to 1.5 km, the BedrettoLab is ideally suited for experiments focused on enhanced geothermal systems (EGS), earthquake physics and other underground processes (Figure 1).

The BedrettoLab is a next-level development that builds on the experience from a number of underground laboratory projects, notably from i) its Swiss predecessor at the Grimsel Test Site (Amann et al 2018), ii) the Mont Terri underground rock laboratory (Bossart et al 2017), iii) the Laboratoire Souterrain à Bas Brut (LSBB) in France[1], iv) the Sanford Underground Research Facility in South Dakota, USA[2], and v) the SKB Äspö Hard Rock Laboratory in Sweden[3]. Among the aspects that set the BedrettoLab apart from other underground laboratories are its larger depth (>1 km average overburden), its location in the midst of the tectonically active southern Swiss Alps, and its extensive and growing research infrastructure tailored for geoscience and geoenergy research projects.

Brief history of the Bedretto tunnel

The Bedretto tunnel was built in 1973 as a side-tunnel of the Furka Base tunnel, with a length of 5'200 meters. It was originally constructed to facilitate the excavation of the Furka Base tunnel. It was abandoned in 1983 after completion of the Furka railroad and was partially blocked by rockfall. In 2000, the first mapping was conducted and research in the accessible sections began. In 2012, it was partially reconditioned to provide ventilation for the Furka tunnel. This reconditioning meant that there was access to the full tunnel for the first time since construction. In 2018, after discussions in the Cantonal Council of Ticino, the tunnel was selected for the BedrettoLab. The Bedretto tunnel is owned by the Canton of Tessin, who have leased it for 100 years to the Matterhorn-Gotthard-Infrastruktur (MGI). ETH Zurich has an agreement with the MGI for use of the tunnel. Between 2018 and 2019, the tunnel was retrofitted with full infrastructure - road construction, securing of unstable rocks, ventilation system, communications network, electricity - from tunnel meter 0 to 2'250. The BedrettoLab was inaugurated in May 2019. A second phase of laboratory and infrastructure expansion started in 2022, with the goal of extending the infrastructure to TM 5'250. The tunnel expansion was finalized in 2023. The first phase of infrastructure development in 2018/2019 was funded by ETH Zurich. The second phase of infrastructure development was funded fully by the Werner Siemens Foundation.

[1] https://lsbb.cnrs.fr

[2] https://eesa.lbl.gov/projects/the-egs-collab-project/

[3] https://www.skb.com/research-and-technology/laboratories/the-aspo-hard-rock-laboratory

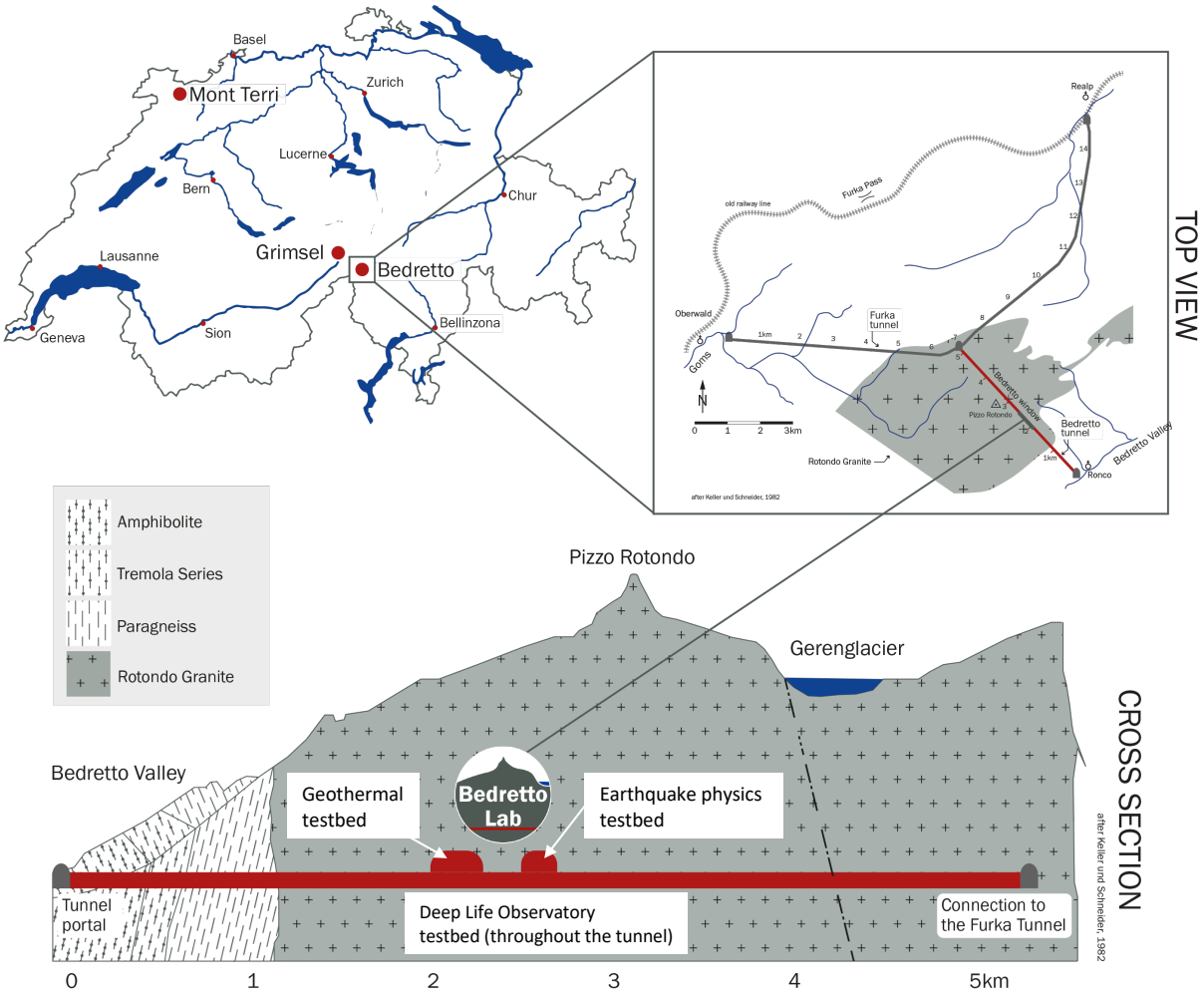

Figure 1: The Bedretto tunnel displaying the Geothermal testbed between tunnel meters 2'000 and 2'100, and the Earthquake Physics testbed between tunnel meters 2'300 and 2'500. The Deep Life Observatory (DELOS) consists of instrumentation and measurement locations throughout the tunnel.

Research at the BedrettoLab

Since its construction in 2018, the BedrettoLab has facilitated a wide range of research projects in the already-operational Geothermal testbed (Ma et al 2022). The Geothermal testbed, located in a niche between TM 2'000 and 2'100, features a major geophysical and rock mechanics monitoring array (Plenkers et al 2023) to study reservoir engineering. Additional instrumentation was supported by the Swiss National Science Foundation (SNF) R'Equip grant 189632 "Monitoring and scientific equipment for the Bedretto Deep Underground Laboratory for Geoenergies". The Geothermal testbed hosted the Bedretto Reservoir Project, which combined 3 projects with complementary targets for the development of large-scale deep reservoirs for the circulation of water and the storage and extraction of geothermal energy. One of the core components of this effort was the Validating Technologies for Reservoir Engineering (VALTER) project, funded by the Swiss Federal Office of Energy (BFE). Construction work on the Earthquake Physics testbed, located between TM 2'300 and 2'500, began in 2022. The Earthquake Physics testbed will host a variety of research projects aimed at a better understanding of earthquake rupture processes. The newly established Deep Life Observatory (DELOS) consists of geobiology field instruments deployed across the tunnel, either near the Geothermal testbed or in other areas (e.g. TM901), and will be used to study organisms living at the energy limit of life. Figure 2 shows a timeline of various projects, past, current, and planned at the BedrettoLab.

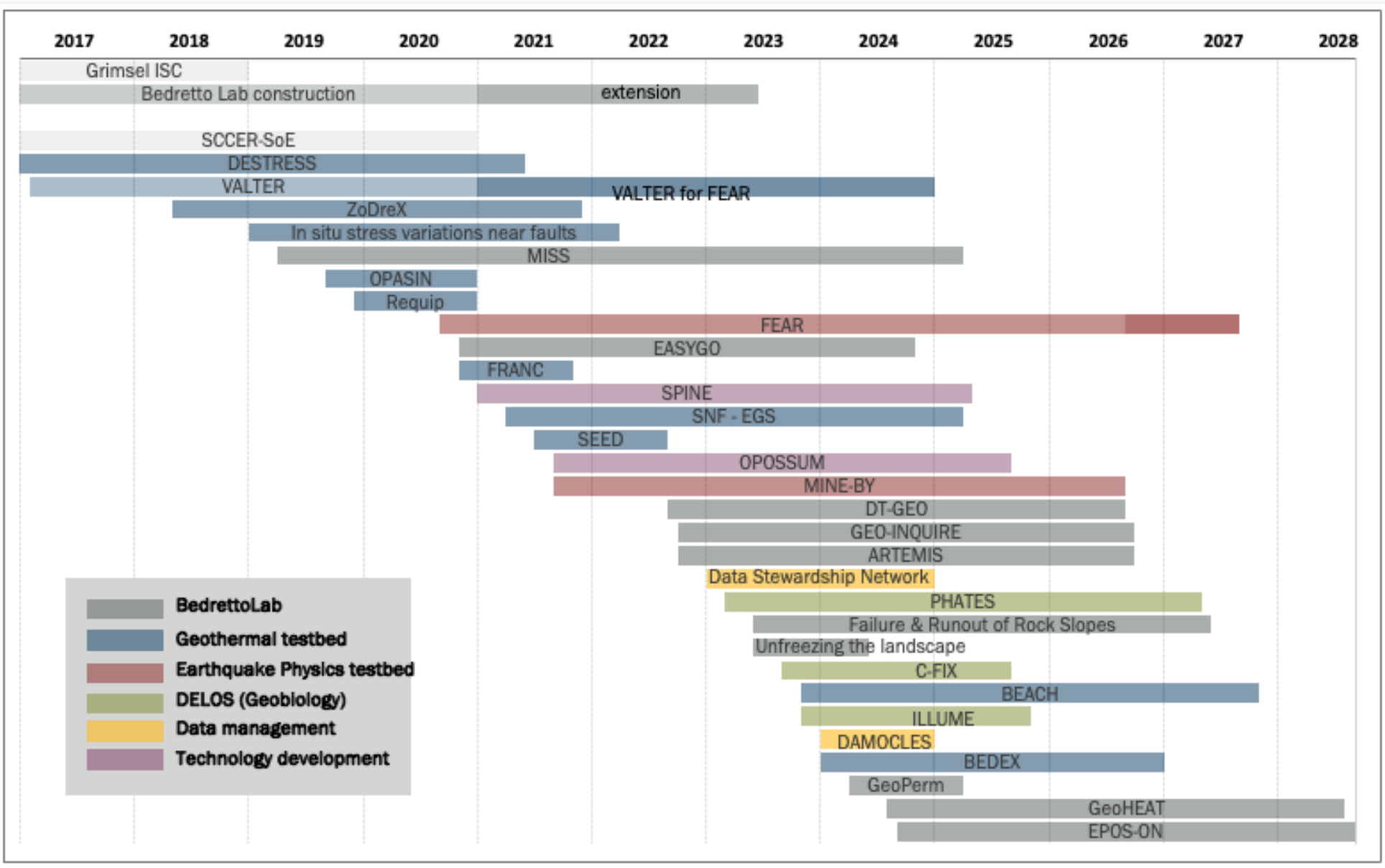

Figure 2: Past, current, and planned projects at the BedrettoLab.

Geothermal testbed

The Geothermal testbed is located between TM 2'000 and 2'100. It is equipped with a 400 m stimulation borehole equipped with a permanent multi-packer system separating the borehole into distinct intervals. Surrounding the injection borehole an array of monitoring boreholes have been drilled. The boreholes are equipped with a variety of sensors and consists of pore pressure sensors, fiber Bragg grating (FBG) sensors to measure strain, various seismic sensors, fiber-optic cables for distributed strain (DSS), distributed acoustic (DAS) and distributed temperature sensing (DTS).

VALTER4FEAR: a task of the FEAR project (p. 20)

PI: D. Giardini & S. Wiemer (ETH), F. Amann (RWTH Aachen), M. Cocco (INGV)
Funding: EU Horizon 2020 Synergy project FEAR "Fault Activation and Earthquake Rupture"

The aim of the VALTER4FEAR task of the FEAR project is to test the hydraulic injection protocols intended for the FEAR fault activation experiments in the VALTER volume.

- Test and quantitatively understand the role of the injection protocol on fault preconditioning
- Measure the dynamic changes of fluid pressure and strains, particularly during slip episodes in the injection and monitoring boreholes
- First opportunity for FEAR working groups and task forces to design, conduct, and analyze data from fault slip experiments

M-zero experiments

In April 2024, the BedrettoLab underwent one of its biggest experiments in the earthquake science World. The experiment aimed to understand and characterize the mechanics and rupture physics of a reservoir to create, predict and estimate the hazard of a given size earthquake. To do so, a complex set of sensors were installed and used to monitor the seismicity induced by injection in a granitic reservoir in the Geothermal testbed, previously studied in the VALTER project. Interval 11 within injection borehole ST1 is selected as it has the most favorable seismicity statistics and is hydraulically “isolated”.

To induce seismicity, a complex injection procedure was put in place and a new remote-controlled software was developed to manage the experiment in the safest conditions namely from ETH Zurich. Around 20 members of the BedrettoLab team were organized to work in shifts covering different tasks, e.g. earthquake picking, flow rate checking, repairs and safety checks.

April 30th at 4:09 UTC the whole Bedretto seismic network (acoustic sensors, tunnel stations, surface stations) recorded the first triggered M -0.4 after only injecting $\sim$100 m3 (Figure 3). The

event occured inside the targeted volume. This is a big accomplishment for the BedrettoLab team and will serve as excellent preparation for the planned experiments within ERC Synergy project FEAR starting in October 2024.

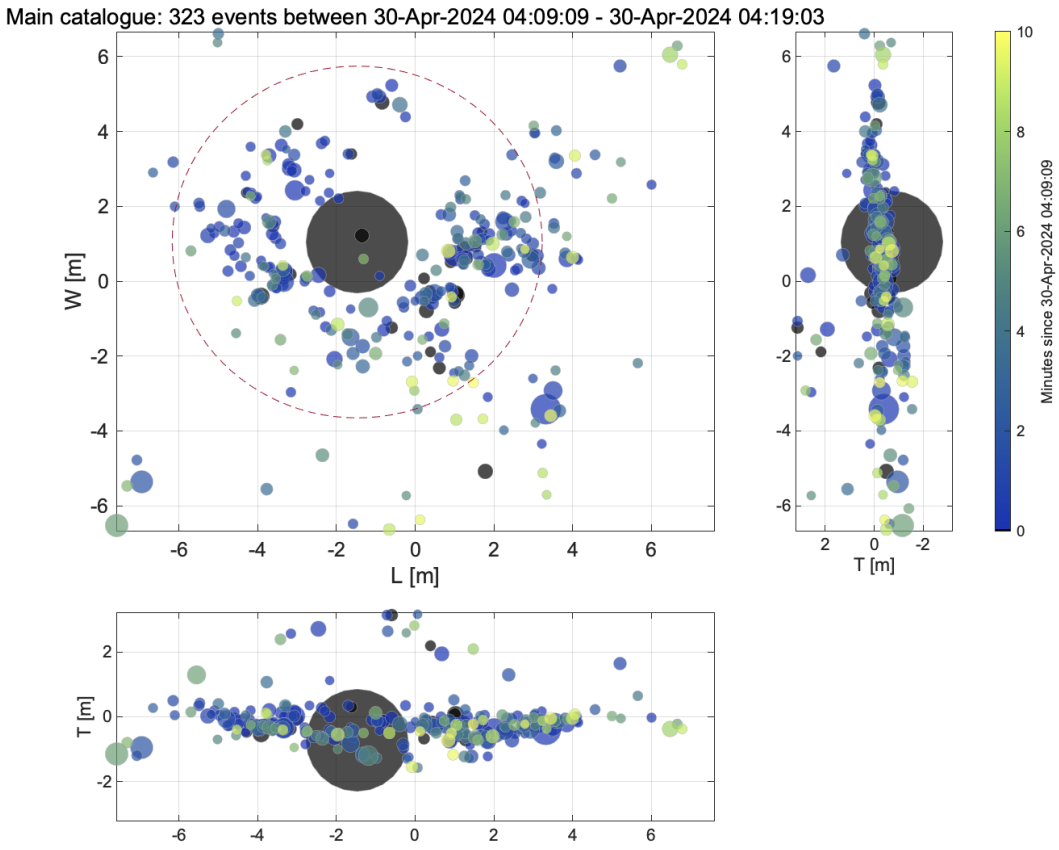

Figure 3: Seismicity of the M-zero experiments. The mainshock is in black and the aftershocks are color coded with time inside the VALTER volume.

Remote Control

Previously, technicians and engineers used a screw wrench to adjust the flow board. Now, small motors are remotely activated from a computer in Zurich to operate the valves and pumps. With the recent completion the M-zero experiment and more large-scale experiments planned, these motors and their remote-control system significantly enhance the safety and reproducibility of experiments. Personnel no longer need to be physically present in the laboratory; all processes can be managed and monitored remotely from Zurich. Moreover, the remote adjustment of valves is far more precise than manual adjustments with a wrench, which is crucial for the reproducibility of experiments.



Figure 4: Remote control, data outcome.

ARTEMIS: Awareness and Resilience Through European Multi-Sensor System

PI: S. Wiemer (Swiss Seismological Service (SED) at ETH Zurich)

The ArtEmis sensor, designed for continuous monitoring of radon, temperature, and acidity in groundwater, was installed during the most recent M-zero experiment in the Geothermal testbed. This installation aims to identify changes in these observables in relation to induced earthquakes. Calibration of the instrument and subsequent data analysis are pending. The ArtEmis project additionally plans to expand sensor usage to monitor such observables for natural seismic events, and has already identified several sites in the Valais region for additional sensor placements. In Bedretto, changes were observed in the dissolved gas partial pressures (He, Kr, Ar, N2, CO2, O2) as measured by the miniRuedi at the ST2 borehole. These changes started to occur as water was injected into ST1 on 25.04.2024 (green dashed line in figures). Figures 5 and 6 show the partial pressures of some of the gasses dissolved in the water outflowing at ST2 over the main injection period. An underlying cyclic signal is apparent on the Kr measurements (observable because the partial pressure is small). The cycle occurs approximately every 6 hours. This could be due to small pressure changes in the BedrettoLab atmosphere affecting the calibration and therefore results. 100 L of Kr loaded water was injected at ST1 in 10 minutes prior to the main injections on 25.04.2024 and 29.04.2024 (at the green dashed line and red dashed lines), which also denotes commencement of the injected water, and the increase in pressure of the injected water, respectively. The M-zero occurrence is indicated by the red solid line. It is not yet clear if the Kr loaded water reaches the ST2 borehole. The second observed ‘peak’ is slightly higher for Kr than for other gases, but further data analysis is required to clarify if this is a result of the Kr loaded water reaching ST2 or not. Data acquired in the months leading up to the M-zero experiment still needs to be filtered for problems during analysis. Data post M-zero is currently being collected for all aforementioned gas species.

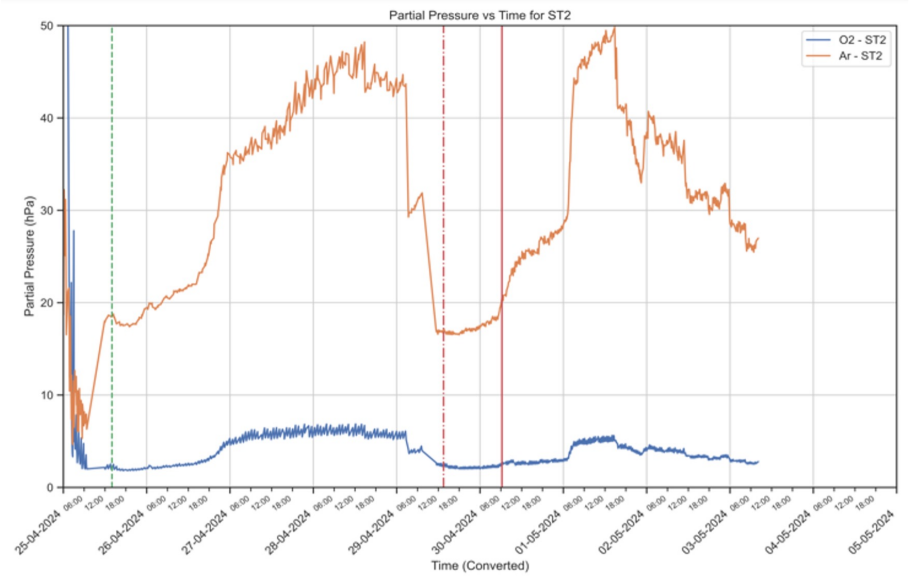

Figure 5: Partial Pressure over time of the gasses Argon and Oxygen.

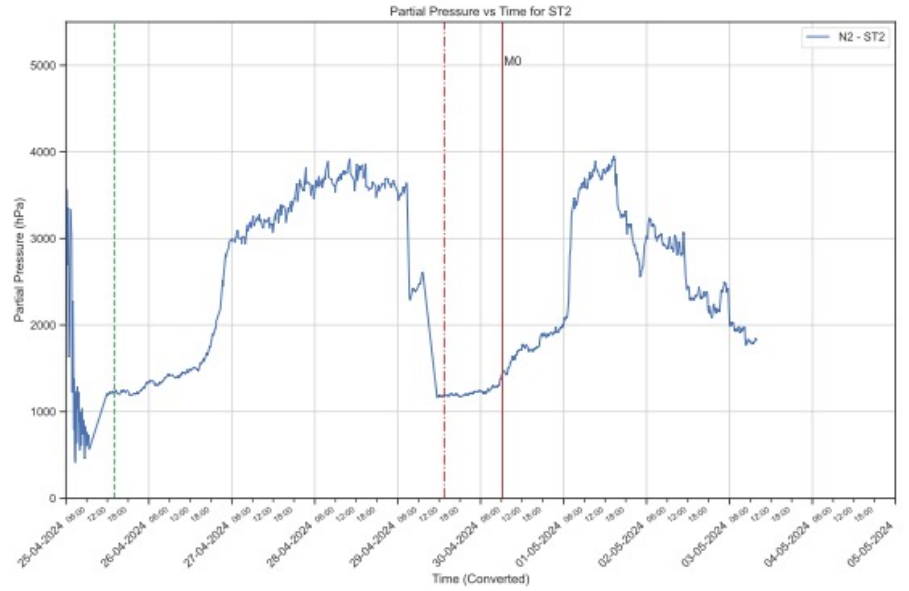

Figure 6: Partial Pressure over time of the gas Nitrogen.

Recent publications

Selection and Characterization of the Target Fault for Fluid-Induced Activation and Earthquake Rupture Experiments

Authors: Achtziger-Zupančič, P., Ceccato, A., Zappone, A. S., Pozzi, G., Shakas, A., Amann, F., Behr, W. M., Escallon Botero, D., Giardini, D., Hertrich, M., Jalali, M., Ma, X., Meier, M.-A., Osten, J., Wiemer, S., and Cocco, M.

Abstract: Performing stimulation experiments at approximately 1 km depth in the Bedretto Underground Laboratory for Geosciences and Geoenergies necessitates identifying and characterizing the target fault zone for on-fault monitoring of induced fault-slip and seismicity, a current challenge in understanding seismogenic processes. We discuss the multidisciplinary approach for selecting the target fault zone for the experiments planned within the Fault Activation and Earthquake Ruptures (FEAR) project, aiming to induce fault-slip and seismicity up

to a magnitude 1.0 earthquake while enhancing monitoring and control of fluid-injection experiments.
Structural geological mapping, remote sensing, exploration drilling and borehole logging, ground-penetration radar, and laboratory investigations were employed to identify and characterize the target fault – a ductile-brittle shear zone several meters wide with intensely fractured volume persisting over 100 m. Its orientation in the in-situ stress field favors reactivation in normal to strike-slip regimes. Laboratory tests showed slight velocity strengthening of the fault gouge. The fault's architecture, typical for crystalline environments, poses challenges for fluid flow, necessitating detailed hydraulic and stress characterization before each of the FEAR experiments. This multidisciplinary approach was crucial for managing rock volume heterogeneity and understand implications for the dense monitoring network. Successfully identifying the fault sets the stage for seismic activation experiments commencing in spring 2024.

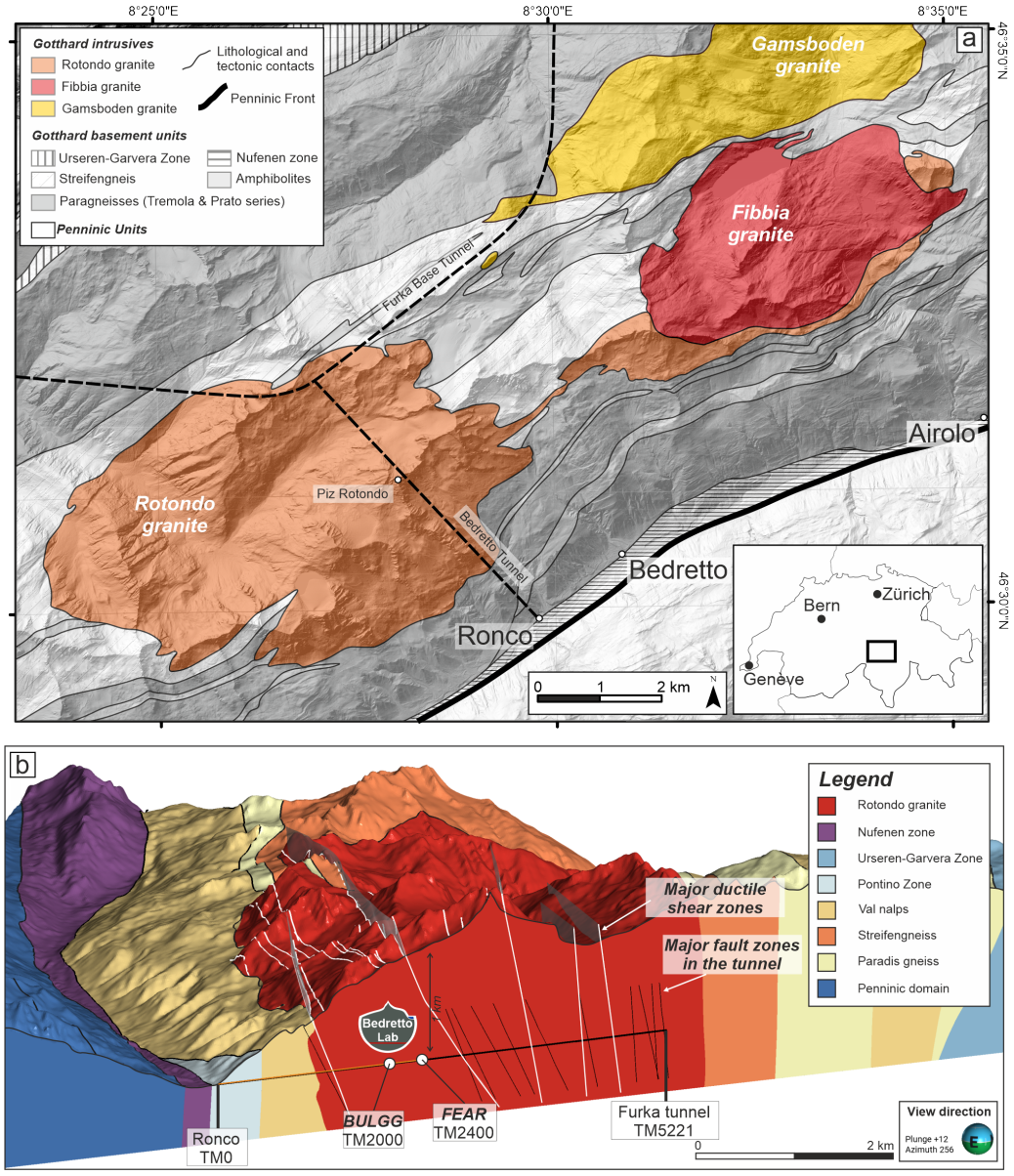

Figure 7: (a) Schematic geological map showing the location of the Bedretto tunnel in the Rotondo granite. (b) 3D Geologic cross section along the Bedretto tunnel highlighting the main geological features of the Rotondo granite.

Exploring the Feasibility of Energy Extraction from the Bedretto Tunnel in Switzerland

Authors: Halter, T., Gholizadeh Doonechaly, N., Notzon, A., Rybach, L., Hertrich, M., and Giardini, D.

Abstract: This feasibility study investigates extracting thermal energy from the Bedretto tunnel in the Swiss Alps, which benefits from subsurface heat flux and rock overburden insulation. Using the simulation software COMSOL Multiphysics, we created a numerical model of the tunnel environment to evaluate which medium between rock, air, and water serves as the most effective heat source. Our findings indicate that flowing water is the most effective heat source. Potential applications include distributing the water to nearby villages and storing remaining heat in the subsurface. Estimates indicate that the total extractable thermal energy ranges between 0.8 MWth and 1.5 MWth after reducing the water temperature to 4 °C via a heat pump. The study identifies the most suitable energy sourcing locations based on efficiency and investment costs. Circulating water to individual heat pumps in Bedretto, with the natural elevation difference, enables water transport without a pump. Cost analyses reveal that the investment in piping and heat pumps can be amortized within the equipment's lifespan with appropriate economic models. With the same initial investments, district heating systems are viable in villages with over 30 connections. The payback periods are 10 years for 60 connections, 4.5 years for 90 connections, and immediate for 200 connections.

Thermal Energy Storage and Recovery in Fractured Granite Reservoirs: Numerical Modeling and Efficiency Analysis

Authors: Halter, T., Gholizadeh Doonechaly, N., Shakas, A., Brehme, M., Hertrich, M., Giardini, D.

Abstract: Fractured media are seldom considered viable for storing excess thermal energy seasonally, compared to the more commonly used porous aquifers, due to their heterogeneity, lower storage capacity, and potential for unpredictable flow paths. This study employs COMSOL Multiphysics to create a numerical model of a fractured granite reservoir located below the BedrettoLab. The energy efficiency of both single-well and doublet systems was evaluated over 25 cycles, each comprising four 91-day phases: injection, storage, production, and resting. Results indicated that the single-well system was more efficient, with energy efficiency increasing with the flow rate. For an injection temperature of 60 °C, the system achieved energy efficiencies of up to 59.3% and 67.7%, after 10 and 25 cycles, respectively, aligning with porous Aquifer Thermal Energy Storage (ATES) system efficiencies at this temperature. Exploration of electricity production using water injected at 120 °C revealed it to be uneconomical and ineffective. However, the most promising use of the retrieved water was found to be direct ground heating for a greenhouse. This technology offers a potential alternative for thermal energy storage in regions lacking suitable porous aquifers, although identifying appropriate locations with the necessary geological characteristics may present significant challenges.

Ongoing research areas (presented on the following pages)

Systematic multi-stage hydraulic stimulation experiments in a hectometer-scale fractured rock volume at the Bedretto Underground Laboratory, Switzerland
Bröker, K., Ma, X., Gholizadeh Doonechaly, N., Rinaldi, A. P., Obermann, A., Rosskopf, M., Hertrich, M., Giardini, D., the Bedretto Lab team

---

Geological contraints on the seismic anisotropy of Rotondo granite within the Bedretto tunnel
Hinshaw, E., Behr, W., Zappone, A., Ceccato, A., Tewksburry-Christle, C.

Seismic and aseismic slip driven by ascending fluids and overpressure pulses on faults
Jiang, D., Dal Zilio, L., Rinaldi, A.

Continuous measurements of radon and other dissolved gas species in groundwater: A crucial step in earthquake precursor research?
Lightfoot, A., Strupler, M., Wiemer, S.

Systematic multi-stage hydraulic stimulation experiments in a hectometer-scale fractured rock volume at the Bedretto Underground Laboratory, Switzerland

Bröker, K.[1,2], Ma, X.[3], Gholizadeh Doonechaly, N.[2], Rinaldi, A. P.[4], Obermann, A.[4], Rosskopf, M.[2], Hertrich, M.[2], Giardini, D.[2] & the Bedretto Lab team

[1] Center for Hydrogeology and Geothermics, University of Neuchâtel, Switzerland
[2] Institute of Geophysics, ETH Zürich, Switzerland
[3] School of Earth and Space Sciences, University of Science and Technology of China, China
[4] Swiss Seismological Service (SED), ETH Zürich, Switzerland

Contact: Abstract:

1 Introduction

Bedretto Underground Laboratory for Geosciences & Geoenergies

- **Scaled-down in-situ hydraulic stimulation experiments** (Ma et al., 2022) in a representative granitic rock volume
- Overburden: > 1000 m and multiple large fault zones in the volume
- Stress state: transitional between normal and strike-slip faulting (Bröker and Ma, 2022), local stress perturbations exist (Bröker et al., 2024)
- **Stimulation borehole ST1** (399 m long, Fig. 1) separated into 14 injection intervals by multi-packer system
- Dense borehole array with multi-sensor monitoring system (Plenkers et al., 2023)

Research question

Stimulation intervals 7-14 contain **similarly oriented pre-existing fractures**, but have different hydraulic transmissivities. How do these intervals react to **comparable fluid injections**? At **which pressures are structures reactivated**?

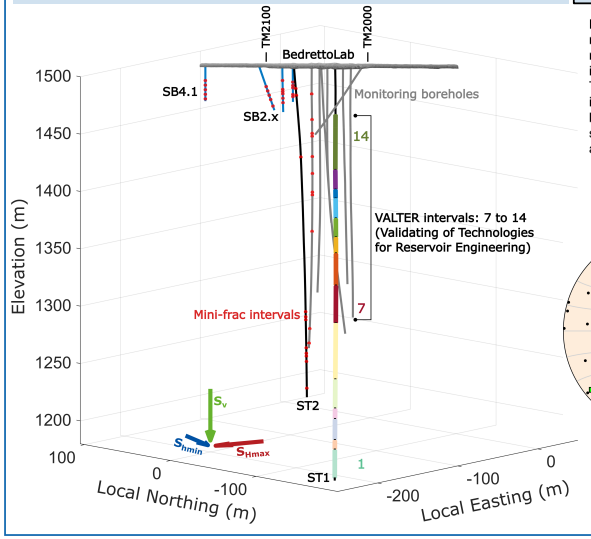

Fig. 1 Stimulation (ST), monitoring (MB) and stress measurement (SB) boreholes in the Bedretto Geothermal Testbed. The 14 stimulation intervals along ST1 and locations of mini-frac tests for stress field characterization are marked.

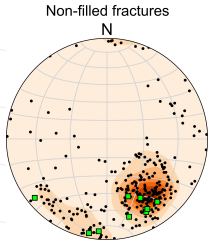

Fig. 2 Lower hemisphere pole plot of non-filled fractures along borehole ST1. Green square denote fracture zones > 10 cm.

3 Hydromechanical Analysis

Fracture reactivation, P-Q analysis

- In 5 intervals a clear **bilinear behaviour indicates fracture reactivation** (= increase in injectivity)
- In 3 intervals **no increase in injectivity** was achieved:
  - Int 7, high transmissivity: high pressure (17.5 MPa), seismicity and pressure-injected volume plot suggest reactivation without injectivity increase
  - Int 13, high transmissivity: pressure was too small for reactivation even at high flow rate (150 L/min), but many seismic events!
  - Int 12, low transmissivity: reached a high pressure (21.4 MPa), but low seismicity → interval hydraulically isolated due to terminating/cemented fracture(s)

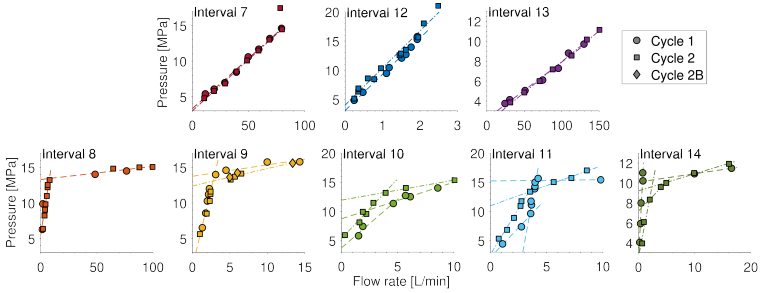

Fig. 4 Pressure-flow rate plots of each hydraulic stimulation. P-Q points were taken at the end of each injection step (Fig. 3). Bilinear behaviour indicates fracture reactivation.

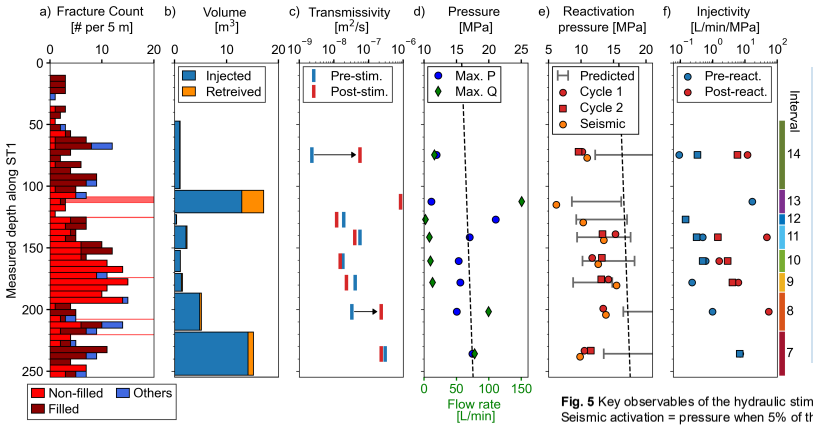

Fig. 5 Key observables of the hydraulic stimulations. Panel e) & f) estimated from Fig. 4. Seismic activation = pressure when 5% of the total events happened

Heterogeneous rock mass response

- Strongly varying initial transmissivities and thus injected volume, flow rate, and max. pressure
- Reactivation pressures from **P-Q plots agree** well with **seismic activation pressures**
- **Reactivation pressures** are **lower than S_3 magnitude**, so hydraulic shearing is more probable than hydraulic jacking & fracturing
- Hydraulic shearing can be predicted using a **Mohr-Coulomb failure** criterion → predicted reactivation pressures consider uncertainties (Monte Carlo simulation with 10000 realizations)
- **Stress perturbation by large fault zone** in int 13 might prohibit reactivation in int 12 → max. pressure above S3 magnitude

2 Multi-Stage Hydraulic Stimulations

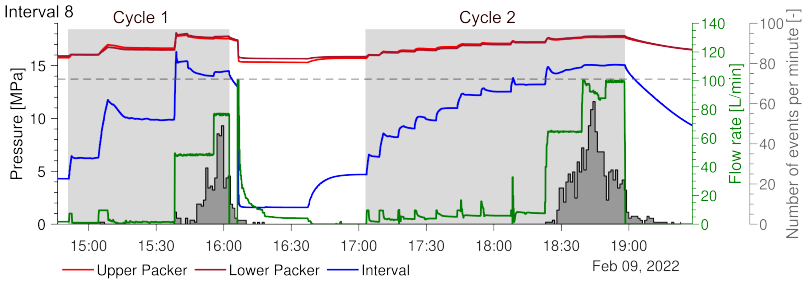

Fig. 3 Injection protocol of pressure-controlled stimulation in interval 8. The interval pressure was measured downhole, while all other parameters were measured at the surface. The dashed line marks the estimated reactivation pressure. Seismic data from Obermann et al. (2024).

Methodology

- **Intervals 7-14** (VALTER volume) lie in or adjacent to the high-resolution monitoring zone → interval length: 7.5 m (int. 12) – 54.8 m (int. 14)
- We injected relatively small water volumes (0.35–14 m³) following a standardized injection protocol to compare the interval response (**seismo-hydromechanical characterization**)
- Depending on the interval transmissivity, injection protocol (Fig. 3) was conducted **pressure-(6 intervals) or flow rate-controlled (2 intervals)**
- We integrate hydromechanical (downhole and surface pressure & flow rate sensors) and seismic (collocated accelerometers and acoustic emission sensors) observations

4 Discussion

- Similar fracture orientations, initial transmissivities and reactivation pressures (int 8-12), but different transmissivity increases and number of seismic events → **geological properties of fractures** (= flow channels) **determine stimulation efficiency**
- **Seismic clouds typically propagate upwards** on parallel planes that seem to a large extent **associated with non-filled fractures**
- **Hydraulic shearing** can explain reactivation pressures, but stress heterogeneity is not fully understood

References

Bröker, K., & Ma, X. (2022). Estimating the least principal stress in a granitic rock mass: Systematic mini-frac tests and elaborated pressure transient analysis. *Rock Mechanics and Rock Engineering*, 55:1931–1954. https://doi.org/10.1007/s00603-021-02743-1

Bröker, K., Ma, X., Zhang, S., Doonechaly, N. G., Hertrich, M., et al. (2024). Constraining the Stress Field and its Variability at the BedrettoLab: Elaborated Hydraulic Fracture Trace Analysis. *In Review (URMMS)*. https://dx.doi.org/10.2139/ssrn.4706040

Ma, X., Hertrich, M., Amann, F., Bröker, K., Gholizadeh Doonechaly, N., et al. (2022). Multi-disciplinary characterizations of the BedrettoLab–a new underground geoscience research facility. *Solid Earth*, 13(2), 301–322. https://doi.org/10.5194/se-13-301-2022

Obermann, A., Rosskopf, M., Durand, V., Plenkers, K., Bröker, K., et al. (2024) Seismic response of hectometer-scale fracture systems to hydraulic stimulation in the Bedretto Underground laboratory, Switzerland. *Submitted to JGR*.

Plenkers, K., Reinicke, A., Obermann, A., Doonechaly, N. G., Krietsch, H., et al. (2023). Multi-Disciplinary Monitoring Networks for Mesoscale Underground Experiments: Advances in the Bedretto Reservoir Project. *Sensors* 23 (6): 3315. http://dx.doi.org/10.3390/s23063315

Seismic and aseismic slip driven by ascending fluids and overpressure pulses on faults

Danyang Jiang[1], Luca Dal Zilio[2] , Antonio Pio Rinaldi[1]

[1]Swiss Seismological Service, ETH Zürich; [2]Seismology and Geodynamics, Institute of Geophysics, ETH Zürich

danyang.jiang@sed.ethz.ch

Introduction

Fault zones may serve as fluid pathways, with fluid pressure and transport properties significantly impacting fault behavior. The Cahuilla swarm in California is one example illustrating the complex interaction between solids and fluids in nature *(Ross et al. 2020)*. Despite evidence suggesting their importance, conventional earthquake models often overlook dynamic fluid pressure and poroelastic effects in fault mechanics. In this study, we would like to present a newly-developed Hydro-Mechanical Earthquake Cycles (H-MECs) model to investigate the influence of ascending fluids and overpressure pulses on both seismic and aseismic slip.

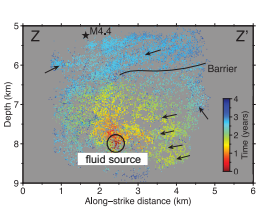

upward migration

After M_w4.4

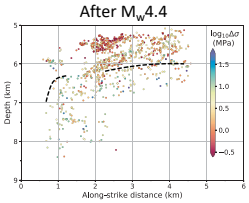

upward migrating microearthquakes after big event (Mw4.4)

***Fig. 1**: The spatio-temporal distribution of Cahuilla swarm (left) and fault valving phenomena (right) (Ross et al. 2020).*

Hydro-Mechanical Earthquake Cycles (H-MECs) model

- 2-D antiplane strike-slip fault model *(Dal Zilio et al. 2022)*
  - fully integrates solid-fluid interactions
  - poro-visco-elasto-plastic compressible medium
  - rate- and state-dependent friction
- **permeability evolution law** *(Zhu et al. 2020)*

$$\frac{\partial k^*}{\partial t} = -\frac{V}{L_k}(k^* - k_{max}) + \frac{1}{T_k}(k^* - k_{min})$$

Permeability increases during the slip and decreases during healing

Model Setup

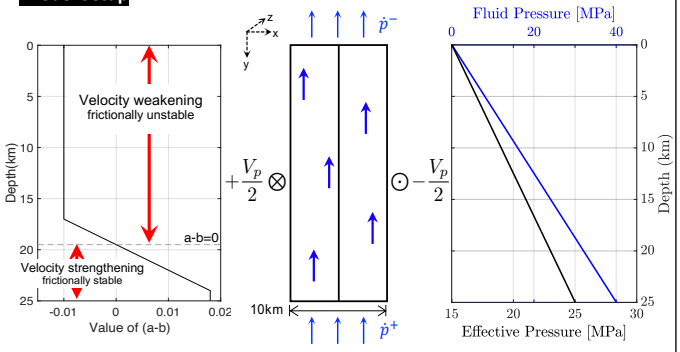

***Fig. 2**: Model setup regarding the rate-and-state friction coefficient (left), fault position and tectonic loading (middle), and initial pressure profiles (right).*

Reference model: without permeability evolution

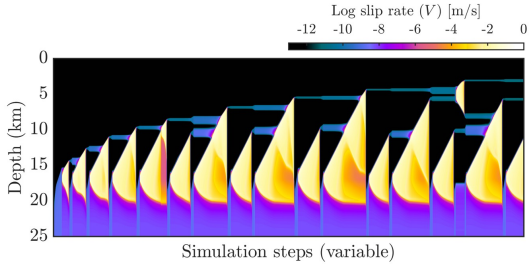

***Fig. 3**: Seismic cycle pattern of reference model.*

Results

1. Permeability evolution law introduces the dynamic fluid pressure in our model, which enables our model to reproduce complex seismic pattern.

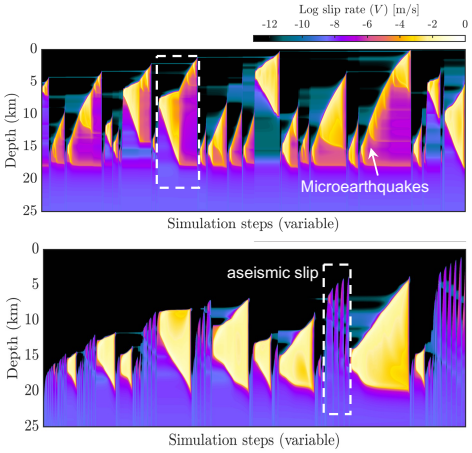

***Fig. 4**: Different seismic cycle pattern with permeability evolution (T_k=231.48 days and L_k=1 m)*

2. Slip on fault triggers an increase in fault permeability, facilitating the migration of over-pressurized ascending fluids. This mechanism initiates and sustains slow-slip events within the seismogenic zone.

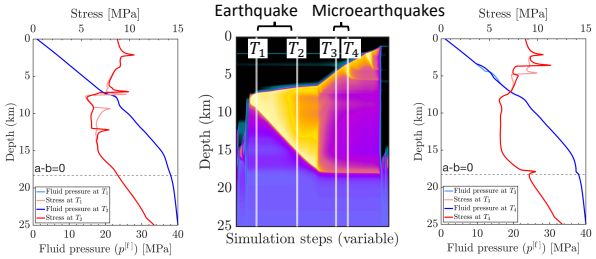

***Fig. 5**: The fluid pressure profiles and stress profiles during earthquake (left) and microearthquake (right). Middle plot shows the chosen time steps on a zoom in slip rate plot.*

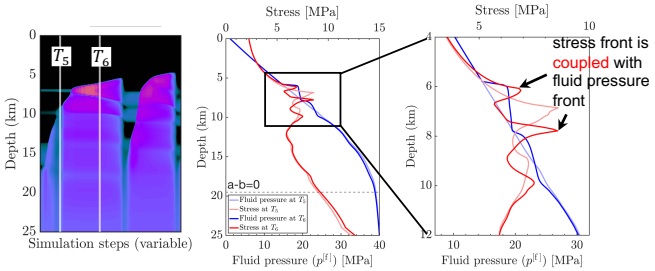

***Fig. 6**: The fluid pressure profiles and stress profiles during aseismic slip (middle) and the zoom in part (right). Left plot shows the chosen time steps on a zoom in slip rate plot.*

Conclusions

- Dynamic fluid pressure introduces aseismic slip and microearthquakes into seismic cycle pattern
- Coupled system is one possible mechanism for aseismic slip
  - Aseismic slip can occur throughout the whole seismogenic zone

References

1. Dal Zilio, L., Hegyi, B., Behr, W., and Gerya, T. (2022). Hydro-mechanical earthquake cycles in a poro-visco-elasto-plastic fluid-bearing fault structure. *Tectonophysics* 838, 229516.

2. Zhu, W., Allison, K. L., Dunham, E. M., and Yang, Y. (2020). Fault valving and pore pressure evolution in simulations of earthquake sequences and aseismic slip, *Nature Communications* 11:4833.

3. Ross, Z. E., Cochran, E. S., Trugman, D. T., and Smith, J. D. (2020). 3d fault archi- tecture controls the dynamism of earthquake swarms. *Science* 368(6497):1357–1361.

Geological constraints on the seismic anisotropy of Rotondo granite within the Bedretto Tunnel

Emily R. Hinshaw[1], Whitney M. Behr[1], Alba Zappone[2], Alberto Ceccato[1], & Carolyn Tewksbury-Christle[3]
[1]Geological Institute, Department of Earth Sciences, ETH Zurich, [2]Institute of Geophysics, Department of Earth Sciences, ETH Zurich, [3]Geosciences Department, Fort Lewis College, Durango, CO, USA
Contact: ehinshaw@ethz.ch

Introduction

The Bedretto Tunnel provides an opportunity to test the geological assumptions made when estimating seismic properties from a rock. In this study, we calculate the seismic properties (velocity and anisotropy) for different structural domains within the Rotondo Granite at various scales (m- to km-) and end-member assumptions (e.g. volumetric averaging methods). We aim to determine which assumptions are more representative of the actual geophysically-determined seismic anistropy. This work will calibrate the often-employed calculation recipes for rock seismic properties when ground-truth geophysical data is not available.

Geological Background

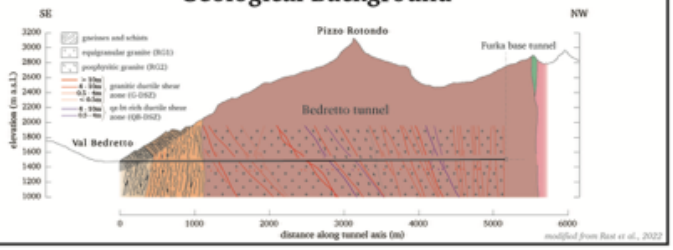

Geological Characterization

Granite shear zone from Tunnel Meter 1350

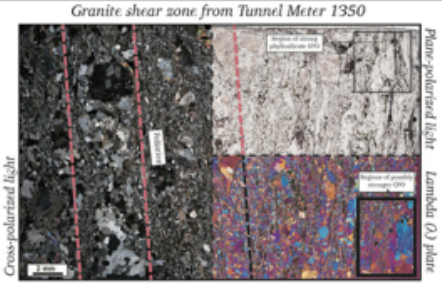

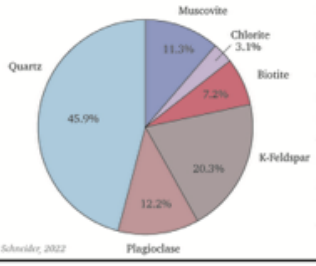

Shear zones have strong foliation fabrics with SPO (shape-preferred orientation), though not necessarily CPO (crystallographic-preferred orientation). Shear zones either have granitic mineral assemblages (left) or quartz-biotite (right).

Quartz-biotite shear zone from Tunnel Meter 2801



Translating Geological Observations to Seismic Estimates

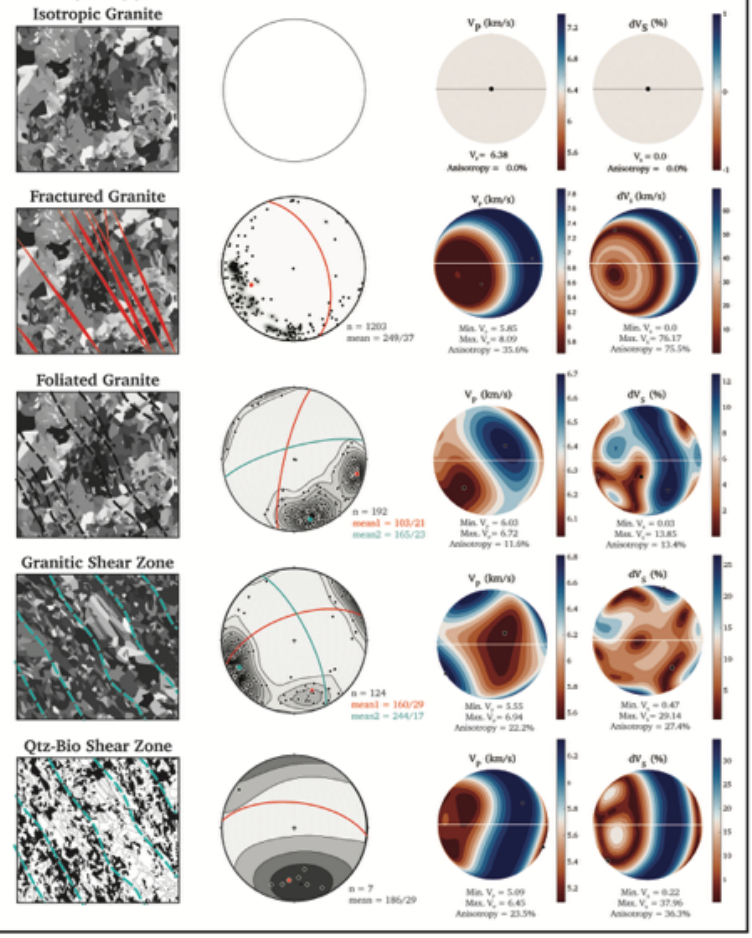

Possible Geological Controls on Anisotropy

Mineralogy

Impact (or extent of control) on the overall anisotropy will depend on the volume percent of certain minerals (e.g. phyllosilicates).

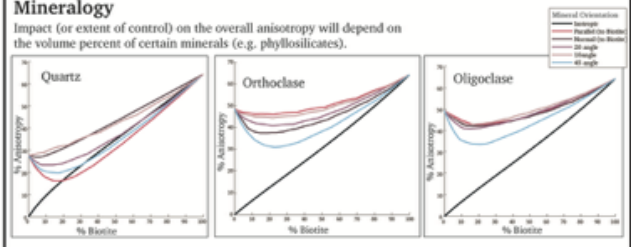

Structural Fabric

Impact (or extent of control) on the overall anisotropy will also depend on the volume percent of certain structural domains. These are examples from end-member assumptions where phyllosilicates are 100% aligned.

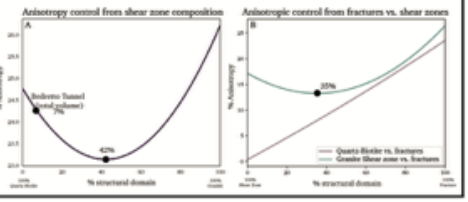

Averaging Assumptions

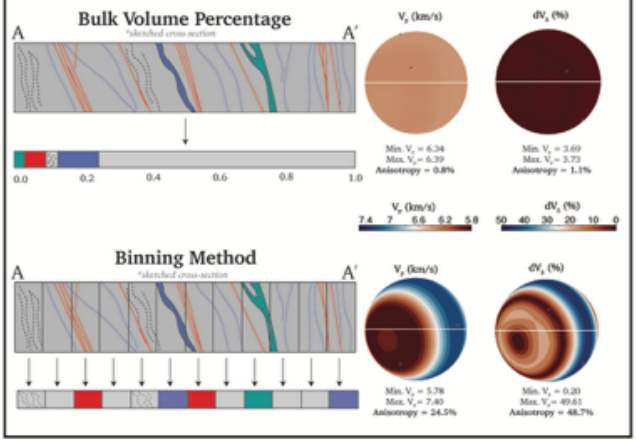

Conclusions

- Calculations are most sensitive to phyllosilicate volume and orientation.
- Structural domains within the Rotondo granite result in highly variable anisotropy.
- Different averaging methods do not change velocity directions, but do change velocity magnitudes.

References

Jordan, D., 2019, Geological Characterization of the Bedretto Underground Laboratory for Geoenergies: , p. 60 p., doi:10.3929/ETHZ-B-000379305.

Keller, E, & Schneider, T R. (1982). Geologie und Geotechnik. Schweizer Ingenieur und Architekt, 100(24), 512–520. https://doi.org/10.5169/seals-74820

Rast, M., Galli, A., Ruh, J.B., Guillong, M., and Madonna, C., 2022, Geology along the Bedretto tunnel: kinematic and geochronological constraints on the evolution of the Gotthard Massif (Central Alps): Swiss Journal of Geosciences

Schneider, C., 2022, Seismic Velocity Anisotropy and Microstructural Characterization of Ductile Shear Zones in the Rotondo Granite: ETH-Zurich, 33 p.

Continuous measurements of radon and other dissolved gas species in groundwater: A crucial step in earthquake precursor research?

ArtEmis: **A**wareness and **R**esilience **T**hrough **E**uropean **M**ulti-**S**ensor **S**ystem

Alexandra Lightfoot[1], Michael Strupler[1], Stefan Wiemer[1]

[1]Swiss Seismological Service (SED), ETH Zurich, Sonneggstrasse 5, 8092 Zurich, Switzerland

(alexandra.lightfoot@sed.ethz.ch)

I. Aim

- **European collaboration project** intended to design, build, and operate a multi-sensor system comprising of more than 100 sensors, which determine Radon (Rn) concentrations in groundwater.
- **Test if changes in radon concentrations can be used as potential precursors to earthquakes** by feeding measurement data into machine learning algorithms and correlate them to seismic data.

→ Can continuous measurements contribute to better earthquake forecasting?

II. Background

^{222}Rn (half-life: 3.8d) is produced in the radioactive decay series of ^{238}U – which is naturally abundant in the Earth's crust.

- Distinct changes in Rn concentrations in air, soil and groundwater have been observed and proposed as earthquake precursors.

Hypotheses: stress increase → larger number of cracks → increased radon emission

III. Locations: Italy, Greece and Switzerland

Ground acceleration hazard map*

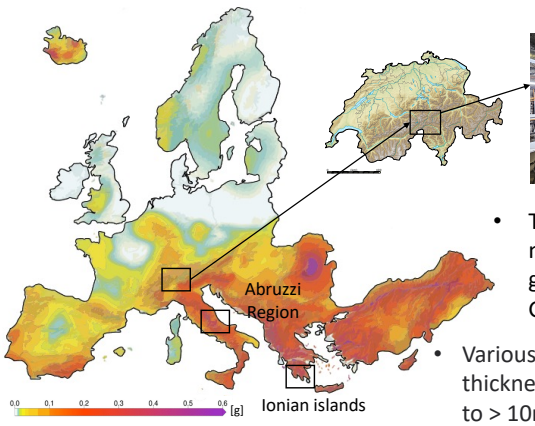

Expected level of ground shaking at a specific location due to future potential earthquakes.

Switzerland's underground rock laboratory, Bedretto

installed boreholes



- The Bedretto tunnel is mostly located in Rotondo granite, a part of the Gotthard massif.**
- Various shear zones with thicknesses between few cm to > 10m.
- Outflows of water from drilled boreholes and fissures.

- Experiments planned with hydraulic stimulation to initiate small non-damaging earthquakes.
- Ideal conditions for measuring Rn time series in groundwater (small temperature and pressure fluctuations).

Tunnel section identifying shear zones

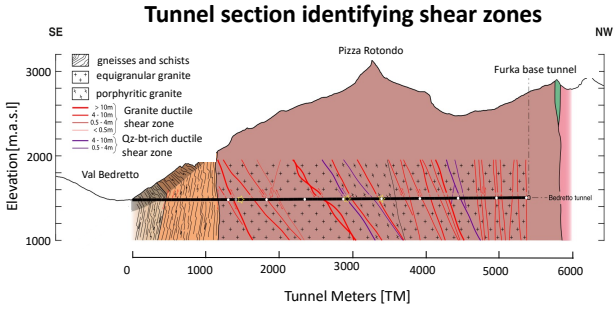

IV. Sensor design

- A scintillation detector - CsI(Tl) crystal detecting both α and γ radiation from Rn decay progenies.

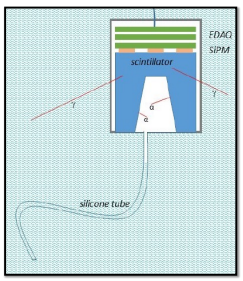

- Sensor additionally measures water temperature and acidity.

Additional dissolved gas analysis

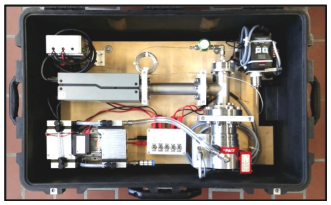

- Portable mass spectrometer: Continuously Analyses e.g., He, Ar, Kr, CO_2, O_2, N_2 in gas/water.

V. Preliminary observations and next steps

Initial Rn concentrations from boreholes/fractures

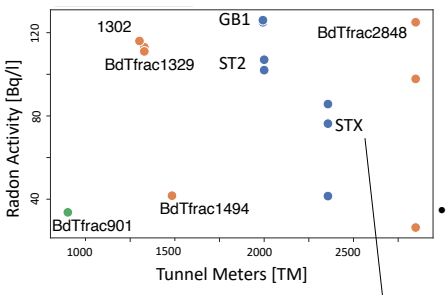

- Selection of ST2 borehole to begin measurements with installation taking place between December 2023 and February 2024.
- Exploring additional potential sites in the Valais to deploy the newly developed sensor.

*Adapted from Danciu L. et al., 2021
**Rast et al., 2022

+41 44 633 83 23
alexandra.lightfoot@sed.ethz.ch

Schweizerischer Erdbebendienst
Service Sismologique Suisse
Servizio Sismico Svizzero
Swiss Seismological Service

ETH zürich

Earthquake Physics testbed

The Earthquake Physics testbed is located 400 m further into the Bedretto tunnel beyond the Geothermal testbed. It is being built around the MC fault zone, a distinct ∼2 m wide fault zone identified as a suitable target for fault activation experiments in the context of the ERC Synergy project FEAR "Fault Activation and Earthquake Rupture" and the Werner Siemens Foundation project MISS "Mitigating Induced Seismicity for Successful Geo-Resources Applications". The MC fault zone steeply dips towards the northwest (∼330°dip direction and ∼70°dip) and crosscuts the Bedretto tunnel at an almost perpendicular angle (Figure 8). It is a reactivated brittle mylonitic shear zone that shows clear evidence of past fault slip episodes in the form of strong shear localization structures, and a distinct, narrow (< 5 mm) fault core with fault gouge (Lützenkirchen & Loew 2011). The fault is favorably oriented to slip in the estimated regional stress field, as inferred from borehole breakouts and hydromechanic characterizations in the boreholes of the Geothermal testbed 400m away (Bröker & Ma 2022).

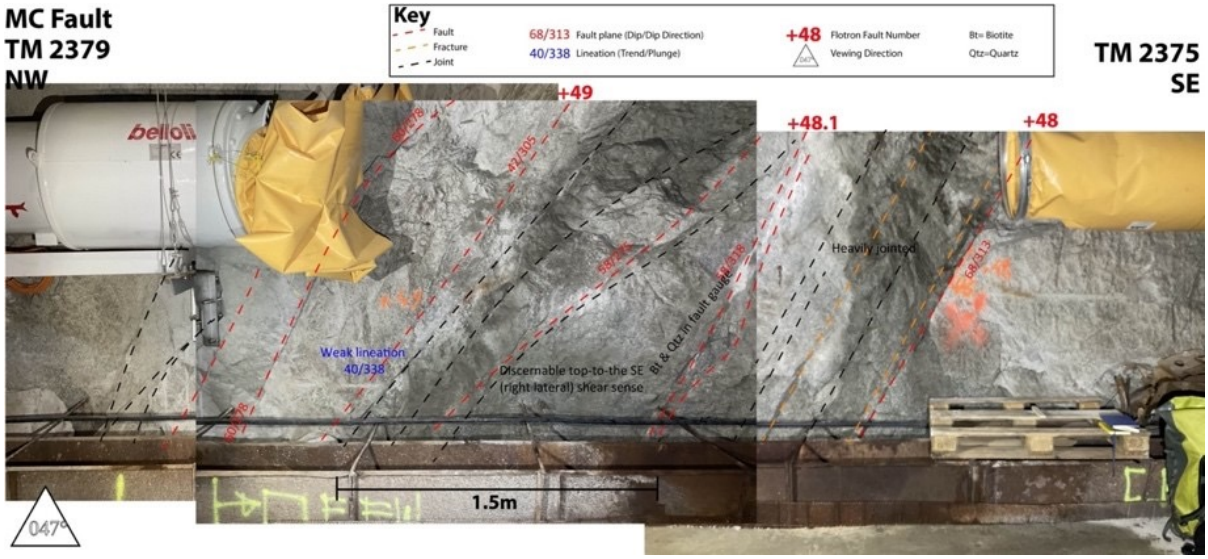

Figure 8: The intersection between the Bedretto tunnel and the target MC fault zone of the Earthquake Physics testbed. The Earthquake Physics testbed is located between tunnel meters 2'300 and 2'500.

The FEAR and MISS projects will perform the first-ever 50-100 m scale fault stimulation experiments at over 1'000 m depth, conditioning the stress distribution on the fault and validating the results of deep experiments with tests in rock deformation laboratories, numerical modeling, and observations from natural earthquakes. The experimental objectives are to induce non-damaging earthquake ruptures (∼Magnitude 1) on a natural fault in order to better understand earthquake rupture processes.

In spring 2022, a detailed characterization campaign of the target fault zone was conducted. This campaign involved drilling 3 prospection boreholes of up to 250 m length. The inference and imaging that these boreholes facilitated have confirmed i) a large enough spatial extent of the MC fault zone (at least 300 m in length), ii) its sufficiently planar geometry, and iii) the

structural and compositional suitability for fault activation experiments.

To better access the target fault zone, the FEAR side tunnel, a 120 m-long access tunnel, is being constructed at a distance of 50 m parallel to the MC fault zone. The tunnel construction will cost 2.4 MCHF, is in itself a well-monitored science and engineering project (project PRE-CODE - Progressive Excavation Damage Zone Evolution During and Post Mine-By Tunneling, BGE, Germany), and is scheduled to be finalized by Q3 2025. Together, the target MC fault zone and the FEAR side tunnel form the core of the Bedretto Earthquake Physics testbed.

From a seismology perspective, the Earthquake Physics testbed is particularly interesting because of the unusually favorable seismic noise conditions. Being located at >2 km inside a mountain, with >1 km of overburden, and far away from external noise sources such as wind and traffic, the Earthquake Physics testbed location is seismically very quiet. A Streickeisen STS-2 seismometer located just ∼130 m away from the MC fault zone, the seismic station '8R.T2246' (Figure 9), is the quietest seismic station in the entire national network operated by the Swiss Seismological Service. These are excellent conditions for building a highly sensitive earthquake observatory.

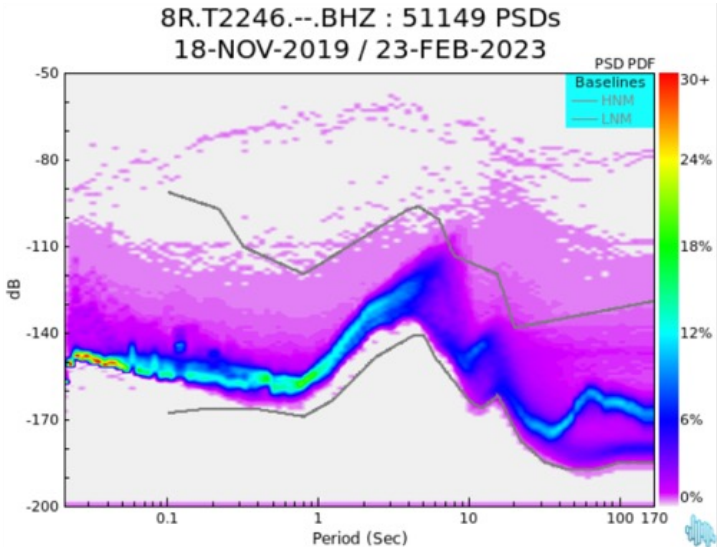

Figure 9: Power spectral density plot for the vertical component of station '8R.T2246', showing the exceptionally low noise levels at the Earthquake Physics Testbed.

FEAR: Fault Activation and Earthquake Rupture

PIs: D. Giardini (ETH), S. Wiemer (ETH), F. Amann (RWTH Aachen), M. Cocco (INGV)
Funding: EU Horizon 2020 Synergy

The FEAR project aims to advance our understanding of earthquake physics by inducing non-damaging earthquake ruptures ∼M1 on a natural fault zone. With ∼50 scientists from ETH Zurich, RWTH Aachen, INGV Rome, and Sapienza University of Rome and a budget of ∼13 MEuros, FEAR is the largest Synergy grant awarded by the European Research Council in the geosciences domain.

The FEAR project consists of 4 main experiments (Figure 10) scheduled to take place between 2024 and December 2026. A first smaller-scale experiment, FEAR Experiment 1, is planned to be conducted before the main part of the FEAR tunnel has been excavated. FEAR Experiments 2-4 will be realized after tunnel completion.

The goals of the project MISS ("Mitigating Induced Seismicity for Successful Geo-Resources Applications", PI: D. Giardini, ETH), funded by the Werner Siemens Foundation, are optimally aligned with those of FEAR.

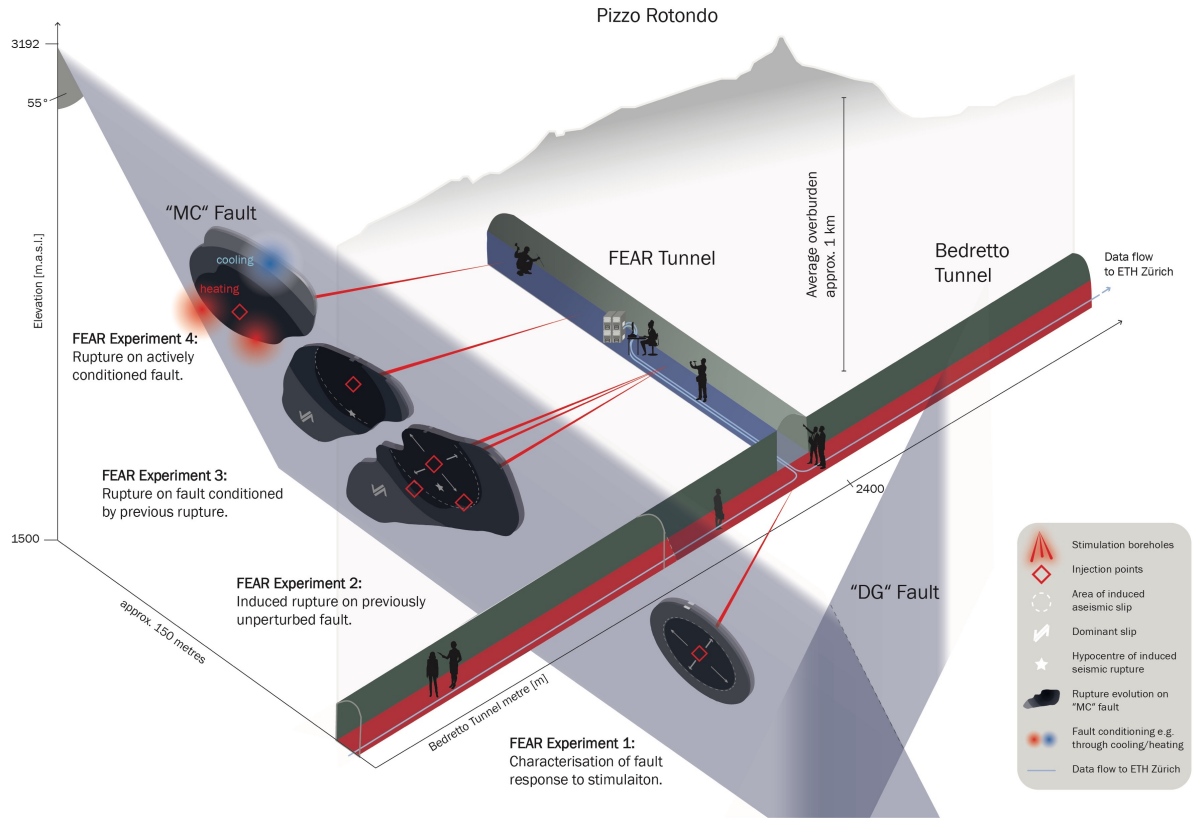

Figure 10: Sketch of the existing Bedretto tunnel, the 120 m-long FEAR tunnel, the target MC fault zone of the Earthquake Physics testbed, and the four main FEAR Experiments.

The main objectives of the FEAR project are to:

- Conduct experiments on rupture surfaces of 50 m, producing events of magnitudes -2 to 1, a scale required to bridge laboratory, previous deep experiments, and natural events.
- Attempt to precondition stress on the target fault.

- Install an unprecedented array of multi-disciplinary, next-generation sensors in boreholes very near the future rupture planes.
- Demonstrate a seamless integration of experimentation, modeling, and hypothesis-driven forecast evaluation.

The research activities in FEAR are distributed among the Geology, Laboratory, Modeling, and Monitoring Working Groups (WGs).

FEAR Geology Working Group

The aims of the FEAR Geology Working Group in this past year:

- Refinement of the fault zone model, especially in light of the new information from the injections and seismicity recorded in the VALTER volume and the upcoming experiments.
- Provide joint effort with the Characterization Task Force for the characterization of the hydraulic connection of fractures across boreholes.
- Define rock facies and provide samples for informed use in laboratory experiments dedicated to assess the permeability and rheology of fault rocks.

Geology Working Group Highlights

- Analysis of core logs of the MC fault to define 5 fundamental facies of the Rotondo granite (Figure 11 a.): F0, intact rock distinguished by the absence of pervasive brittle deformation and prevalence of magmatic fabrics, F1, presence of cohesive closed fractures decorated by minerals such as biotite and quartz, F2, presence of fractures which are mostly non cohesive and open, F3, dilated open fractures and breccias with at least one principal segment characterize by the presence of fault gouge, F4, cohesive cataclasites and fractures with high interconnected porosity. F3 and F4 are mostly associated with a cataclasite precursor mineralize with zeolites. The facies were qualitatively classified in a permeability-cohesion diagram (Figure 11 b.) to assess the potential for reactivation and hydraulic pathways.
- Definition of i) a practical MC fault model composed of two sub-parallel main planes defined by the connection of facies F3 and F4, and a ii) ideal MC fault model where hydraulic connectivity between the two main planes is controlled by sets of open fractures prevalently sited in a restricted damage zone comprised between the two.
- Publication of Article: "Selection and Characterization of the Target Fault for Fluid-Induced Activation and Earthquake Rupture Experiments" which collects the collective effort of the Geology and other working groups in the description of the MC fault zone. The geological fault model is discussed extensively in the manuscript (Achtziger-Zupančič et al. 2024).
- Characterization of the deformation history of MC-like faults using as representative the fault at TM 2’848 (named “Waterfault”) including dating of fault gouges. The deformation history suggests limited brittle reactivation that occurred around 12 Ma along pre-existing cohesive shear zones with evidence of coseismic damage (Figure 12).
- Improvement of the characterization of the fracture network of the FEAR injection volume and analysis of the fracture pattern around the MC fault zone in Borehole BFE_A_05 and BFE_A_06, in order to constrain the fractures controlling the hydraulic connectivity between the two boreholes and affecting the injection procedures on the fault.

- Qualitative analysis of the geometry and distribution of the microseismicity cloud in the VALTER volume generated by the M-zero event to improve our understanding of the geometry of the fracture and fault pattern, and comparison with the geometry of faults and fracture zones exposed at the surface (surface geology).
- Work on the noble gases concentration impacted during injection and production cycles of the M-zero experiment.

Geology Working Group Next Steps

- Analysis of the seismicity pattern after FEAR experiment 1 to better constrain the fault zone geometry and refine the geological model.
- Retrospective examination of experimental volume changes: Following the completion of the seismic experiments, the test volume will be examined again to evaluate any alterations to its properties, structures, and geometries.
- Joint analysis of the geometry of the microseismicity in the VALTER volume generated during the M-zero experiments in order to define, by means of comparison with fault structures at the surface, the geometrical model of the activated fault zone and provide further information on the triggering and propagation mechanisms.
- The continuation of the noble gases measurements on the M-zero volume and sampling of the MC waters.

Ongoing research in the FEAR Geology Working Group (presented in the following pages)

3D geological models of the Rotondo granite and fault zone geometries
Ceccato, A., Behr, W., Zappone, A. & the FEAR Geology WG

Characterization and 3D geometrical modeling of a complex fault zone for earthquake rupture experiments
Ceccato, A., Behr, W., Zappone, A. & the FEAR Geology WG

The candidate fault for fluid-induced earthquake rupture experiments in the Rotondo granite
Pozzi, G., Achtziger-Zupančič, P., Aldega, A., Ceccato, A., Collettini, C., Escallon, D., Hertrich, M., Ma, X., Meier, M-A., Osten, J., Shakas, A., Spagnuolo, E., Volpe, G., Zappone, A., Amann, F., Cocco, M., Giardini, D., Wiemer, S.

Tectonic and structural evolution of the Rotondo granite
Ceccato, A., Behr, W., Zappone, A., Tavazzani, L., Giuliani, A.

Assortment of past, recent and future petrophysical data from BULGG
Schaber, T., Osten J., Ceccato, A., Jalali M., Amann, F.

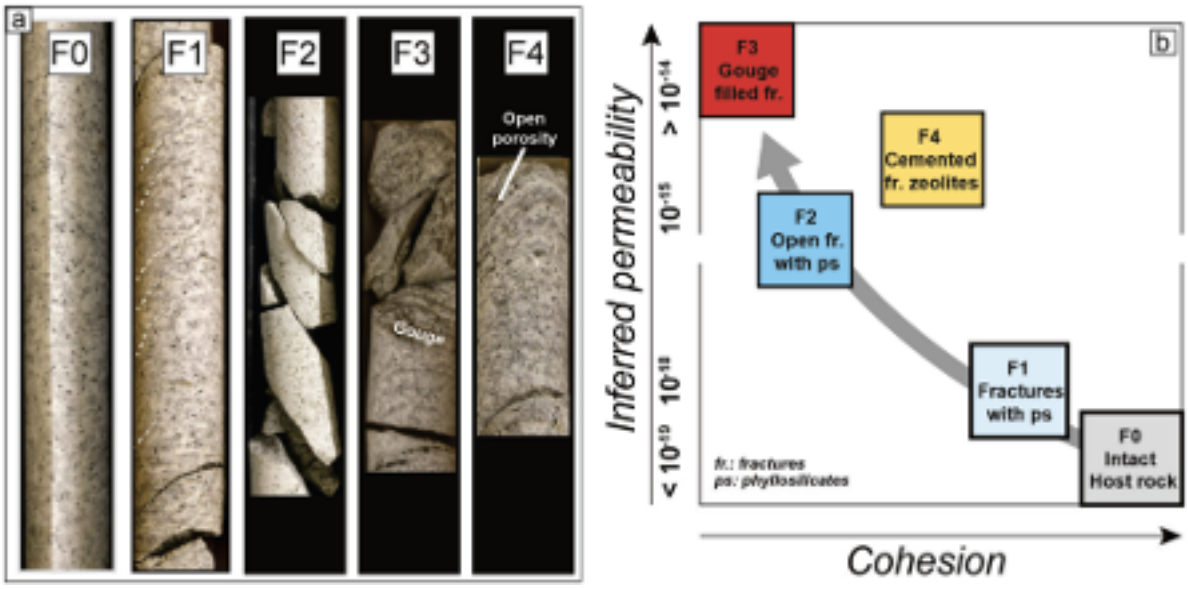

Figure 11: MC fault facies: a) in the borehole logs; b) as a function of inferred permeability (from the work of Osten et al.) and cohesion control.

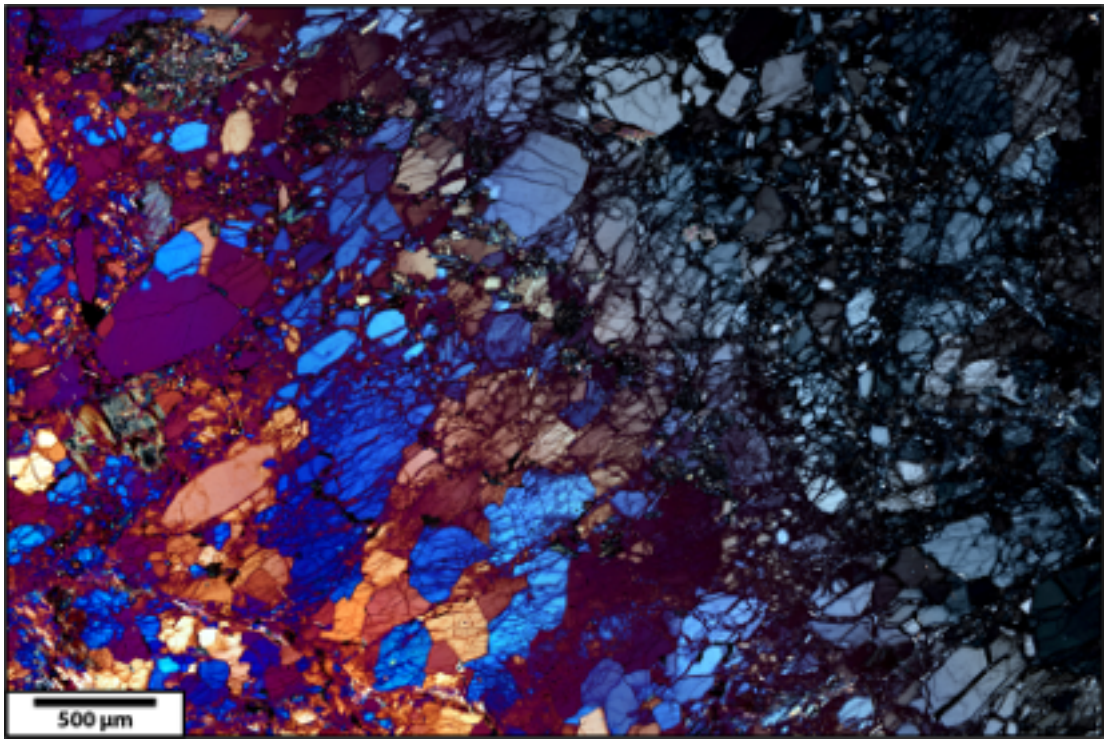

Figure 12: Breccia fragments within the damage zone of the Waterfault showing pervasive fragmentation by shattering (< mm in size) without displacement of the fragments. Right half, crossed polars view in optical microscope of a thin section, left half, interference colors enhanced with the gypsum lamina to better evidence the lack of displacement of fragments.

3D geological models of the Rotondo granite and fault zone geometries

Alberto Ceccato, Whitney M. Behr, Alba S. Zappone
aceccato@erdw.ethz.ch
Department of Earth Sciences, ETH Zurich, Sonneggstrasse 5 8092 Zurich

1. Research questions

What is the 3D geometry of deformation zones in the Rotondo granite?

2. Methods

Field surveys, remote sensing, structural analyses and 3D modelling with Leapfrog

3. Results

- A **3D geological model** of the geology of the Rotondo granite and its **deformation zones** using Leapfrog Geo
- **Mesoscale 3D fault zone geometry** and **fault zone classification**

Contribution to FEAR: these results provide an overview of the fault zone geometries to be expected in the experimental volume.

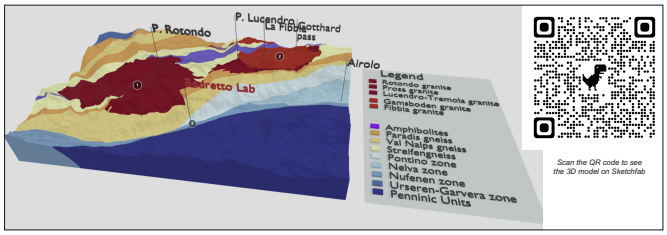

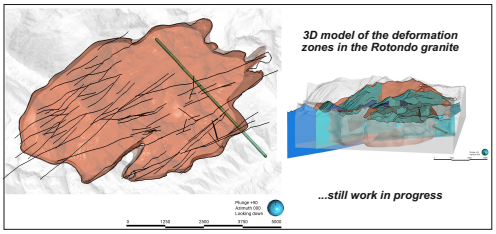

Regional scale 3D geological modelling

- 3D geological modelling based on existing geological maps (Geological Atlas of Switzerland, 1:25000; SwissTopo); and integrating the **results of field structural analyses** and **remote sensing** on the Rotondo granite.

3D models computed with leapfrog

... fundamental for the interpretation of local natural seismicity and hydrogeological characteristics at the regional scale.

Fault zone geometry and classification

Fault zones composed of shear fractures - MC-type fault zones

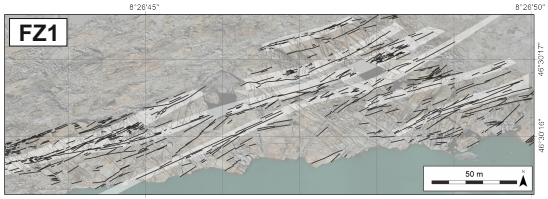

- Fault zone extends for over 200-300 m along strike
- Each shear fracture/fault plane is <30-50m in length
- Many shear fractures with overtepping; average spacing of stepovers <~1m?
- Possible reactivation of the entire fracture network

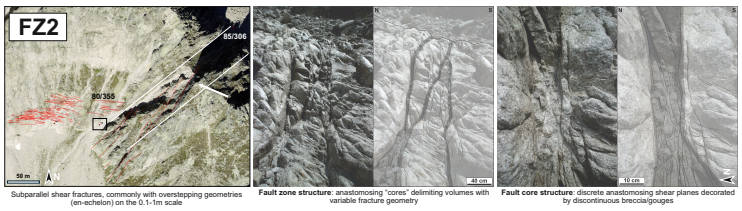

Subparallel shear fractures, commonly with overstepping geometries (en-echelon) on the 0.1-1m scale

Fault zone structure: anastomosing "cores" delimiting volumes with variable fracture geometry

Fault core structure: discrete anastomosing shear planes decorated by discontinuous breccia/gouges

Intermediate fault zone geometry

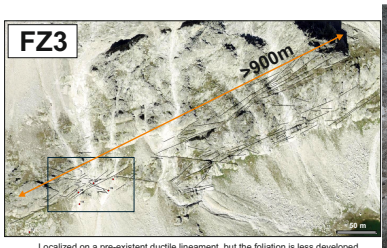

Localized on a pre-existent ductile lineament, but the foliation is less developed

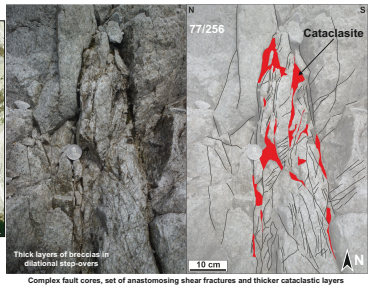

Complex fault cores, set of anastomosing shear fractures and thicker cataclastic layers

Fault zone localized on thick (>>1 m) mylonitic shear zone

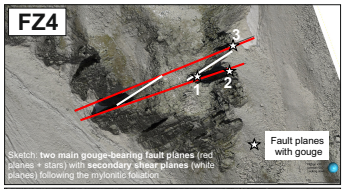

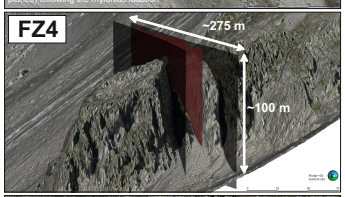

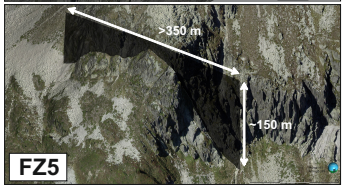



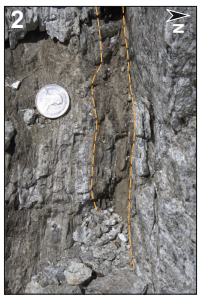

Main gouge-bearing planes: continuous over 200-300 m along strike, 100 m vertical extension exposed)

Secondary planes follow the mylonitic foliation
- 60-100 m along strike
- vertical extension not well constrained

Summary of fault outcrops and geometry types

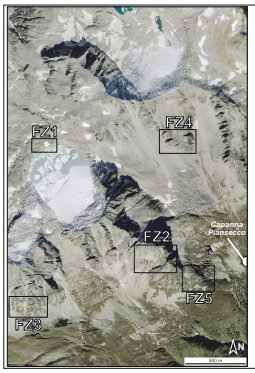

FZ1 FZ2 — **Fault zones composed of shear fractures - MC-type fault zones**

FZ3 — **Intermediate fault zone geometry**

FZ4 FZ5 — **Fault zone localized on thick (>>1 m) mylonitic shear zone**

Small — Scale — Large

Type 1 (FZ1-2): MC-type fault zones exploiting pre-existent fractures, mainly composed by shear fractures
- dominated by bare-rock contacts, thin breccia/cataclasite layers <5cm, irregularly distributed in the fracture network
- no significant differences between fault core and damage zone
- Roughness dependent on micro-scale asperities on shear plane + large-scale overstepping between shear fractures (~0.1-1m)

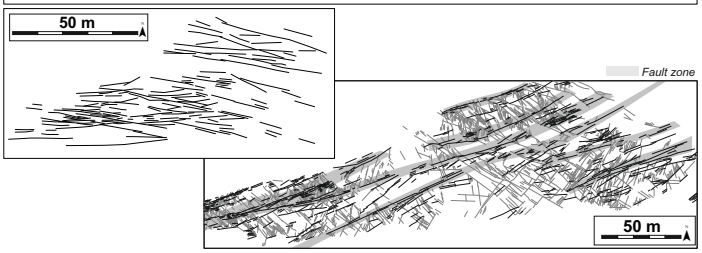

Intermediate (FZ3): Increasing strain, exploiting pre-existent fractures and major lineaments
- occurrence of larger patches of cataclasites/gouges, with a discontinuous distribution along principal slip surfaces and secondary planes
- fault core composed of a 10-20 cm thick zone of high fracture density.

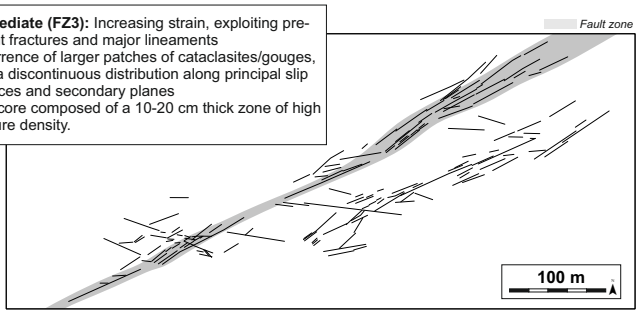

Type 2 (FZ4-5): large scale faults localized on pre-existent large-scale lineaments (ductile shear zones), localized at lithological contacts (e.g., mylonitic shear zones against undeformed granite)

- continuous over hundreds of m
- planes decorated by continuous(?) gouge layer, as thick as 5-10 cm
- Gouge/cataclasites dominating over bare-rock contacts
- Roughness dependent on shear plane asperities
- No overstepping between shear planes

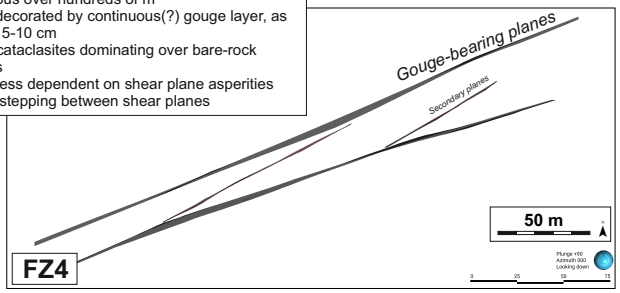

Characterization and 3D geometrical modelling of a complex fault zone for earthquake rupture experiments

Alberto Ceccato[1] (aceccato@erdw.ethz.ch), Peter Achtziger-Zupančič[2,3], Giacomo Pozzi[4], Alexis Shakas[1], Alba Simona Zappone[1], Daniel Escallon[1], Marian Hetrich[1], Mohammadreza Jalali[2], Xiaodong Ma[1], Men-Andrin Meier[1], Julian Osten[2], Whitney M. Behr[2], Florian Amann[2], Massimo Cocco[4], Domenico Giardini[1], and Stefan Wiemer[1]

1 ETH Zurich, Geological Institute, Department of Earth Sciences, Zurich, Switzerland (aceccato@erdw.ethz.ch)
2 Department of Engineering Geology and Hydrogeology, RWTH Aachen University, Germany
3 Fraunhofer Research Institution for Energy Infrastructures and Geothermal Systems IEG, Aachen, Germany
4 Istituto Nazionale di Geofisica e Vulcanologia, Italy

1. Introduction and motivations

Fault zone geological and geometrical complexities are prime parameters playing a fundamental role in controlling the characteristics of both natural and induced seismicity. In the Bedretto tunnel (Switzerland), the Fault activation and Earthquake Rupture (FEAR) project aims at triggering a M_w = 1 seismic event through fluid injection and stimulation of a natural fault zone situated in a large scale (> 10^7 m^3) fractured granite reservoir. The limited exposure of the fault zone in the tunnel, however, restricts the possibility to constrain in detail the geometrical and geological characteristics of the experimental target. Therefore, in order to constrain the geological and geometrical characteristics of the target fault zone, we have integrated structural analyses, borehole and core logging, and borehole ground penetrating radar (GPR).

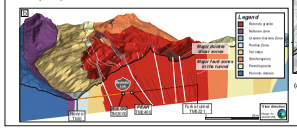

2. Geological setting of the Bedretto Lab

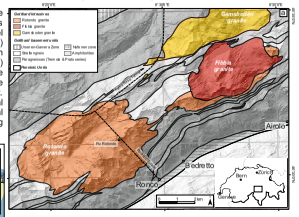

(a) Schematic geological map showing the location of the Bedretto Tunnel in the Rotondo granite. (b) 3D Geologic cross-section along the Bedretto Tunnel highlighting the main geological features of the Rotondo granite. Modified from Ceccato et al. (2024)

3. Required fault properties for the FEAR project experiments

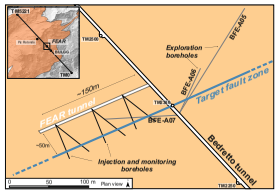

Schematic plan view on the experimental setup of the FEAR project, highlighting the Bedretto tunnel, the planned fault-parallel access tunnel (FEAR tunnel), the steeply dipping target fault zone (blue), and the planned boreholes hosting the monitoring instrumentation and the injection system.

Experimental requirements: The primary objective of FEAR is to induce seismic activity (with maximum approximate magnitude Mw = 1.0) through hydraulic stimulation within a natural fault zone, equipped with a multidisciplinary monitoring network with unprecedented spatial resolution and proximity to the source zone.

(1) Geometrical and spatial requirements. Planar, single structure that is continuous over 30 to 50 meters capable of hosting a Mw = 1.0, favorably oriented with respect to the in-situ stress field, with a high slip tendency and critically stressed.

(2) Monitoring requirements. A fault of limited persistence and thickness is necessary to minimize the extension of the monitoring network and the necessary equipment to provide high resolution data within a (limited) volume around the fault zone.

(3) Hydraulic requirements. The fault permeability should be high enough to ensure the pressurization of a large volume to induce seismic slip but needs to be limited to prevent rapid pressure dissipation and effective pump control (injection flow rate and pressure).

(4) Geological requirements. Geological characteristics of the faults suggesting past seismic activity in geological or recent times, as well as geological characteristics favouring the nucleation and propagation of seismic rupture during fault (re-)activation (e.g., gouges and velocity-weakening fault rocks), are preferred for the fault zone.

4. A Multidisciplinary Approach to Fault Selection and Characterization

- Geological characterization at the field and tunnel scale, in order to illuminate the geological characteristics of the faults in the Rotondo granite, their geometrical properties and spatial extents;
- Borehole drilling, logging and core analyses;
- Geophysical investigations with Ground Penetrating Radar;
- Laboratory- and sample characterization;
- Hydro-mechanical characterization.

in three stages

1. Structural inventory
2. Fault Zone Selection
3. **Fault zone characterization**

In the following, we describe the results of the **Fault zone characterization**, resulting from:

- **(5.1-5.3)** detailed geological and structural characterization in the tunnel and comparison with surface geology
- laboratory characterization of the mineralogy and microstructure of fault rocks, including experimental deformation to constrain the frictional, mechanical, and permeability properties of the fault rocks in the selected fault zone (Volpe et al., 2023; Osten et al., 2024);
- **(5.4)** drilling of exploration boreholes at an angle to the selected fault zone to constrain the actual lateral extent and continuity; logging of cores retrieved from boreholes; borehole logging adopting Acoustic and Optical Televiewer;
- **(5.5)** Single borehole GPR logging.

Preliminary field investigations in the tunnel allowed to identify the complex fault structure characteristics, fault rock properties, and slip tendency in the current stress field of the selected fault zone. These results were compared to the structural observations obtained from field surveys and remote sensing, constraining the slip history, and lateral extent of the set of natural fault zones occurring on the surface above the Bedretto tunnel. Indeed, the lateral extent of the selected fault has been confirmed through the logging (optical/acoustic televiewer, fracture intensity, fracture typology) of exploration boreholes and the analyses of the related cores. The comparison between the geological characteristics of fault zones in the cores and the characteristics of the selected fault zone exposed in the tunnel allowed to confirm the occurrence of the same typology of fault zone further away from the exposure in the tunnel. In addition, GPR logging of the exploratory boreholes provided fundamental insights on the lateral continuity of the identified fault zones on the tunnel wall, as well as those identified in the borehole/core logging.

5. Multiscale Characterization of Fault Zones in the Rotondo Granite and the Resulting Target Fault Zone

5.1 Structural inventory above the Bedretto Tunnel

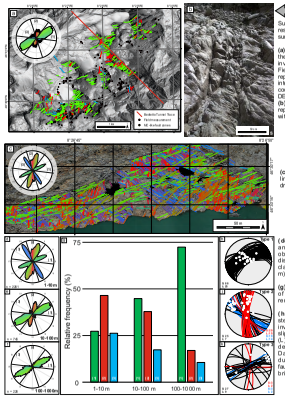

Summary figure presenting the preliminary results of the remote sensing data and field survey in the Rotondo granite area.

(a) DTM of the Rotondo granite area showing the trace of the Bedretto Tunnel relative to the investigated points on the surface (red dots). Field occurrences of MC-like fault zones are represented by yellow dots. The lineaments interpreted from remote sensing are color coded according to their strike (Hillshaded DEM from SwissALTI3D).
(b) Field example of MC-like fault zones, represented by a narrow fracture corridor with multiple principal slip planes.

(c) Interpreted outcrop map with the traced lineament. Ortho-images obtained from drone surveys.

(d-f) Rose diagrams obtained from the analyses of the lineament length data obtained from remote sensing, showing the distribution of lineament strike for each length class (c: 1-10 m; d: 11-100 m; e: 101-1000 m).

(g) Histogram showing the relative frequency of the lineament sets (1-3) identified by remote sensing at the mesoscale/outcrop scale.

(h-k) Equal area, lower-hemisphere stereographic projections of the structural inventory from field analyses. Great circles: slip planes (S). Dots and contour lineations (L). Blue and red planes and dots represent dextral and sinistral kinematics, respectively. Data from Ceccato et al. (2024). (h) Type 1 ductile shear zones. (j) Type 2 brittle-ductile faults. (k) Type 3 Zeolite- and gouge-bearing brittle fault zones.

5.2 Faults sand shear zones in the Bedretto Tunnel

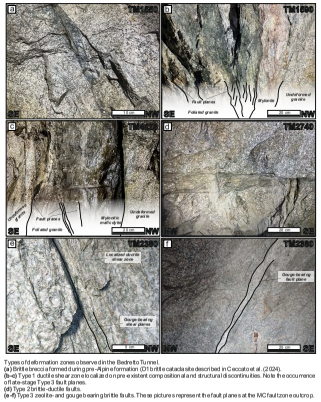

Types of deformation zones observed in the Bedretto Tunnel.
(a) Brittle lineaments formed during pre-Alpine intrusion (D1) brittle cataclasite described in Ceccato et al. (2024).
(b-e) Type 1 ductile shear zone localized on pre-existent compositional and structural discontinuities. Note the occurrence of late-stage Type 2 fault planes.
(d) Type 2 brittle-ductile faults.
(e-f) Type 3 zeolite- and gouge-bearing brittle faults. These pictures represent the fault planes at the MC fault zone exutorio.

5.3 Target fault zone in the tunnel

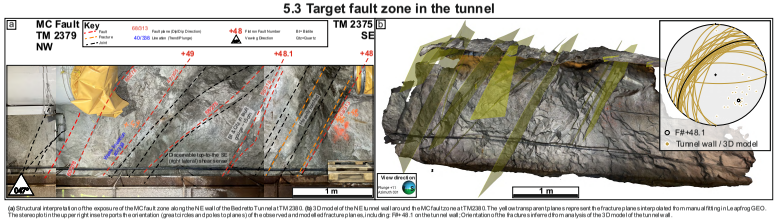

(a) Structural interpretation of the exposure of the MC fault zone along the NE wall of the Bedretto Tunnel at TM2380. (b) 3D model of the NE tunnel wall around the MC fault zone at TM2380. The yellow transparent planes represent the fracture planes interpolated from manual fitting in Leapfrog GEO. The stereoplot in the upper right inset reports the orientation (great circles and poles to planes) of the observed and modelled fracture planes, including F#=48.1 on the tunnel wall. One relation of the fractures inferred from analysis of the 3D model of the tunnel wall.

5.4 Borehole Logs, Cores and Facies Description

In order to identify the occurrence of the MC fault zone at depth along the boreholes, rock cores from BFE_A05, _A06, _A07 were analyzed and classified in different Core Facies, representing segments of the cores with similar geological characteristics. Comparing the Core Facies to the characteristics of the MC fault along the tunnel wall, and defining the position of the different Core Facies along the boreholes we constrained the overall geometry and occurrence of the MC fault at depth.

Facies definition
F0: Intact rock with rare (<< 5/m) thin cohesive fractures filled with phyllosilicates
F1: Dense set of oriented cohesive fractures filled with phyllosilicates, exploiting mylonitic fabric
F2: Same as F1 but fractures are not cohesive, host with enhanced matrix porosity
F3: Severely damaged rocks with oriented fractures and presence of fine gouge
F4: Cataclasite cemented by zeolites with high matrix porosity

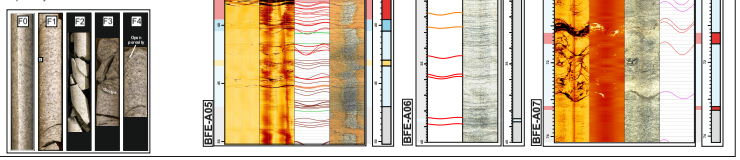

5.5 Single-Hole GPR-Imaging

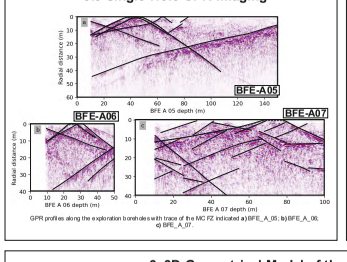

GPR profiles along the exploration boreholes with trace of the MC PZ indicated a) BFE_A_05; b) BFE_A_06; c) BFE_A_07.

6.1 Validation of 3D model against synthetic GPR profiles

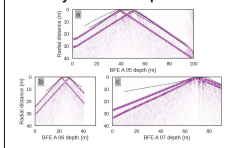

GPR forward model using the methodology from Shakas and Linde (2015) and the 3D geometry for the MC fault zone, both planes 48 and 49. The simulation aimed to reproduce the results observed in borehole BFE_A_05. The (dashed) line superimposed on the image is the trace of the MC FZ picked from field observations.

6. 3D Geometrical Model of the MC Fault Zone

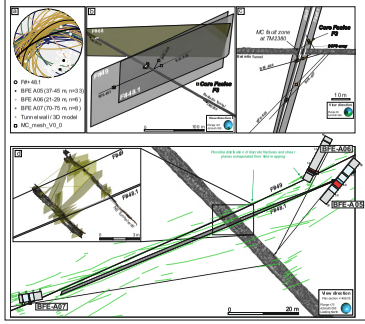

All geological and geometrical information have been integrated into a preliminary 3D geometrical model (in Leapfrog Geo), representing the overall geometry of the selected fault zone. This preliminary geometrical model has been validated against synthetic GPR profiles, computed through GPR forward modelling along the exploration boreholes.

3D Geometrical model of the MC fault zone from tunnel observation, core facies distribution, and borehole logging.
(a) The stereoplot in the upper right inset reports the orientation (great circles and poles to planes) of the observed and modelled fracture planes, including F#=48.1 on the tunnel wall; orientation of the fractures in BFE boreholes as inferred from OTV/ATV logging. Orientation of the fractures inferred from analysis of the 3D model of the tunnel wall; orientation of the two main meshes (MC_mesh_V0_0) defined through interpolation of tunnel, core and borehole data.
(b) Overview of the 3D model of the MC fault zone, composed of two main surfaces (meshes F#=49 and F#=48.1 bounding a zone of high fracture intensity.
(c) Side view of the 3D model showing the distribution of the borehole arrays and the location of the F3 facies in each borehole.
(d) Plan view of the MC fault zone showing the two main surfaces interpolated from core facies distribution. The light green traces represent the likely heterogeneous distribution of discrete fractures and shear planes as inferred from field mapping of structures similar to the MC fault. The inset shows the fractures interpreted from LiDAR scanning and structural analysis of the tunnel wall. Note the slight difference in orientation between the tunnel wall fractures and the interpolated surfaces.

7. Conclusions

The integrated results define the selected fault zone as a 3-7 m wide zone of higher density (up to 5/m), of variably oriented secondary fractures, and bounded by two main slip surfaces.
The slip surfaces are irregularly decorated by phyllosilicate-rich gouge patches, filling the roughness of the fault surface. The lateral extension of each discrete fracture does not exceed 30 m in length, but the overall lateral continuity of the fault zone exceeds several hundreds of meters.
The presented integrated characterization approach allowed us to constrain a geologically-sound, first-order 3D geometrical model of a complex natural fault zone, validated against geophysical forward modelling. These preliminary results have fundamental implications for the expected experimental planning and outcomes, modelling and injection strategies, project logistics, as well as the design and deployment of the monitoring network around the stimulated fault zone.

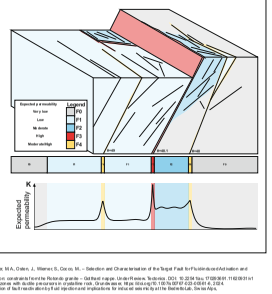

References
Achtziger-Zupančič, P., Ceccato, A., Zappone, A. S., Pozzi, G., Shakas, A., Amann, Behr, W. M., Escallon, D., Giardini, D., Hetrich, M., Jalali M., Ma, X., Meier, M-A., Osten, J., Wiemer, S., Cocco, M. – Selection and Characterization of the Target Fault for Fluid-induced Activation and Earthquake Rupture Experiments in the Rotondo Granite, Switzerland. Solid Earth. https://doi.org/10.5194/egusphere-egu23-15966, 2023
Ceccato, A., Pozzi, G., Antonioli, A., Basagni, A., Kotronakis, M., Tartaglia, G., Viganò, A., Di Toro, G. – Multi-scale characterization of the exhumed Nubian-Pan African seismogenic crust: fault rocks and earthquake scaling parameters of the Bellagio Fault Zone (Southern Alps, Italy). Solid Earth, 12, 1995–2032. https://doi.org/10.5194/se-12-1995-2021, 2021
Ceccato, A., Antonioli, A., Kotronakis, M., Tartaglia, G., Viganò, A., Di Toro, G. – Structural and petrophysical characterization of an exhumed paleo-earthquake hypocentral section. Tectonophysics, 817, 229047. https://doi.org/10.1016/j.tecto.2021.229047, 2021
Ceccato, A., Simpson, G., Viganò, A., Di Toro, G. – Pervasive folding and fracturing of foliated cataclasites in the frictional regime of the seismogenic crust. Journal of Structural Geology, 125, 90–110. https://doi.org/10.1016/j.jsg.2018.08.007, 2019
Ceccato, A., Pennacchioni, G., Menegon, L., Tarantola, A. – Influence of chlorite and dynamic recrystallization on the strength of experimentally deformed granite at the brittle-plastic transition. Journal of Structural Geology, 125, 231–248. https://doi.org/10.1016/j.jsg.2018.08.007, 2019
Ceccato, A., Viganò, A., Di Toro, G. – Mechanisms of strain localization in pseudotachylyte-bearing faults exhumed from the seismogenic crust. Tectonophysics, 733, 201–226. https://doi.org/10.1016/j.tecto.2017.11.038, 2018

The candidate fault for fluid-induced earthquake rupture experiments in the Rotondo granite.

FEAR Fault Activation and Earthquake Rupture

Giacomo Pozzi, Peter Achtziger-Zupančič, Luca Aldega, Alberto Ceccato, Cristiano Collettini, Daniel Escallon, Marian Hertrich, Xiaodong Ma, Men-Andrin Meier, Julian Osten, Alexis Shakas, Elena Spagnuolo, Giuseppe Volpe, Alba Zappone, Florian Amann, Massimo Cocco, Domenico Giardini, Stefan Wiemer

HPHT LAB

Field mapping

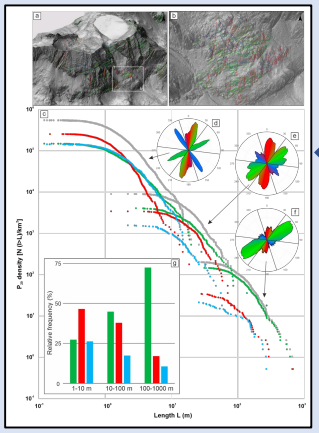

NE-SW faults (including the MC)
Have high lateral persistency

BULGG

The main aim of the ERC Synergy project "Fault Activation and Earthquake Rupture" (FEAR) is instrumenting and stimulating a fault to study seismic slip in a natural, but controlled environment.
Experiments will be performed in the Bedretto Underground Laboratory for Geosciences and Geoenergies (BULGG), an experimental facility located at 1 km of depth in the Swiss Alps.
To select a candidate fault we integrated structural geology field work, near- and far-field remote sensing, geophysical investigations, borehole logging, mineralogical and petrological analysis, and experimental rock deformation.

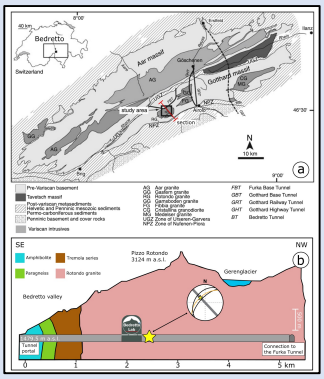

GPR in tunnel, borehole log and fault model

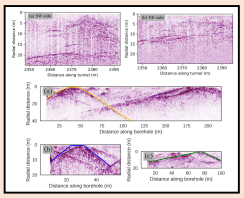

3D MC model

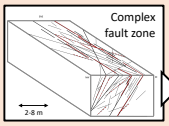

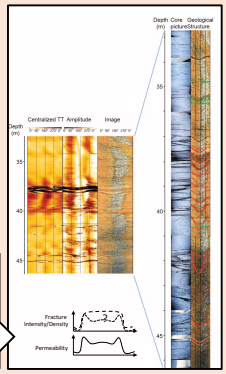

Initial selection criteria

a) Brittle shear zone
b) Presence of gouge
c) Small water inflow

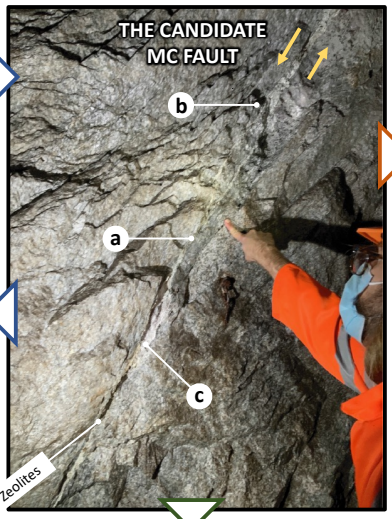

Fault zone facies and in-situ permeability

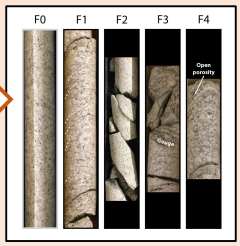

F0 Intact rock with rare (<< 5/m) thin cohesive fractures filled with phyllosilicates
F1 Dense set of oriented cohesive fractures filled with phyllosilicates, exploiting mylonitic fabric
F2 Same as F1 but fractures are not cohesive, host with enhanced matrix porosity
F3 Severely damaged rocks with oriented fractures and presence of fine gouge
F4 Cataclasite cemented by zeolites with high matrix porosity

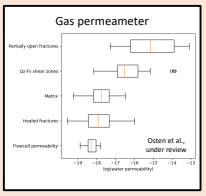

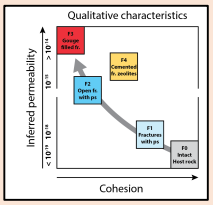

Microstructures

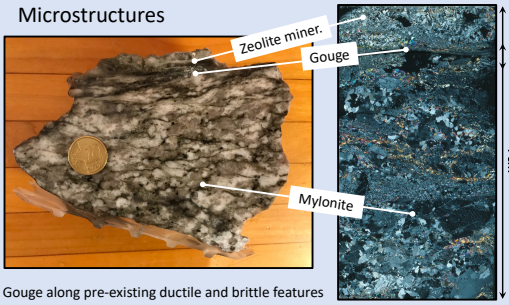

Gouge along pre-existing ductile and brittle features

Gouge composition (XRPD)

GRANULAR MATERIALS						PHYLLOSILICATES		
Quartz	Albite	K-Feldspar	Stilbite	Laumontite	Cabasite	Muscovite	Clinochlore	Biotite
46%	19%	12%	0.60%	0.40%	x	22%		x

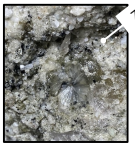

A similar fault: the Waterfault

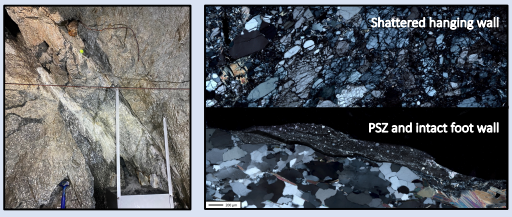

"Sister" fault bears evidences of seismic reactivation

Experimental results: frictional properties and simulation of fluid injection

Friction

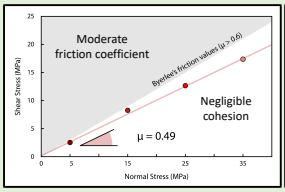

Rate and state

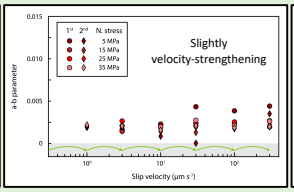

Frictional healing

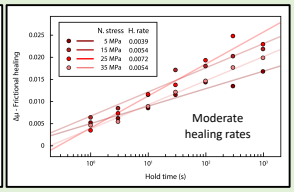

Experimental fabric

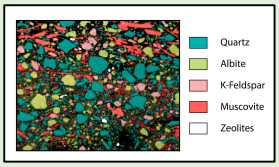

Cataclasis is the main deformation mechanism, but part of the deformation is accommodated by frictional sliding along the phyllosilicates folia reducing hard interaction within granular fraction.

Injection and reactivation

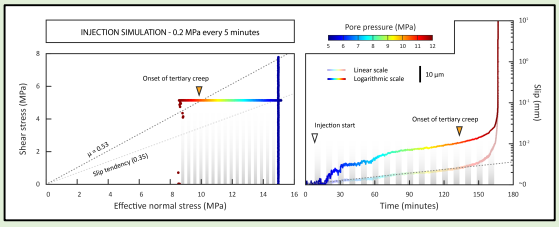

Fluid pressurization induced weakening overcomes the slightly rate strengthening behaviour of the gouge, promoting a laboratory earthquake during injection.

Relevant articles

Xiaodong et al. 2022

Volpe et al. 2023

Details of laboratory injection experiment

Confining pressure (~lithostatic)	= 15 MPa
Hydrostatic pore pressure	= 5 MPa
Effective normal stress	= 20 (15) MPa
Slip tendency	= 0.35
On-fault shear stress	= 5.25 MPa
Pore pressure at reactivation	≈ 12 MPa
Permeability (before injection)	≈ $9.32 \cdot 10^{-17}$ m²
Permeability (after injection)	≈ $2.90 \cdot 10^{-17}$ m²

Tectonic and structural evolution of the Rotondo granite

Alberto Ceccato, Whitney M. Behr, Alba S. Zappone, Lorenzo Tavazzani, Andrea Giuliani

aceccato@erdw.ethz.ch
Department of Earth Sciences, ETH Zurich, Sonneggstrasse 5 8092 Zurich

1. Research questions

- What are the deformation features characterizing the **structural evolution** of the Rotondo granite?
- What is it its **tectonic evolution**?
- How **strong** was the Rotondo granite during the orogenic collision?
- What is the r**heological evolution** of the Rotondo grnaite through the Alpine orogenesis?

Contribution to FEAR:
- Geological characterization of the structural features occurring in the experimental volume.

2. Methods

- Structural map and field investigation sites
- Analysis of Pressure and Temperature conditions of deformation (Perple_X)
- Geochronology of deformation structures (U-Pb and Rb/Sr geochronology)

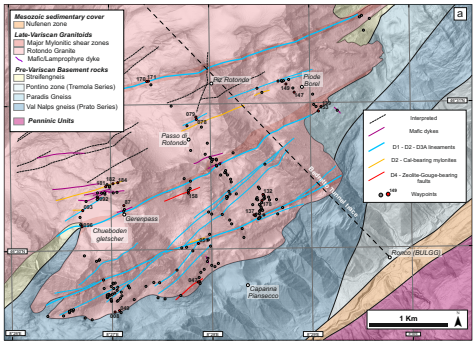

3. Results

Structural Evolution and deformation sequence

- **D_1**: brittle shear fractures, cataclasites and breccias, containing a fine-grained matrix of quartz + biotite; steeply-NW-dipping, sub-vertical lineation? no clear kinematics;
  - e.g., FA fault.
- **D_2**: ductile, mylonitic shear zones; very well foliated and fine-grained, mylonitic foliation defined by biotite + muscovite; steeply-NW-dipping, developed exploiting D1 structures; reverse, top-to-SE kinematics;
  - e.g., main DG fault-mylonite.
- **D_{3A}**: ductile shear zones with strike-slip (dextral) kinematics, reactivating D2 shear zones; mylonitic foliation defined by biotite + muscovite + chlorite;
- **D_{3B}**: brittle-ductile faults, defining a conjugate of strike-slip faults with oblique lineation; usually associated with quartz + chlorite veins (nice little crystals!!)
- **D_{3C}**: discrete, brittle-ductile faults with normal kinematics, NW-SE-trending;
- **D_4**: zeolite- and gouge-bearing faults, exploiting pre-existent foliations and fault planes; sub-horizontal lineation with strike-slip kinematics.
  - e.g., MC fault zone.

4. Discussion & Conclusions

- **Structural evolution**: 4 main phases of deformation: D1 to D4, related to the evolution of Alpine tectonics. Garnet U-Pb, mica Rb-Sr dating constrain exhumation of Rotondo granite from amphibolite facies at 34-20 Ma to greenschist facies at 15-14 Ma
- **Tectonic evolution**: Fast exhumation (~3 mm/yr) accommodated by weak ductile shear zones localized on pre-collisional brittle deformation structures - followed by strike-slip tectonics at the regional scale and decreased exhumation rates.
- **Rheological evolution**: The European crust was extremely weak during collision, rheology was controlled by metamorphic and fluid evolution in localized shear zones. The occurrence of inherited tectonic and primary (e.g., magmatic) fabrics and structures, although highly misoriented, clearly controlled strain geometry and localization throughout their entire rheological and metamorphic evolution.

3. Structural evolution - Deformation sequence

D_1 *Quartz-biotite shear fractures, breccias and cataclasites* ⇨ *Most pervasive feature in the tunnel!!!*

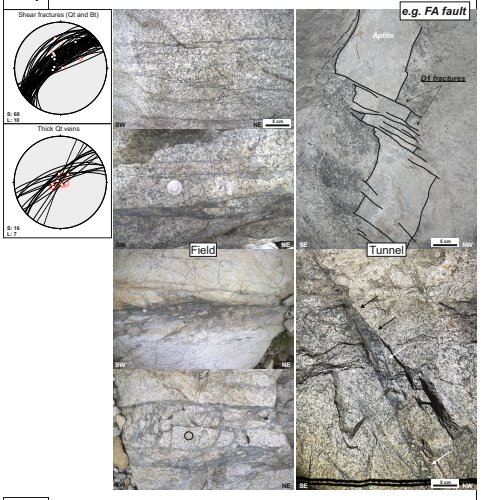

D_2 *Ductile shear zones - Dip-slip, reverse kinematics* ⇨ *Mylonites with dip-slip lineation*

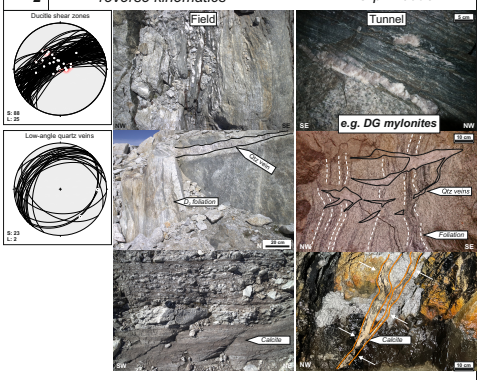

D_{3A} *(Brittle-)Ductile shear zones - Strike-slip kinematics* ⇨ *Mylonites with horizontal lineation*

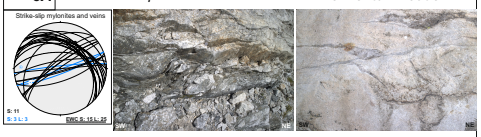

D_{3B} *Brittle-ductile faults: strike-slip and normal kinematics* ⇨ *"Tunnel-parallel" fracture system*



D_{3C}

D_4

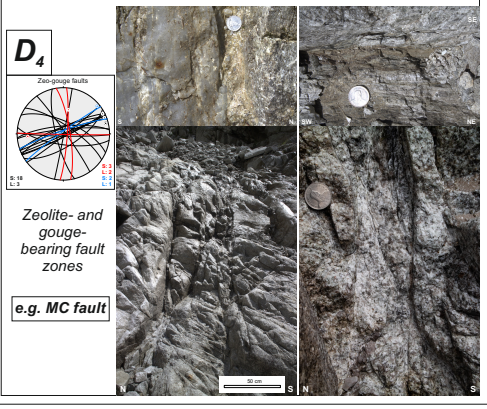

Zeolite- and gouge-bearing fault zones

e.g. MC fault

4. Discussion & Conclusions

P-T conditions of deformation & exhumation/cooling rates

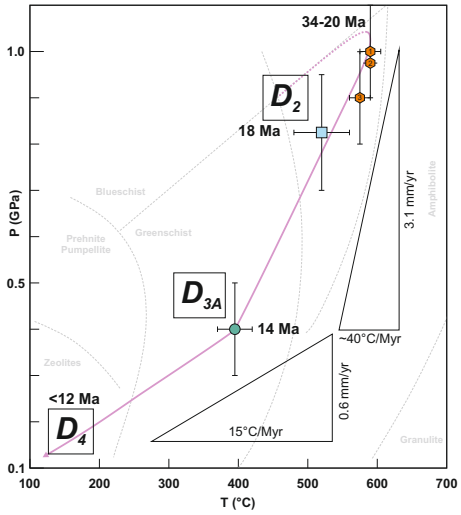

Tectonic evolution during Alpine collision

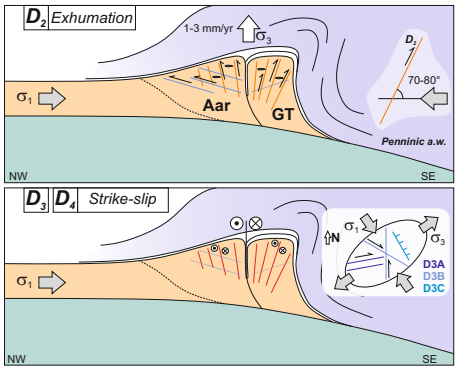

Rheological evolution during Alpine collision

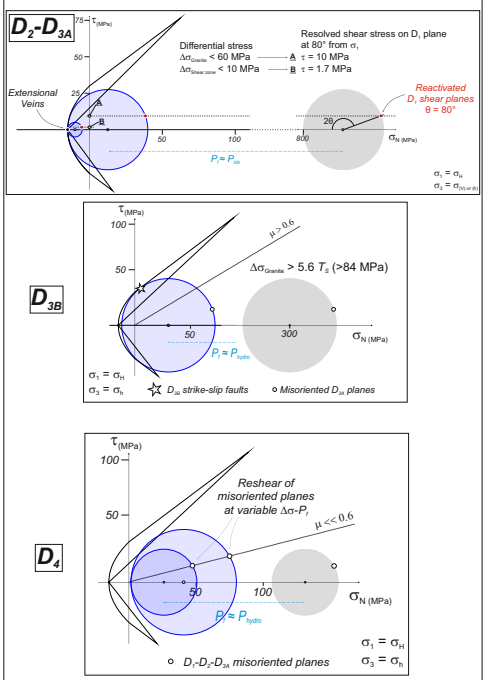

Acknowledgement: AC wish to thank the CAS-SAC crew of the Capanna Piansecco for their warm hospitality and support during fieldwork. The FEAR project has received funding from the European Research Council (ERC) under the European Union's Horizon 2020 research and innovation programme (grant number 856559).

Assortment of past, recent and future petrophysical data from BULGG

Tom Schaber[1], Julian Osten[1], Alberto Ceccato[2], Mohammadreza Jalali[1], Florian Amann[1,3]

[1]*Department of Engineering Geology & Hydrogeology , RWTH Aachen, Aachen, Germany*
[2]*Department of Earth Sciences , ETH Zürich, Zürich, Switzerland*
[3]*Fraunhofer Research Institution for Energy Infrastructures and Geothermal Systems IEG, Kockerellstraße 17, 52062 Aachen, Germany*

Overview

- Petrophysical lab measurements act as complementary data to in-situ measured field data
- Current and future work focus on the characterization of the MC fault zone, as it was selected as candidate fault zone for reactivation experiments
- Obtaining parameters as permeability, porosity and p-wave velocity amongst others allow for a detailed hydraulic and partly structural characterization of the investigated rock volume
- Foreseing the shear zone/fault stimulation and reactivation experiments in the FEAR project, insights about hydraulic behaviour is key for the determination of the right injection location, as well as choosing appropriate pressures and volumes

Past work

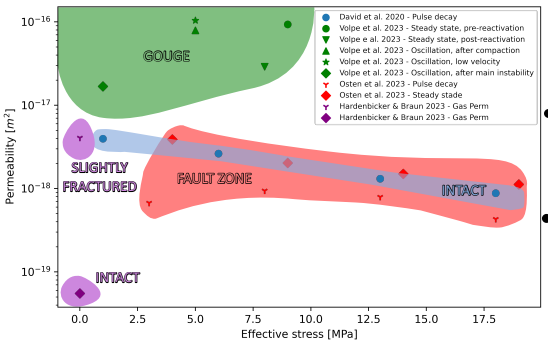

- Past petrophysical work focused on specific aspects, either: intact granite, gouge, EDZ, or entire fault zone characterization
- Fundamental insights were the fracture dominated fluid transport and low matrix permeability and porosity
- Especially permeability is altering depending on structural geological aspects that were not necessary considered in all of the work

Current state

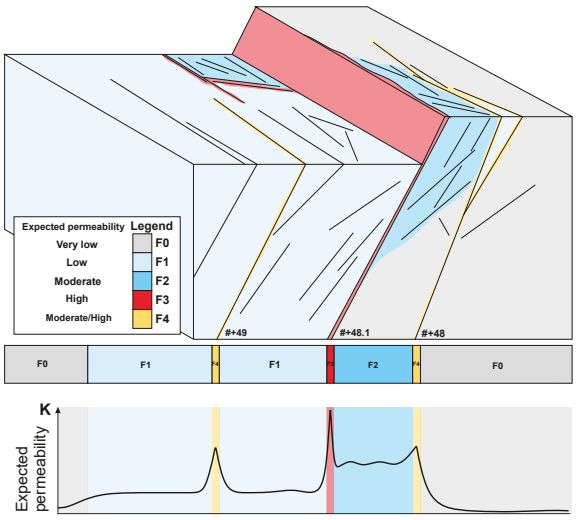

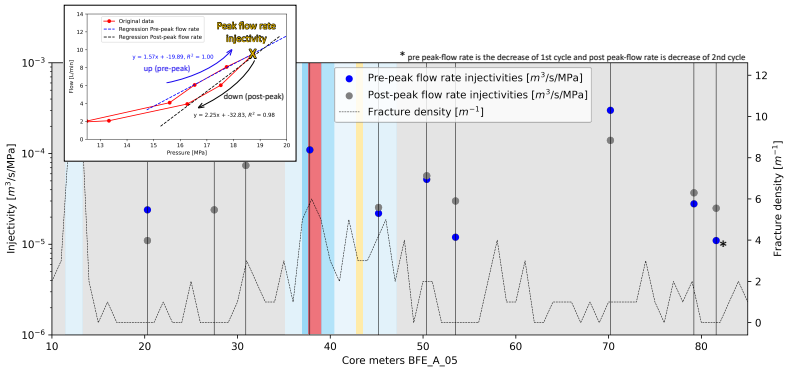

- MC shear zone experienced two deformation events that also affected its hydraulic behaviour
- The first event led to the development of a zone of higher fracture intensity. Fractures are now sealed and closed. The second event was also the last brittle event which created the fault core (gouge) and partially reactivated/re-opened the pre-existing fractures
- Due to erratic testing protocols and often non isolated single fractures in BFE_A_05 it was not possible to derive coherent values for hydraulic conductivity of several tested intervals using pulse tests ("pressurized slug test"). P vs Q plots, and thereby injectivity allowed for a much better inference of the hydraulics along the borehole which is disecting MC fault zone

Future work

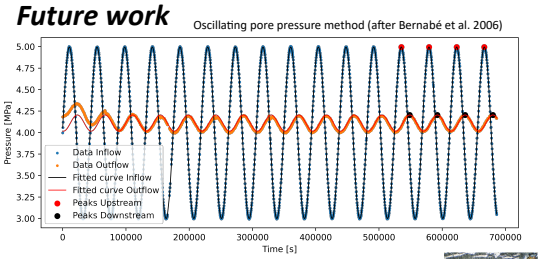

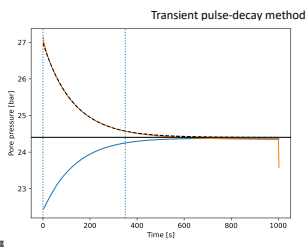

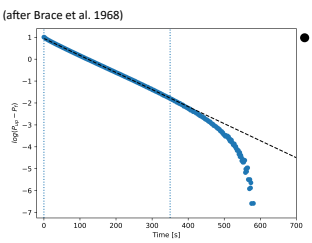

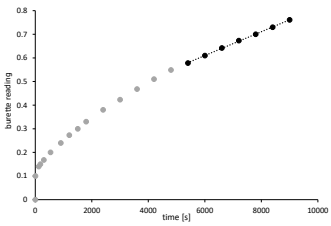

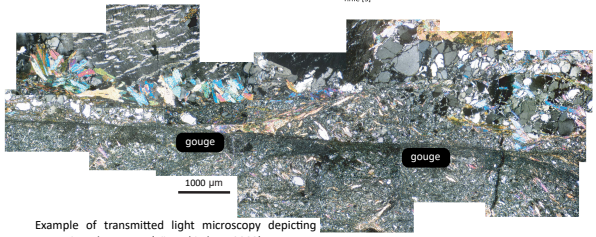

Example of transmitted light microscopy depicting gouge in a shear zone (Lützenkirchen, 2002)

- Besides permeability, other potentially useful parameters and methods include: SEM, gamma density, (un)-connected porosity, (un)-saturated p-wave velocity, transmitted light microscopy
- Different permeability measurement techniques allow the targeting of a sample's varying structural aspects (matrix, discontinuity)
- Understanding the hydraulics of the different facies, as well as from diverse fracture types is key
- Rating the impact of anisotropy with regard to foliation (even if only minor)
- Getting a complete hydraulic characterization of the MC fault zone which allows to infer a reasonably structured injection campaign

References:
- Braun, J.: PRECODE project: Hydro-mechanical characterization of the candidate location for grout injections at Bedretto Laboratory,Switzerland. RWTH Aachen University, Aachen (2023), Master's thesis
- David, C., Nejati, M., Geremia, D., (2020) On petrophysical and geomechanical properties of Bedretto Granite, ETH Zurich, https://doi.org/10.3929/ethz-b-000428267
- Hardenbicker, L.R.: PRECODE project: rock-mechanical characteriza-tion of the candidate location for grout injections at Bedretto laboratory, Switzerland. RWTH Aachen University, Aachen (2023), unpublished Master Thesis
- Lützenkirchen, V.H.: Structural geology and hydrogeology of brittle fault zones in the central and eastern Gotthard massif, Switzerland. ETH Zürich, Zürich (2002). Doctoral Thesis
- Osten, J., Schaber, T., Gaus, G., Hamdi, P., Amann, F., Achtziger-Zupančič, P., (2024) A multi-method investigation of the permeability structure of brittle fault zones with ductile precursors in crystalline rock, RWTH Aachen University, https://doi.org/10.1007/s00767-023-00561-6
- Volpe, G., Pozzi, G., Collettini, C., Spagnuolo, E., Achtziger-Zupančič, P., Zappone, A., Aldega, L., Meier, M.A., Giardini, D., Cocco, M., (2023) Laboratory simulation of fault reactivation by fluid injection and implications for induced seismicity at the BedrettoLab, Swiss Alps, Tectonophysics, https://doi.org/10.1016/j.tecto.2023.229987https://doi.org/10.1007/s00767-023-00561-6

FEAR Laboratory Working Group

The aims of the FEAR Laboratory Working Group in this past year:

- The prediction of the type of reactivation of the fault.
- The behavior of the fault hydraulically and mechanically under stimulation and its hydro-mechanical effects.
- The experimental schemes: sensor type, near and far field data availability, chain of processes...

Laboratory Working Group Highlights

The Laboratory Working Group is divided in the different partner universities: RWTH Aachen (WG1), INGV (WG2) and ETH (WG3). The highlights of this year are as follow:

- WG1: First, the reactivation of a fault in a true triaxial (TAURUS), was monitored with the mini-SIMFIP and a clear precursory sliding signal was observed with AE sensors (paper in prep). The current state of the experimentation is summarized in Figure 13. Second, the petrophysical characterization of the Rotondo Granite (Osten et al. 2024).
- WG2: First, the reactivation of the Rotondo granites was tested to gain understanding of the role of bare rock in the possible style of reactivation (Aretusini et al., in prep) and to compare it to the MC fault. Second, the derivation of the slip weakening constitutive laws in the earthquake rupture was calculated and prepared (Cornelio et al in prep). Third, a technical update on the MEERA (Spagnuolo et al. in prep) or the multipress designed for the study of rupture propagation was completed. (Figure 14) Fourth, a temperature modeling of the M-zero event (Aretusini, Cornelio, Gholizadeh et al. in prep.) due to the frictional heating has been calculated.
- WG3: First, the investigation of pre-Failure Strain Localization (Bianchi et al. 2024) with a combination of laboratory and numerical techniques. (Figure 15) Second, the aseismic strain localization prior to failure and associated seismicity in crystalline rock (Salazar et al, under review at Communications Earth & Environment). Third, the evolution of frictional properties on a frictional discontinuity due to wear (Michail et al, in preparation) as it is uncertain in real geologic settings, as found in the MC fault zone, how reactivation may change the frictional response of the interface. Fourth, the Effects of Fluid Preconditioning on the Deformation Response of a Laboratory Fault (Bianchi et al, in preparation). To reactivate faults, a so-called “fluid hammer” has been proposed to be effective in field tests (Moein et al. 2023) and the M-zero experiments. (figure 16) Finally, the understanding and data reduction of ultrasonic acoustic surveys in intact and fractured granite specimens (Wu, Paul Antony Selvadurai, et al. 2023; Wu, Paul A Selvadurai, et al. 2023). This activity studies the effects of fluid imbibition into dry (Wu, Paul Antony Selvadurai, et al. 2023) and fractured (Wu, Paul A Selvadurai, et al. 2023) granite samples in unconfined conditions.

Laboratory Working Group Next Steps

- Continue the in-depth characterization campaigns.
- Hypothesis testing and model transfer to the larger scale.
- Which data are in the near field / far field?

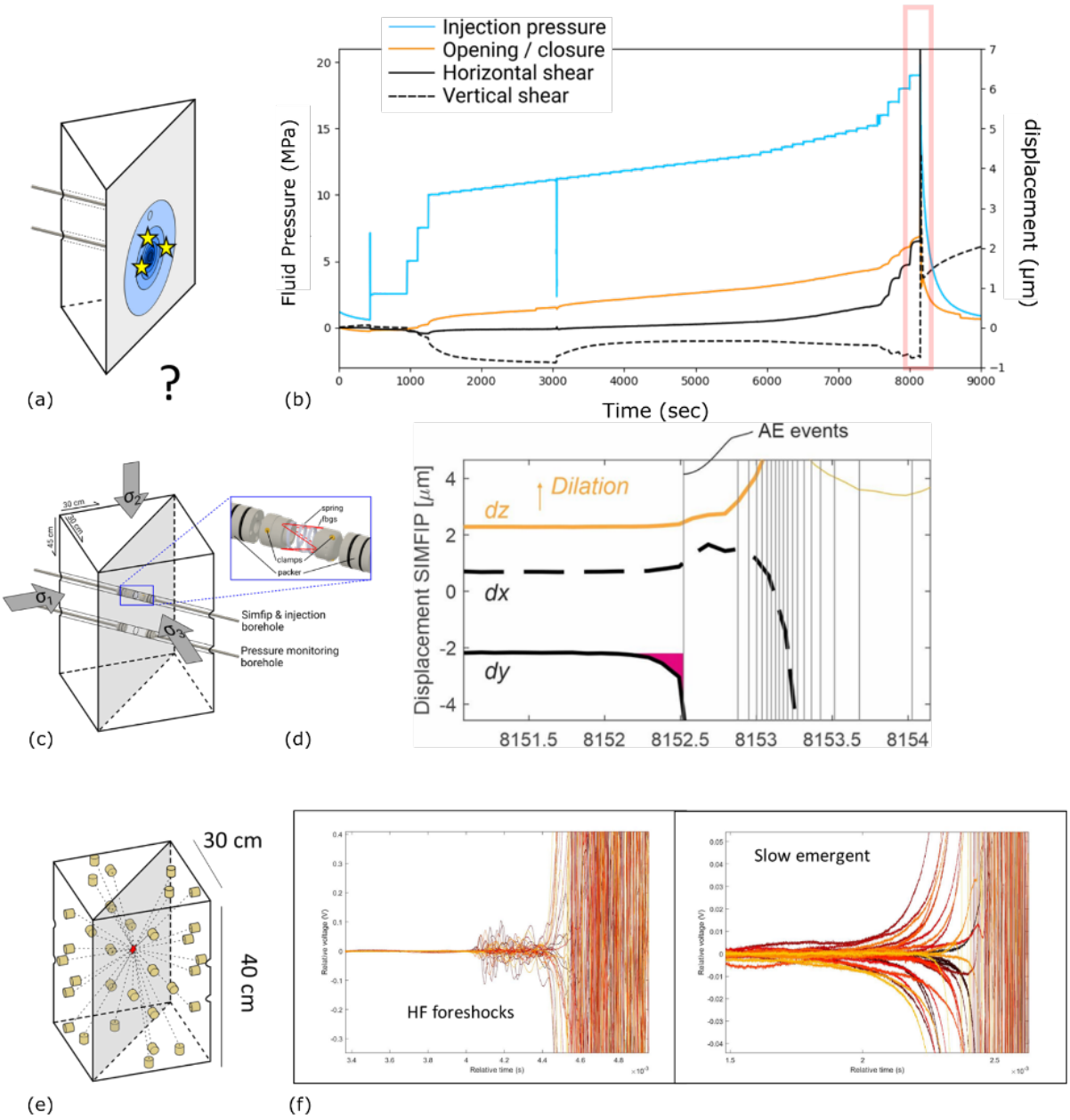

Figure 13: (a) A schematic diagram of the fluid overpressure produced at the injection site of the true triaxial apparatus. (b) Main experimental observations of a fluid reactivation of a critically stressed fault. The fluid pressure (blue) was increased in a stepwise manner and the mechanical response was recorded on the mini-SIMFIP in a monitoring borehole which tracked the opening (orange), and horizontal (black) and shear (dashed) motions. (c) An overview of the stress state and an in-set visualization of the mini-SIMFIP probe that straddled the fault. (d) A Zoomed view of the mechanical responses moments before failure. The fault showed a complex motion that appears to have slow premonitory displacements before the onset of acoustic emissions (AEs). (e) The acoustic emission array with 32 passive sensors. (f) Examples of distinct variations and foreshocks detected in the initiation phase.

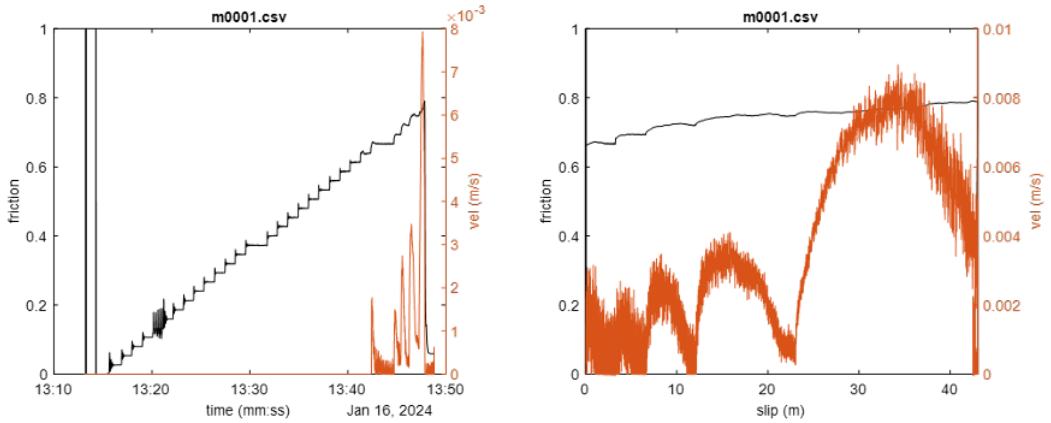

Figure 14: Left panel: black solid line, friction coefficient vs. time after a stepwise increase in shear stress. Slip rate (m/s) is in orange. Right panel: friction coefficient and slip rate vs. slip. Spontaneous oscillations in slip before the main frictional instability occur and reach slip rates of 8 mm/s. Normal laid (averaged on the fault surface) was 5 MPa.

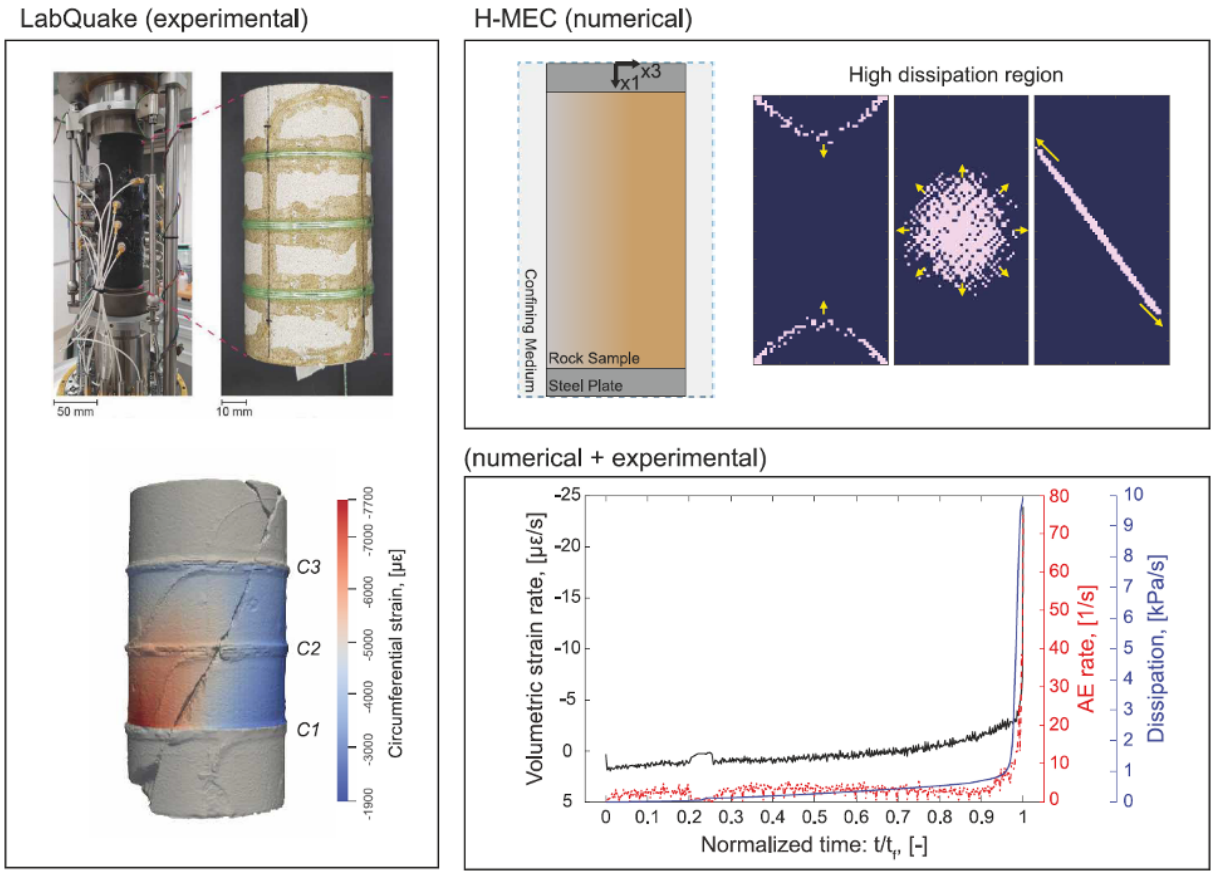

Figure 15: An overview of the research published in Bianchi et al (2024) is summarized. The laboratory campaign collected AE and DSS data and was used to verify a comprehensive Hydro-Mechanical Earthquake simulator (H-MEC). The comparison of the two results enabled a first effort look at the explanations into the mechanics governing failure in the homogeneous but brittle sample.

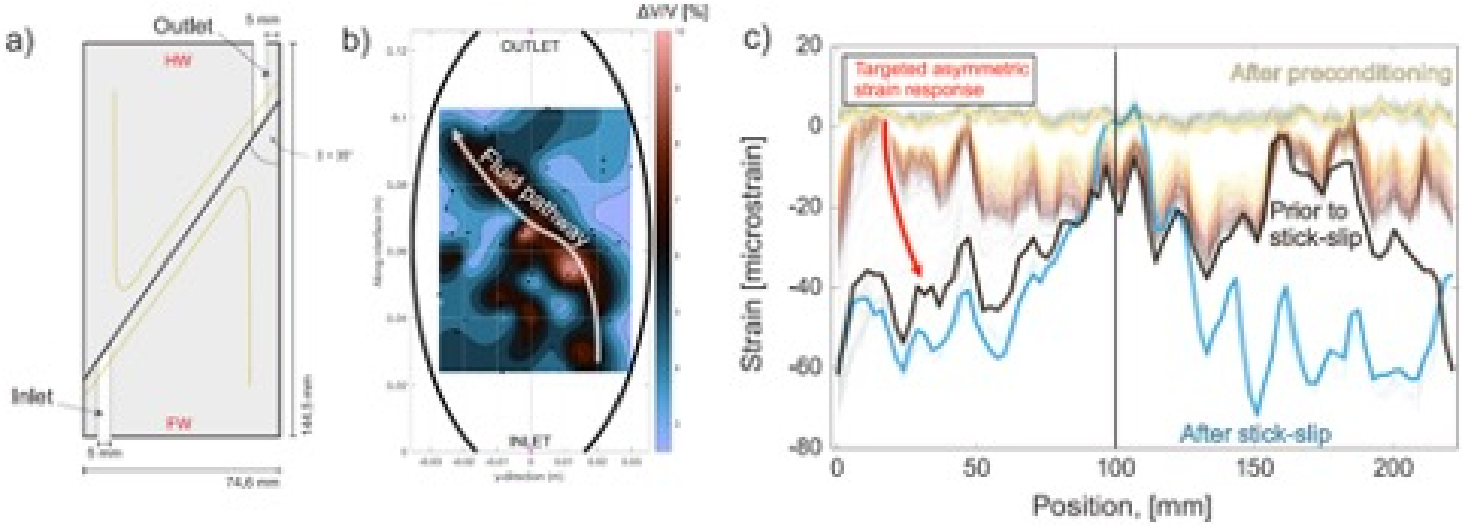

Figure 16: (a) Layout of saw-cut Rotondo sample used to test the effects of fluid preconditioning in a triaxial setting. (b) Relative changes in seismic velocities are determined using ultrasonic surveys during a characterization test where low pressure water was introduced on the dry fault. The fluid pathway was determined from an increase in seismic velocity theoretically predicted with the introduction of fluids into the fracture pore space. (c) Strain response captured on fault parallel strain on the DSS array. Strain shows an asymmetric response to the fluid hammer in this preconditioned case. (not shown) the response was more isotropic in the non-preconditioned scenario.

Ongoing research in the FEAR Laboratory Working Group (presented in the following pages)

Exploring fault preparation and earthquake nucleation from the laboratory
Bianchi, P., Selvadurai, P. A., Dal Zilio, L., Vásquez, A. S., Madonna, C., Gerya, T., Wiemer, S.

Fault preparation and earthquake nucleation from the integration of laboratory and numerical techniques
Bianchi, P., Selvadurai, P.A., Dal Zilio, L., Vásquez, A.S., Madonna, C., Gerya, T., Wiemer, S.

Multiple seismic slip-rate pulses and mechanical and textural evolution of calcite-bearing fault gouges
Cornelio, C., Aretusini, S., Spagnuolo, E., Di Toro, G., Cocco, M.

High-Resolution GPR Imaging of Fracture Apertures
Escallon, D., Shakas, A., Maurer H., Madonna C., and the Bedretto Team

---

The Impact of Injection Protocol and Stress Preconditioning on the Hydro-Mechanical Response of the Crystalline Rock
Jalali, M., Selvadurai, P., Spagnuolo, E., Meier, M-A., Dal Zilio, L., Gholizadeh Doonechaly, N., Bröker, K., Osten, J., Rosskopf, M., Obermann, A., Amann, F., and the FEAR Team

---

3D Fault Displacement During Fluid-Driven Reactivation Experiments in Lab-Scale
Osten, J., Selvadurai, P., Spaguolo, E., Cook, P., Jalali, M., Cadmus, A., Fuentes, R., Guglielmi, Y., Amann, F.

Updates from SaMiEx: Towards an Intrisic Understanding of Acoustic Emission Sensors
Selvadurai, P., Villiger, L., Plenkers, K., Delcourt, T., Marty, P.J., Ermet, L., Boese, C., Kwiatek, G., Obermann, A., Rosskopf, M., Meier, M.A., Haag, T., Knornschild, N., Tinti, E., Dal Zilio, L.

Laboratory Insight into the Evolution of the Seismic Potential of an Asperity due to Wear
Michail, S., Selvadurai, P.A., Rast, M., Salazar Vásquez, A.F., Bianchi, P., Madonna, C., Wiemer,S.

The Life Cycle of an Asperity: Insights from the Laboratory
Michail, S., Selvadurai, P.A., Rast, M., Salazar Vásquez, A.F., Bianchi, P., Madonna, C., Wiemer, S.

Exploring fault preparation and earthquake nucleation from the laboratory

Patrick Bianchi[1], P. A. Selvadurai[1], L. Dal Zilio[2,3,4], A. Salazar Vásquez[1,5], C. Madonna[6], T. Gerya[2], S. Wiemer[1]

[1]Swiss Seismological Service, ETH Zurich; [2]Institute of Geophysics, ETH Zurich;
[3]Earth Observatory of Singapore, Nanyang Technological University; [4]Asian School of the Environment, Nanyang Technological University;
[5]University of Applied Sciences of Eastern Switzerland, Rapperswil; [6]Geological Institute, ETH Zurich

This presentation participates in OSPP

Outstanding Student & PhD candidate Presentation contest

1 Introduction

The initiation of **unstable fault slip** leading to earthquakes involves intricate physical processes and interactions. Investigations at both field and laboratory scales have highlighted the existence of **spatio-temporal variations in seismic or aseismic observations** near the epicenter of a major seismic event[1,2].

These variations are often associated with the **preparatory phase of major earthquakes** and are believed to involve processes resulting from **progressive localization of deformation,** around the eventual rupture zone, that **accelerates leading up to failure**. However, the time and spatial scales of this behavior are not well understood due to **our lack of understanding into the physical mechanisms within the preparatory zones**.

2 Material and methods

We perform a triaxial test on a sample of **Berea sandstone**. **16 piezo-electric transducers** (PZTs) are used **passively** to detect **acoustic emissions** (AEs) and **actively** to construct a **P-wave velocity model**. **Distributed strain sensing** (DSS) with **optical fibers** is employed to measure axial and circumferential strain (Fig. 1).
We conduct simulations using **H-MEC**[3], which is a 2D fully coupled and continuum based seismo-hydro-mechanical poro-visco-elasto-plastic numerical modeling code (Fig. 2). We track the **dissipation of mechanical energy**, which is related to **irreversible processes** consuming strain energy: $\boldsymbol{D = \sigma'_{ij} \cdot \dot{\boldsymbol{\varepsilon}}'_{ij}}$.

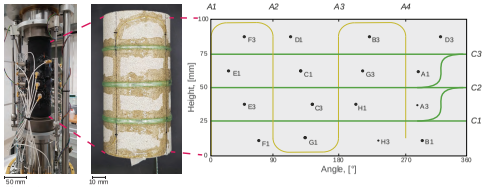

Figure 1

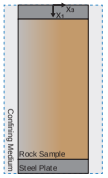

Figure 2

The following **protocol** is used:

- a **confining pressure** (blue line, Fig. 3) of **20 MPa** is applied to the sample and is kept constant,
- **differential stress** (red line, Fig. 3) is increased with a **constant piston displacement rate** (0.33 µm/s) until the **failure of the sample** is reached with associated major stress drop.

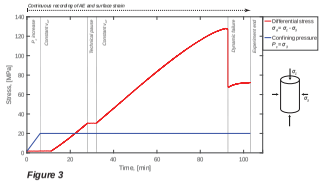

Figure 3

3 Laboratory Results

We observe the formation of **two clusters of AEs at the top and bottom of the sample** (Fig. 4) during approximately the entire test. Shortly (<5 min) before the macrofracture nucleation, the **AEs localize** on one side of the bottom half of the sample. Then, the macrofracture nucleates and propagates upwards.

The last interpolated DSS measurement of circumferential strain (Fig. 5) shows **deformation localization spatially correlating with the last cluster of AEs** that anticipated the nucleation of the macrofracture.

By repeatedly pulsing from each PZT sensor, we construct P-wave velocity models and investigate their **spatial variations** (Fig. 6). **Central regions** of the sample experience a **stronger velocity decrease** significantly earlier than the macrofracture nucleation. However, **no seismic activity** is detetced there before failure (Fig. 4).

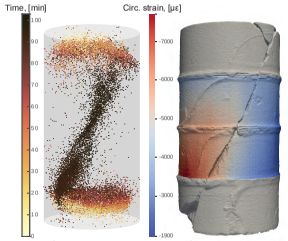

Figure 4

Figure 5

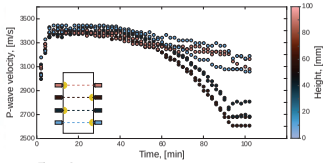

Figure 6

4 Numerical Results

We build a binary mask that isolate regions of the sample with **high dissipative levels** (Fig. 7) to track **irreversible deformation** in the sample. The simulations reveal **three distinct stages of preparatory processes:**

1) highly dissipative fronts propagate towards the middle of the sample correlating with the observed **AE locations** (Fig. 7, left)
2) dissipative regions are individuated in the middle of the sample and could be linked to the discernible **decrease of the P-wave velocities** (Fig. 7, middle)
3) a system of **conjugate bands** form, coalesce into a single band that grows from the center towards the sample surface and is interpreted to be due to the **preparation of a weak plane** (Fig.7, right).

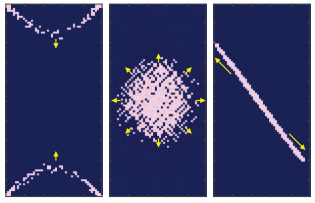

Figure 7

5 Discussion

The **mean volumetric strain rate and AE rate temporally correlate** and are both indicative for a **preparatory process** prior to the sample failure (Fig. 8, top). The increased seismic activity could be caused by the **localization of deformation**.

The **simulated dissipation** also shows an **abrupt increase** prior to failure (Fig. 8, bottom). The cause of this increase might be related to a **preparatory process** also responsible for the **acceleration** of the volumetric strain and AE rates. The model appears to capture this **accelerated behavior**.

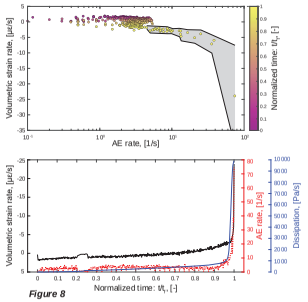

Figure 8

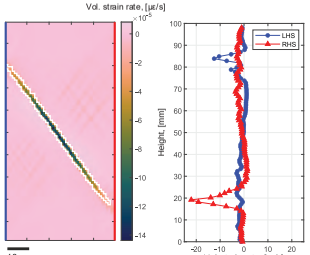

Figure 9

Volumetric strain rate localization is also observed **numerically** (Fig. 9) and spatio-temporally correlates with the laboratory observations. This process is observed as soon as the weak plane **approaches the sample surface** and **interacts** with it.

Due to our choice of using H-MEC in a **quasi-static** manner, our numerical results are deemed reliable only **up to the onset of fracture nucleation**; dynamic propagation is not currently considered in this investigation.

6 Conclusions

This study investigated both **aseismic and seismic preparatory processes linked to strain localization** preceding rock failure. **By combining laboratory measurements and numerical simulations**, we were able to capture a large variations of processes leading up to the nucleation of the shear fracture. **Developing models that capture a range of behaviors** at various scales, including the laboratory, is a necessary step **to properly upscale research efforts** to the reservoir and field scales.

References

[1] Kato, A., & Ben-Zion, Y. (2021). The generation of large earthquakes. *Nature Reviews Earth & Environment*, *2*, 26–39. doi: 10.1038/s43017-020-00108-w
[2] Campillo, M., & Paul, A. (2003). Long-Range Correlations in the Diffuse Seismic Coda. *Science*, *299* (5606), 547-549. doi: 10.1126/science.1078551
[3] Dal Zilio, L., Hegyi, B., Behr, W., & Gerya, T. (2022). Hydro-mechanical earthquake cycles in a poro-visco-elasto-plastic fluid-bearing fault structure. *Tectonophysics*. doi: https://doi.org/10.1016/j.tecto.2022.229516

Fault preparation and earthquake nucleation from the integration of laboratory and numerical techniques

Patrick Bianchi[1], P. A. Selvadurai[1], L. Dal Zilio[2], A. Salazar Vásquez[1,3], C. Madonna[4],T. Gerya[2], S. Wiemer[1]
[1]Swiss Seismological Service, ETH Zurich; [2]Institute of Geophysics, ETH Zurich; [3]University of Applied Sciences of Eastern Switzerland, OST Rapperswil; [4]Geological Institute, ETH Zurich

1 Motivation

An important question related to the FEAR project is ***how does the MC fault reactivate?***

Different rock facies with different properties (hydraulic and mechanic) govern preparatory processes that occur within this fault volume. **Understanding how various facies interact during reactivation** is an overarching goal of the framework presented here.

In this study we investigate **strain localization (a)seismic deformation** preceding failure from the **combination of laboratory tests and physics-based numerical models**.

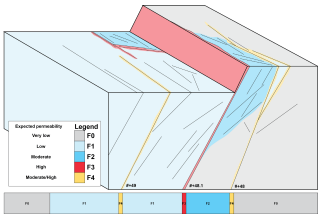

2 Methods Overview

We conduct a **failure test** on a confined sample of **Berea sandstone.**

We deploy **16 piezo-electric transducers** (PZTs) **passively** to detect **acoustic emissions** (AEs) and **actively** to construct a **P-wave velocity model**.

Distributed strain sensing (DSS) with optical fibers (polymide and acrylate) is em axial and circumferential strain.

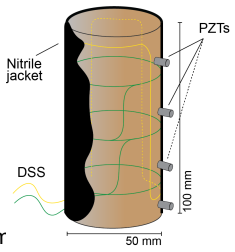

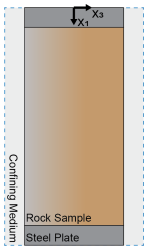

H-MEC [1] is a 2D **fully coupled and continuum-based** seismo-hydro-mechanical poro-visco-elasto-plastic numerical modeling code.

We model the **rock sample**, the **steel plate,** a **confining medium** and a **fluid phase** (i.e., air).

The **dissipation of mechanical energy** is a term related to irreversible processes consuming strain energy stored in the rock: $\boldsymbol{D = \sigma'_{ij} \cdot \dot{\varepsilon}'_{ij}}$.

3 The Laboratory Test

Confining pressure is set to **20 MPa** during the entire test.

Differential stress is increased with constant piston velocity until the **failure of the sample.**

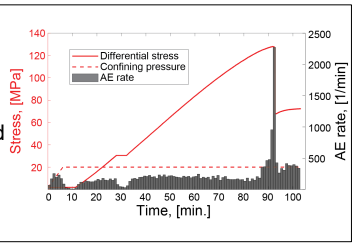

4 Results and Discussion

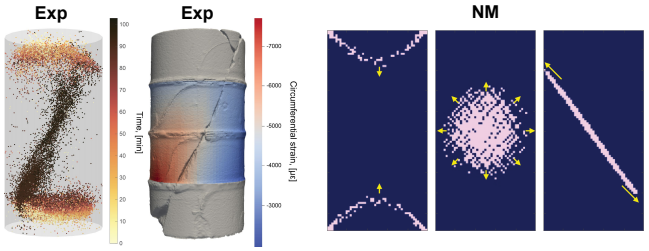

The region of the sample **experiencing higher extension matched the AEs cloud**.

We built a binary mask to isolate regions with **high dissipation levels**.

Three distinct stages are determined by tracking the **evolution of high dissipative regions** and correlate with the **laboratory observations**.

Dissipation shows a **sharp increase preceding failure** and temporally correlates with the increase of the **volumetric strain and AE rates**.

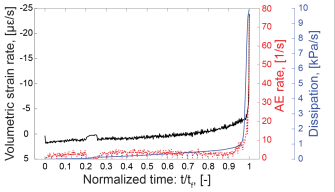

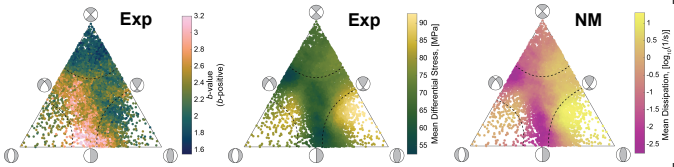

We investigate the relation of **faulting style** with **b-value** and **differential stress**[2]**.**

Correlations are found between these **laboratory** (Exp) parameters and the numerical **dissipation** (NM).

5 Outlook

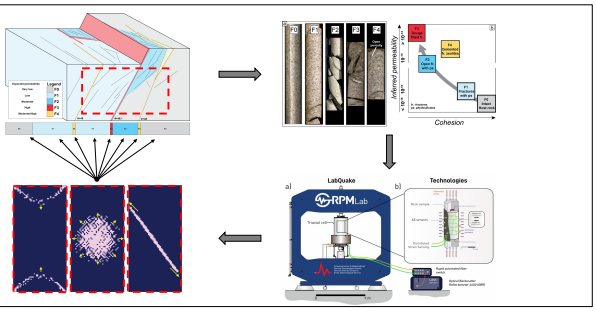

References

1. Dal Zilio, L., Hegyi, B., Behr, W., & Gerya, T. (2022). Hydro-mechanical earthquake cycles in a poro-visco-elasto-plastic fluid-bearing fault structure. Tectonophysics. doi: https://doi.org/10.1016/j.tecto.2022.229516
2. Petruccelli, A., Schorlemmer, D., Tormann, T., Rinaldi, A., Wiemer, S., Gasperini, P., & Vannucci, G. (2019). The influence of faulting style on the size-distribution of global earthquakes. Earth and Planetary Science Letters, 527 , 115791. doi: https://doi.org/10.1016/j.epsl.2019.115791

Partner/Sponsor:

Multiple seismic slip-rate pulses and mechanical and textural evolution of calcite-bearing fault gouges

C. Cornelio[1], S. Aretusini[1], E. Spagnuolo[1], G. Di Toro[1,2], M. Cocco[1]

[1] Istituto Nazionale di Geofisica e Vulcanologia, Rome, IT
[2] Dipartimento di Geoscienze, Università di Padova, Padua, IT

1 Introduction

Natural faults are complex, non-spatially homogenous systems. Rock deformation experimental studies usually simplified the complexity of natural structures either as a surface discontinuity between intact rocks or a thick gouge layer. However, depending on the simplified fault type and its slip history, the response to seismic deformation can vary. During the FEAR project the fault will be reactivated multiple times and its frictional properties can change. In this work, thanks to a combination of experiments and microstructures, we establish the evolution of mechanical properties with up to four consecutive seismic slip-rate pulses in a homogeneus material as a preliminary study for the Bedretto gouge.

2 Experimental approach: SHIVA

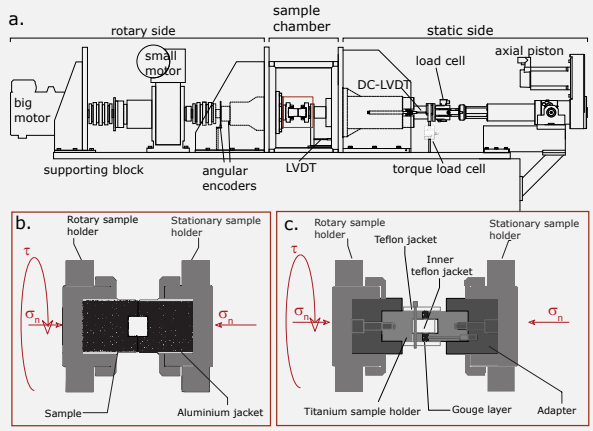

Conditions:
- Room humidity
- Normal stress : 10-20-30 MPa
- Lithology : Carrara Marble

- Trapezoidal slip-rate function: acc/dec = 6.4 m/s^2 , V_{plat} = 1 m/s, slip = 1 m
- Hold time : 120 sec

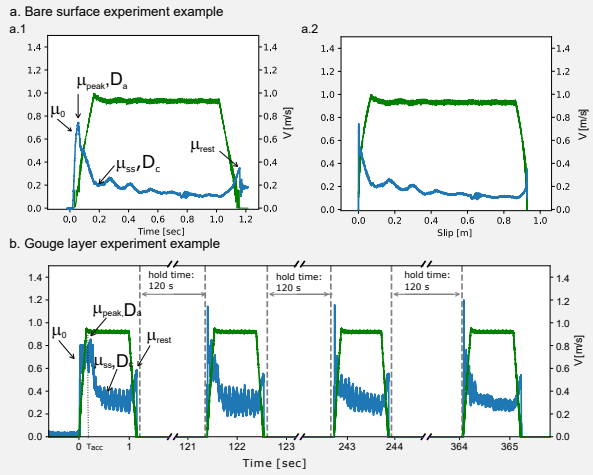

3 Microstructural investigation

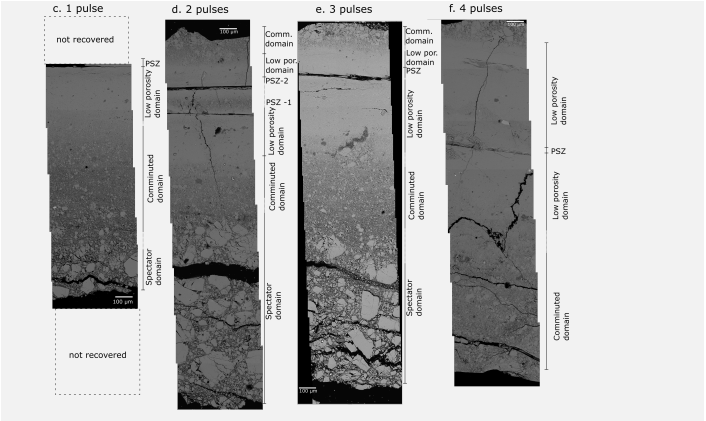

4 Microstructural investigation details

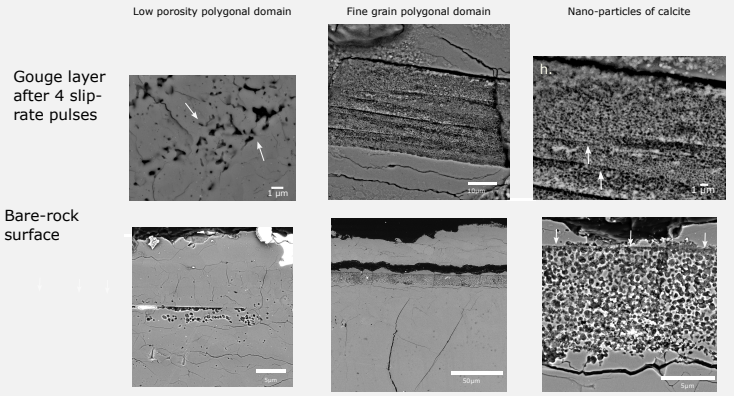

5 Mechanical parameters investigation

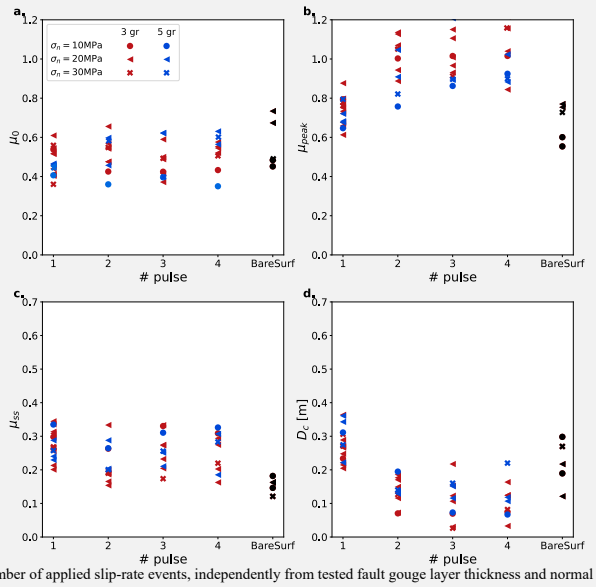

With the number of applied slip-rate events, independently from tested fault gouge layer thickness and normal stress, μ_0 and μ_{ss} are constant, μ_{peak} increases, D_c decreases. The larger change occurs between the first and the second slip-rate pulses: the second shows similar mechanical parameters to bare surface experiments.

6 Energy partitioning

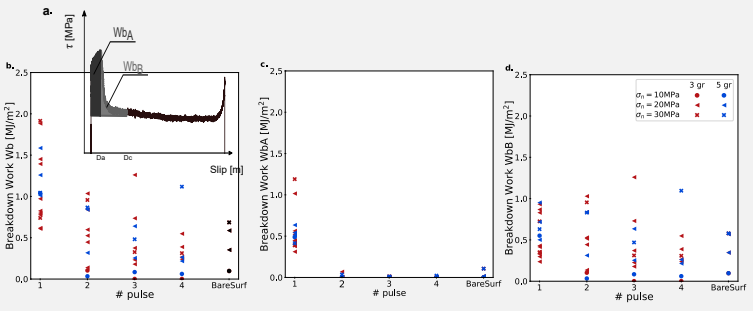

Breakdown Work (W_b) decreases with the number of applied slip-rate pulses and tends to approach the Wb of the bare surfaces.
After the first event, the energy computed before the weakening stage (W_{bA}) drastically decreases after the first slip rate event, the following three events have similarly low values also comparable to the bare rocks.

7 Conclusions

We suggest that the seismic slip history affects the mechanical evolution of the faults. Faults which experienced a larger number of seismic slip events have a mechanical behaviour more similar to well-localized shear zones (bare surfaces).
For future work, we plan to perform experiments with multiple slip-rate events on the MC fault material (gouge and bare surface).

High-Resolution GPR Imaging of Fracture Apertures

Escallon, Daniel; Shakas, Alexis; Maurer Hansruedi; Madonna Claudio and the Bedretto Team
Department of Earth Sciences, ETH Zurich, 8092 Zurich, Switzerland
Author email: daniel.escallon@erdw.ethz.ch

Sub-Fresnel Resolution in GPR - Insights from a controlled laboratory experiment

INTRODUCTION

- Ground Penetrating Radar (GPR) is vital for exploring the near-surface across various scales, particularly in detecting **rock fractures**. Despite its utility, characterizing complex fracture properties like **aperture** and **roughness** remains challenging.
- Current approaches use of a thin-layer model that simulates arbitrary fracture reflections and can help quantify aperture [1]. Various experiments have demonstrated that amplitude changes correlate with aperture, but inferring aperture from GPR reflection amplitudes remains a challenge due to several factors: the complexity of fracture systems, ambiguity in amplitude changes, limited resolution of GPR systems, variability in dielectric properties, and/or the complexity of solving inverse problems.
- To address this, we conducted a high-resolution laboratory experiment using a synthetic 3D fracture, in which we densely scanned the sample with a GPR system, ensuring full coverage, in an effort to explore the resolution capabilities of the device.

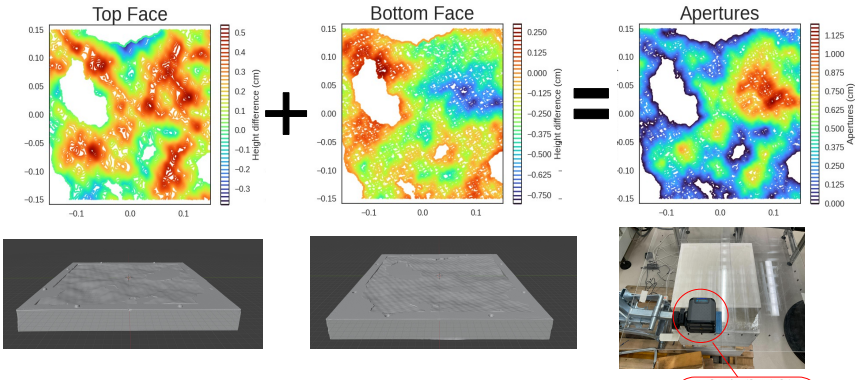



METHODOLOGY

- **Synthetic Fracture Design**: Utilized the geostatistical Python package "GSTOOLS" to design a synthetic fracture. Two distinct 2D spatially correlated random fields were generated employing a *Matérn covariance model*.
- **Fracture Fabrication**: Generated surfaces with *3D Printer* to serve as a mold for casting two Gypsum/Concrete blocks of W:34cm, L:34cm, and H:~12cm, with the fracture positioned at their intersection.
- **Data Acquisition**: Conducted line scans using the Proceq GP8800 GPR device at intervals of 1.12 cm in both directions within a grid setup.
- **Signal Analysis**: Identified the time window containing reflections and plotted the maximum amplitude from these reflections for analysis.

RESULTS AND DISCUSSION

- Notable correlation found between GPR signal changes and fracture apertures.
- GPR capable of identifying features smaller than theoretical Fresnel zone calculations.
- Observations validated by numerical simulations using effective-dipole model [2]. Simulated response reveals small GPR amplitude changes due to fracture roughness.
- **Major findings**: GPR offers sub-Fresnel zone imaging capabilities.

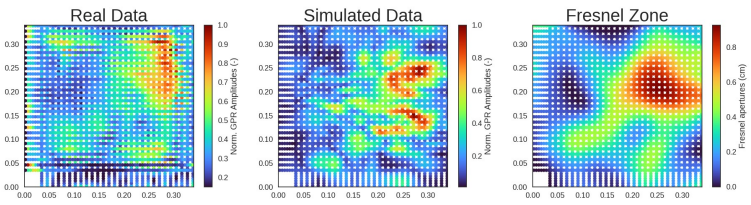

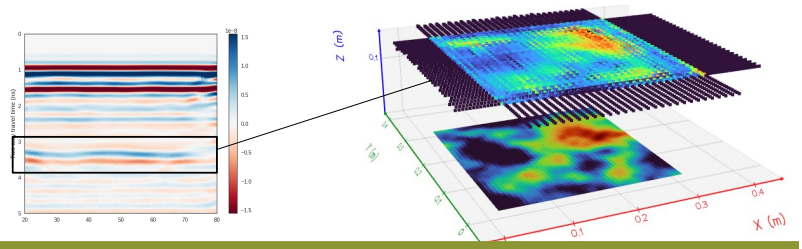

REFERENCES

[1] Sambuelli, Luigi & Calzoni, C. (2010). Estimation of thin fracture aperture in a marble block by GPR sounding. BOLLETTINO DI GEOFISICA TEORICA ED APPLICATA. 51. 239-252.

[2] Shakas, A., & Linde, N. (2015). Effective modeling of ground penetrating radar in fractured media using analytic solutions for propagation, thin-bed interaction and dipolar scattering. Journal of Applied Geophysics, 116. doi:10.1016/j.jappgeo.2015.03.018.

Bedretto Lab | ETH zürich | erc | FEAR Fault Activation and Earthquake Rupture

Take a picture to **download** more information

The Impact of Injection Protocol and Stress Preconditioning on the Hydro-Mechanical Response of the Crystalline Rock

Mohammadreza Jalali[1], Paul Selvadurai[2], Elena Spagnuolo[3], Men-Andrin Meier[2], Luca Dal Zilio[4], Nima Gholizadeh Doonechaly[4], Kai Bröker[5], Julian Osten[1], Martina Rosskopf[4], Anne Obermann[2,4], Florian Amann[1,6], and the FEAR Team

[1] Department of Engineering Geology & Hydrogeology, RWTH Aachen, Aachen, Germany (jalali@lih.rwth-aachen.de)
[2] Swiss Seismological Service, ETH Zürich, Zürich, Switzerland
[3] National Institute of Geophysics and Volcanology (INGV), Rome, Italy
[4] Institute of Geophysics, ETH Zürich, Zürich, Switzerland
[5] Center for Hydrogeology and Geothermics (CHYN), University of Neuchâtel, Neuchâtel, Switzerland
[6] Fraunhofer Research Institution for Energy Infrastructures and Geothermal Systems IEG, Aachen, Germany

FEAR Fault Activation and Earthquake Rupture

EGU General Assembly 2024

Introduction

Fault Activation and Earthquake Rupture (FEAR) project aims to induce a M1 earthquake on a well characterized and monitored fault to further our understanding of earthquake rupture processes such as nucleation and premonitory slip. Injection protocols are investigated to enhance our knowledge of the hydro-mechanical properties and testing hypothesis on reactivation style. For doing so, a series of stress-preconditioning injection protocols were tested in the Bedretto Underground Laboratory for Geoenergies and Geosciences, Switzerland (Ma et al., 2022), using an existing stimulation and monitoring array (Plenkers et al., 2023).

The main objective of these tests was to develop atypical injection protocols that could be implemented in different geological conditions that target aspects of induced seismicity associated with high-pressure fluid injection.

We performed two injections and monitored the rock mass response using six monitoring boreholes each equipped with multi-component seismic monitoring systems, pressure, temperature, and distributed strain sensing arrays. Two different injection protocols have been applied in the same structure, allowing us to characterize the hydro-mechanical response of the rock mass around these intervals. Each test was associated with pre- and post-characterization tests including hydraulic and hydro-mechanical tests such as Hydraulic fracturing (HF) and Hydraulic tests on pre-existing fractures (HTPF) tests.

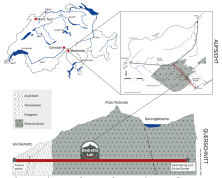

Map view of the Bedretto Tunnel and the hosting Rotondo granite, as well as a cross-sectional view of the BedrettoLab with respect to the tunnel

VALTER for FEAR Experiment

VALTER is a running geothermal-related project in the adjacent volume of the FEAR fault target. ST1 borehole of the VALTER project is well instrumented to test the seismic response of the pre-existing fractures to fluid stimulation. VALTER for FEAR is an experiment that benefits from the synergy between the VALTER and FEAR projects to examine the following objectives:

- Precondition fault zone for seismically activating a larger part of the target fault by long-term high-pressure fluid injection into the ST1 borehole – interval 12
- Test and quantitatively understand the role of the stimulation protocol for fault pre-conditioning

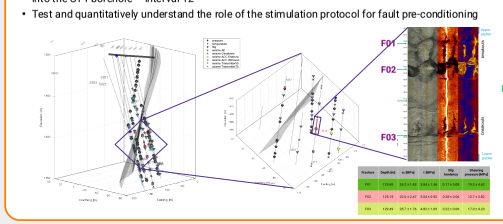

Stress Pre-Conditioning Scenarios

Scenario I
Fluid Pressure

Decrease the fault clamping stress by increasing the fluid pressure around the injection borehole. This could be done by constant pressure injection slightly below jacking pressure for a while and then increasing the pressure to induce slip.

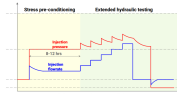

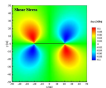

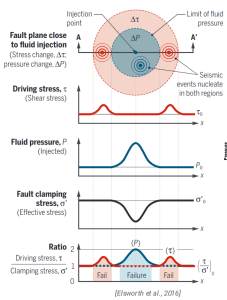

[Ellsworth et al., 2016]

Scenario II
Driving Stress

Induce shear (driving) stresses around the injection borehole via depletion and then rapid injection. This scenario will move the shear (driving) stresses toward the injection borehole and then rapid injection will induce the slip at the vicinity of the injection borehole.

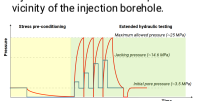

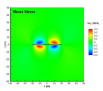

Hydro-Mechanical Observations

Scenario I

This scenario consists of four cycles:

- HF cycle to break down the cement and open the fractures hydraulically
- HTPF cycle (I) to measure the jacking and shut-in pressure before the stress pre-conditioning cycle
- Pre-conditioning cycle to pressurize the fractures and increase the pressurized volume
- HTPF cycle (II) to measure the jacking and shut-in pressure after stress pre-conditioning cycle

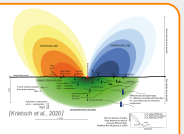

Hydro-mechanical response during scenario I injection

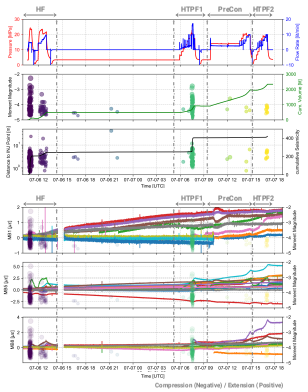

Spatio-temporal distribution of seismic events

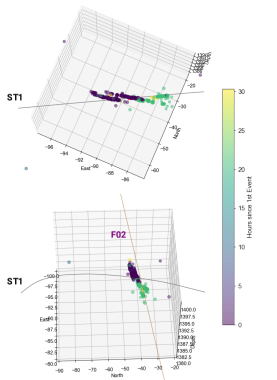

The spatio-temporal distribution of seismic events suggests the evolution of seismicity along a preexisting fracture (F02) (fluid migration along pathways)

Scenario II

This scenario consists of three cycles:

- HTPF cycle (I) to measure the jacking and shut-in pressure before the stress pre-conditioning cycle
- Pre-conditioning cycle to de-pressurized the fractures and then rapid injection cycles to induce slip
- HTPF cycle (II) to measure the jacking and shut-in pressure after stress pre-conditioning cycle

Hydro-mechanical response during scenario II injection

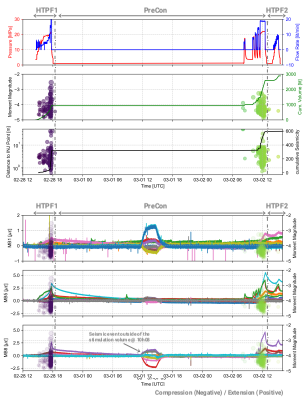

Spatio-temporal distribution of seismic events

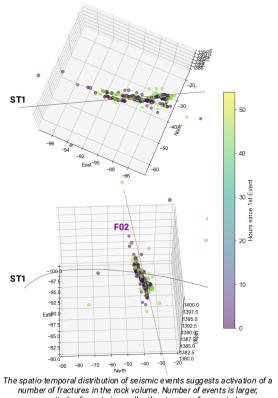

The spatio-temporal distribution of seismic events suggests activation of a number of fractures in the rock volume. Number of events is larger, magnitude of events is smaller than in case of scenario I. (distributed seismicity on small fractures)

Spatial-Temporal Distribution of Strain & Strain Rate

Strain distribution @MB5 borehole during Scenario I injection

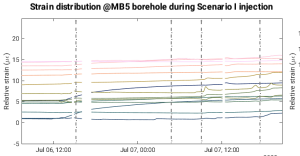

Strain distribution @MB5 borehole during Scenario II injection

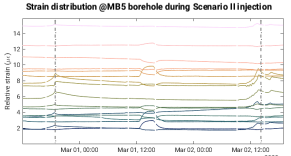

Strain rate distribution @MB5 borehole during Scenario I injection

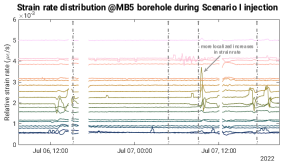

Strain rate distribution @MB5 borehole during Scenario II injection

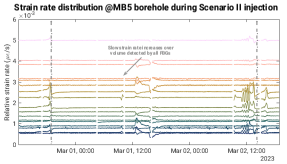

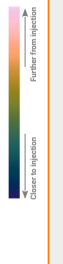

Scenario I – slow preconditioning then fast injection

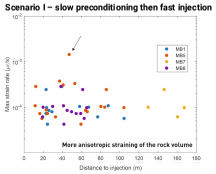

Maximum strain rate is higher perhaps due preferential structure ?

Scenario II – depletion then fast injection

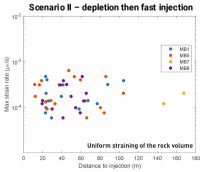

Average strain rate is higher and more uniform

Summary

- Seismicity during both phases depends on the injection pressure as well as flow rate increments.
- The total number of events after the stress pre-conditioning during scenario II was higher than in scenario I.
- The strain rate is more even through the volume during scenario II.
- The local strain rate corresponds to the preferential flow paths (scenario I) whereas the uniform strain rate corresponds to the rock volume response.
- Interval 12 might not be the most interesting section in the context of FEAR objectives to evaluate the effect of injection scenarios on the size of pressurized volume and seismicity
  - Insufficient pressure monitoring system (hydraulically disconnected)
  - The existence of three distinct fractures rather than a fault structure
  - In the vicinity of the Bad Boy structure which might induce stress shadowing



Acknowledgment

The FEAR project has received funding from the European Research Council (ERC) under the European Union's Horizon 2020 research and innovation program (grant number 856559).

FEAR Project

EGU23-14916

References

- Dal Zilio, L., Hegyi, B., Behr, W., & Gerya, T. (2022). Hydro-mechanical earthquake cycles in a poro-visco-elasto-plastic fluid-bearing fault structure. Tectonophysics, 838, 229516.
- Ellsworth, D., Spiers, C. J., & Niemeijer, A. R. (2016). Understanding induced seismicity. Science, 354(6318), 1380-1381.
- Ma, X., Hertrich, M., Amann, F., Bröker, K., Gholizadeh Doonechaly, N., et al. (2022). Multi-disciplinary characterizations of the Bedretto Lab–a new underground geoscience research facility. Solid Earth, 13(2), pp.301-322.
- Krietsch, H., Gischig, V. S., Doetsch, J., Evans, K. F., Villiger, L., Jalali, M., et al. (2020) Hydromechanical processes and their influence on the stimulation effected volume: observations from a decameter-scale hydraulic stimulation project, Solid Earth, 11, 1699–1729.
- Marone, C. (1998). The effect of loading rate on static friction and the rate of fault healing during the earthquake cycle. Nature, 391(6662), 69-72.
- Plenkers K, Reinicke A., Obermann A., Gholizadeh Doonechaly N., Krietsch H., et al. (2023). Multi-disciplinary monitoring networks for mesoscale underground experiments: Advances in the Bedretto Reservoir Project. Sensors, 23(6): 3315.
- Rice, J. R., Lapusta, N., & Ranjith, K. (2001). Rate and state dependent friction and the stability of sliding between elastically deformable solids. Journal of the Mechanics and Physics of Solids, 49(9), 1865-1898.
- Ruina, A. (1983). Slip instability and state variable friction laws. Journal of Geophysical Research: Solid Earth, 88(B12), 10359-10370.

3D Fault Displacement During Fluid-Driven Reactivation Experiments in Lab-Scale

Julian Osten[1], Paul Selvadurai[2], Elena Spaguolo[3], Paul Cook[4], Mohammadreza Jalali[1], Alexander Cadmus[5], Raul Fuentes[5], Yves Guglielmi[4], Florian Amann[1]

[1]Department of Engineering Geology and Hydrogeology, RWTH Aachen
[2]Swiss Seismological Service, ETH Zürich
[3]Instituto Nationale di Geofisica e Vulcanologia
[4]Lawrence Berkley National Laboratory
[5]Chair of Geotechnical Engineering and Institute of Geomechanics and Underground Technology, RWTH Aachen

1. Experimental Setup

Injection

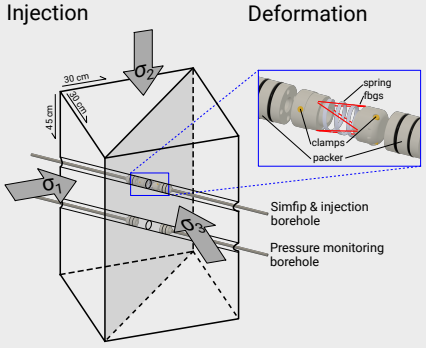

A diagonally fractured granite block is confined individually in σ_1, σ_2 and σ_3 direction by 3 sets of oil filled flatjacks. Two boreholes enable fluid injection and pressure monitoring into the fracture. Fracture boundaries are opn to the atmosphere.

Deformation

A newly developped 3D borehole deformation probe (mini-SIMFIP) measures relative fracture displacement of the two rock parts due to fluid is injection in either of the boreholes.

Acoustic Emission

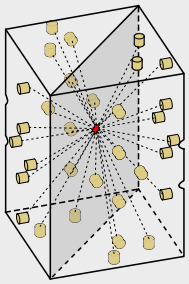

Seismic events are captured by 32 AE sensors mounted around the sample. In active mode, seismic tomography could be used to monitor the propagation of a pressure front during fluid injection.

2. Characterization

Roughness

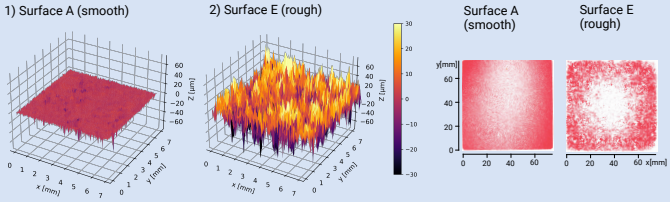

Asperity heights of two different samples of #40 and #1200 grit polish measured by Schaaf (2020) on analogue samples with a white light interferometer.

Stress distribution captured by pressure sensitive film on two analogue samples of same properties.

Stiffness

To investigate fracture deformation and SIMFIP behaviour under compression, the samples were isotropically loaded. As expected the rough sample is less stiff than the rough sample.
Fracture closure and opening behaviour is oppposite to common observations such as Bandis et al. 1983.

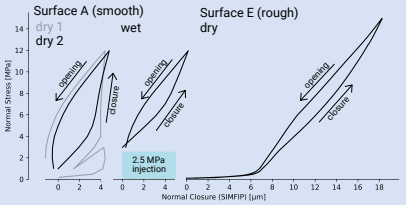

3. Results

Surface A (smooth)

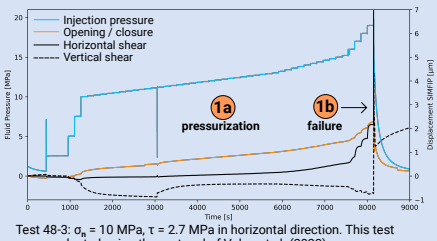

Test 48-3: σ_n = 10 MPa, τ = 2.7 MPa in horizontal direction. This test was conducted using the protocol of Volpe et al. (2023).
27 seismic events were triggered at injection pressure of 20 MPa.

Failure in Detail

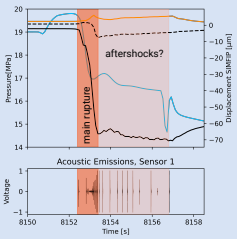

27 seismic events

→ time sync. of AE corrected manually

Surface E (rough)

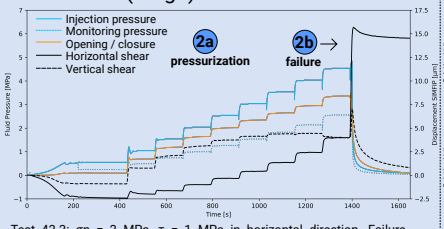

Test 43-3: σn = 3 MPa, τ = 1 MPa in horizontal direction. Failure occured at 4.5 MPa injection pressure. No sesimic data aquisition. Aseismic behaviour observed for previous tests on same samples.
Plot colorscheme based on Cappa et al. (2019).

Event Nucleation

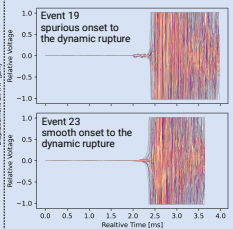

Waveform of all 32 sensors. A changing nucleation pattern can be observed between the different events.

4. Discussion

Mohr-Coulomb and Terzaghi do not apply!

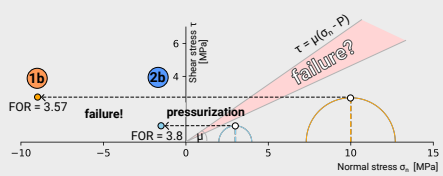

For both cases, the failure occured way beyond the Mohr-Coulomb failurec criterion expanded by Terzaghi's law of effective stress τ = μ(σn - P). Thus, the expected pressure at failure is $P_{exp} = \sigma_n-(\tau/\mu)$. From the real fluid pressure at failure $P_{failure}$ the fluid overpressure ratio FOR can be calculated (Ji & Wu 2021).

Expected failure pressure

$P_{exp} = \sigma_n-(\tau/\mu)$

↓

Failure pressure way above expected pressure

↓

Fluid Overpressure Ratio (FOR)

$FOR = P_{failure} / P_{exp}$

Strong pressure concentration expected

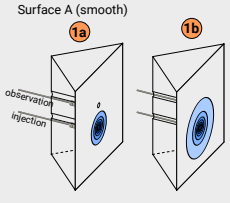

The smooth fracture has a low permeability. The pressurized area is initially very small and fluid injection is not captured in the observation borehole. Fracture opening during reactivation creates a connection between injection and observation borehole.

The rough fracture has a high permeability. The pressurized area goes beyond the observation borehole and water leaks out to the atm fracture boundary.

Pressure Diffusion

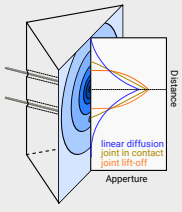

Picture based on Murphy et al. (2004); Pressure diffusion before, during and after fracture activation are not fully understood. Pressure from the one or further monitoring boreholes could give insight to underlaying priniciples.

5. References

Bandis, S.C., Lumson, A.C., Barton N.R. (1983) Fundamentals of Rock Joint Deformation. Int. J. Rock. Mech. Min. Sci. & Geomech. Abstr. 20(6): 249-268
Cappa, F., Scuderi, M.M., Colletini, C., Guglielmi, Y., Avouac, J.-P. (2019) Stabilization of fault slip by fluid injection in the laboratory and in situ. Sci. Adv. 5:eaau4065
Ji, Y., Fang, Z., Wu, W. (2021) Fluid Overpressurization of Rock Fractures: Experimental Investigation and Analytical Modeling. Rock Mechanics and Rock Engineering 54:3039–3050
Murphy, H., Huang, C., Dash, Z., Zyvoloski, G., White, A. (2004) Semianalytical solutions for fluid flow in rock joints with pressure-dependent openings. Water Resources Research 40:W12506
Schaaf, R. (2020) Comparative investigations to determine the surface roughness of solid rocks. Master Thesis, RWTH Aachen
Siebert, P. (2017) Laborversuche zur hydraulischen Risserzeugung in dreiaxial belasteten Granitquadern. Doctoral Thesis, RWTH Aachen
Volpe, G., Pozzi, G., Colletini, C., Spagnuolo, E., Achtziger-Zupančič, P., Zappone, A., Aldega, L., Meier, M.A., Giardini, D., Cocco, M. (2023) Laboratory simulation of fault reactivation by fluid injection and implications for induced seismicity at the BedrettoLab, Swiss Alps, Tectonophysics 862:229987

Updates from SaMiEx: Towards an Intrinsic Understanding of Acoustic Emission Sensors

Selvadurai, P.A.[1], Villiger, L.[1], Plenkers, K.[2], Delcourt, T.[3], Marty, P. J.[3], Ermert, L.[1], Boese, C.[4], Kwiatek, G.[4], Obermann, A.[1], Rosskopf, M.[1], Meier, M.-A.[1], Haag, T.[5], N. Knornschild[5], Tinti, E.[6], Dal Zilio, L.[3,7]

1: Swiss Seismological Service, ETH Zurich, CH, 2: GMuG, DE, 3: Department of Geophysics, ETH Zurich, CH, 4: GFZ Potsdam, DE 5: BULGG, ETH Zurich, CH, 6: Sapienza Università di Roma, IT, 7: Nanyang Technological University, SG

1 Introduction

In Jan-Feb 2023 a **salt mine experiment (SaMiEx)** was conducted in the Merkers mine in Krayenberggemeinde (DE). The test targeted a salt pillar (~ 40 m x 35 m in cross-section) with the aim to **understand the behavior of dynamic sensors** most commonly used to study pico-seismicity (Manthei and Plenkers, 2018). This compliments the goals of the FEAR project. We present preliminary results from SaMiEx and the **potential sensor calibration** in deepening our comprehension of seismic source processes and earthquake mechanics. Our preliminary results study the wavefield produced by pendulum impacts on the face of the salt pillar using computational models in SALVUS. **Modelled P waves** are **compared to the experiments** made using the **acoustic emission sensors** and the **instrument response is computed.**

2 SaMiEx Experiments

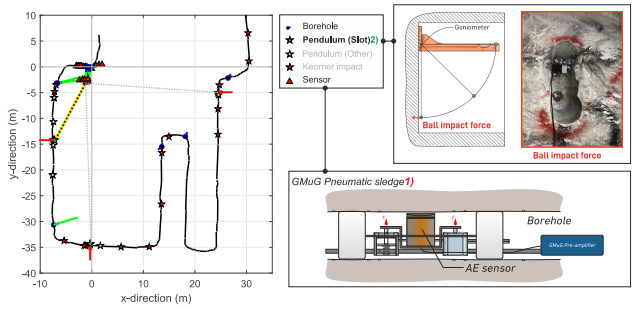

(Left) Map view of the salt pillar. **(top right)** The schematic view of the pendulum impact mechanism used to apply a ball impact force-time function to the wall with various diameter of the impactors. The pendulum was installed in a slot to reduce the loss of energy through the damaged salt pillar wall. **(Bottom right)** A schematic view of the GMuG pneumatic sledge used mount the AE sensors to the inside of the borehole.

1) Other sensor deployment methods were used (cemented, face mounted) but only the preliminary sledge mounted results are presented.
2) Three pendulum slots were used but only the highlighted configuration is on map diagram is shown next.

3 Numerical modelling

SALVUS is numerical tool that uses the **spectral-element method** to solve complex abstractions of the wave equation (Afanasiev et al., 2019). The approach is well-suited for accounting for the **geometric complexities present within the mine**. Our first model uses a **2D isotropic, homogeneous model with no intrinsic attenuation.**

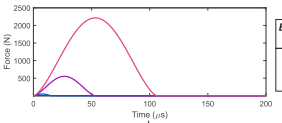

Ball size (mm)	Corner (kHz)
20	9.5
10	18.8
3	62.7

Property	Value	Study	First 2D model
Density	[2200] kg/m³	Wang et al., 2007	2180 kg/m³
V_P	[4350 to 4700] m/s	Popp and Kern, 1998 (varies with confinement)	4370 m/s
V_S	[2490 to 2600] m/s	Popp and Kern, 1998 (varies with confinement)	2590 m/s 3)
Q_P	67 (Gorlenben), 140 (GoM)	From Zong et al (2020): Using: 4.525 km/s	N/A
Q_S	25 (average)	From Zong et al (2020): Using: 2.545 km/s	N/A

3) Estimates of the wave velocities were performed by using various phase arrivals and comparing with experimental observations. These values are the result of an initial parameter refinement exercise.

$$\dot{u}_k(\boldsymbol{x},t) = \overline{f_j(\boldsymbol{\xi},\tau)} * \dot{g}_{kj}(\boldsymbol{x},t;\boldsymbol{\xi},\tau) \quad (1)$$

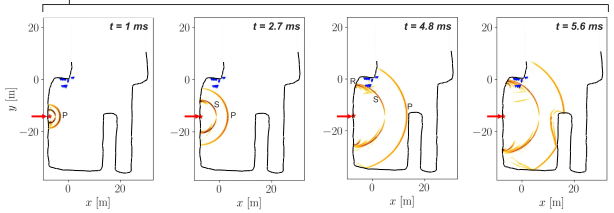

4 Results and Discussion

For an example, we **compare the waveform** of two sensors **versus** the modelled results from **SALVUS** for a 10 mm diameter pendulum impact (f_c = 18.8 kHz)

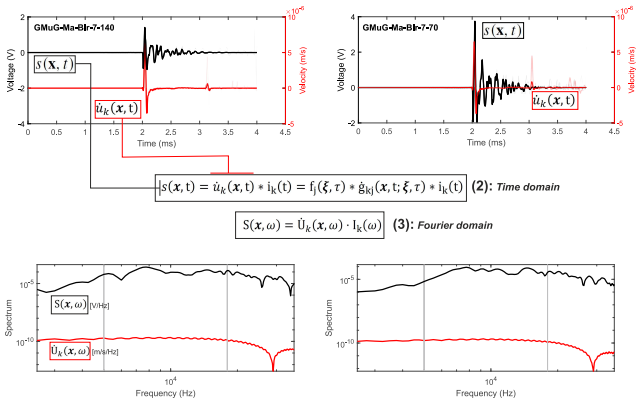

Experimental signals and numerically **computed velocity seismograms** are aligned and windowed about the **direct P wave** arrival. These are then converted into the Fourier domain using the Discrete Fourier transform (DFT). The **instrument response** i_k is then computed via **spectral deconvolution** (e.g. Selvadurai et al., 2022):

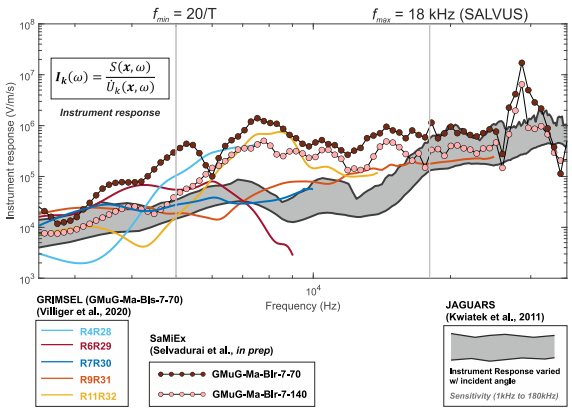

5 Conclusion

These preliminary results offer **insight into the instrument response of AE sensors** via **absolute calibration techniques**. This could be used to better constrain the seismologically inferred properties of acoustic emission in mining and underground research laboratory settings; however, more work is required.

References

1. Manthei and Plenkers (2018) *Appl. Sci.*, 8(9), 1595.
2. Afanasiev et al. (2019) *Geophys. J. Int.*, 216(3), 1675-1692.
3. Wang et al., (2007) in "Mechanical Behaviors of Salt" ISBN 978-0-415-44398-2
4. Popp and Kern (1998) Phys. Chem. Earth., 23(3), 373-378.
5. Zong, et al. (2020) *J. Geophys. Res.: Solid Earth*, 125,e2019JB019025.
6. Selvadurai et al (2022) J. Nondestruc. Eval. 41:23.
7. Villiger et al. (2020) Solid Earth, 11, 627–655.
8. Kwiatek et al. (2011) Bull. Seis. Soc. Am.,101(6), 2592–2608.

Partner/Sponsor:

Laboratory Insight into the Evolution of the Seismic Potential of an Asperity due to Wear

Sofia Michail[1], P.A. Selvadurai[1], M. Rast[2] , A.F. Salazar Vásquez[1,3], P. Bianchi[1], C. Madonna[2], S. Wiemer[1]

[1]Swiss Seismological Service , ETH Zurich; [2]Geological Institute, Department of Earth Sciences, ETH Zurich;
[3]School of Architecture, Civil Engineering, Landscape Architecture Spatial Planning, Eastern Switzerland University of Applied Sciences

Photography not allowed

This presentation participates in OSPP
Outstanding Student & PhD candidate Presentation contest

Introduction and Motivation

Faults in nature exhibit complex surface characteristics, such as the presence of contact asperities, which affect the potential for earthquake nucleation. A common metric to study frictional stability is the nucleation size h^*, which can change due to spatial heterogeneity(1) and wear. Here we use novel laboratory methods to investigate parameters controlling h^* (2,3) and how they likely changed during our experiment. Wear created surface conditions that eliminated off-fault strain accommodation and nullified the asperities seismogenic potential of the fault.

$$h^* \sim \frac{G D_c}{(b-a)\sigma_n}$$

- G : Shear modulus
- $(b-a)$: Rate and state friction parameter(3)
- D_c : Critical Slip distance
- σ_n : Normal stress

Methodology

We performed a triaxial experiment at sequentially increasing confining pressures (Pc = 60, 80, 100 MPa) on a saw- cut sample of Carrara marble.

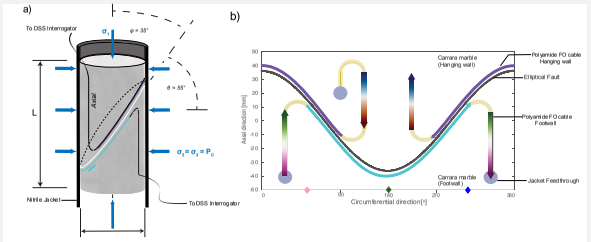

Figure 1. (a) Schematic representation of the saw-cut sample of Carrara marble under triaxial loading. The location of the FO cables attached to the sample's surface is shown as black and purple curves on the hanging wall and as cyan and black curves on the footwall. (b) The distributed strain sensing (DSS) layout is shown on an unwrapped perspective.

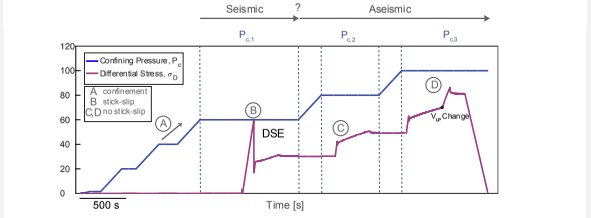

Figure 2. Temporal evolution of the confining pressure P_c and differential stress σ_1–σ_3 during the experiment. The three frictional tests are depicted with $P_{c,1}$, $P_{c,2}$, and $P_{c,3}$ and the stick slip event DSE.

Mechanical Data and Numerical Model

$P_{c,1}$: The fault was **seismic** with **nucleation size $h_0^* < L$**

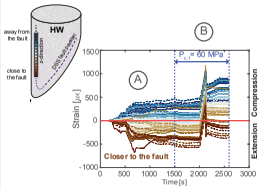

Figure 3. Spatio-temporal evolution of the DSS axial strain of the hanging wall (HW).

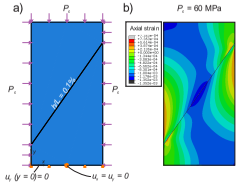

Figure 4. (a) FEM model used to simulate contact stresses in a triaxial with curved interface geometries. (b) Axial stress (LE22 in ABAQUS) through the sample for confining pressure $P_{c,1}$= 60 MPa.

C D $P_{c,2}$, $P_{c,3}$: Our hypothesis that **increased normal stress σ_n** would lead to **smaller nucleation size h^*** and therefore dynamic nucleation was not confirmed.

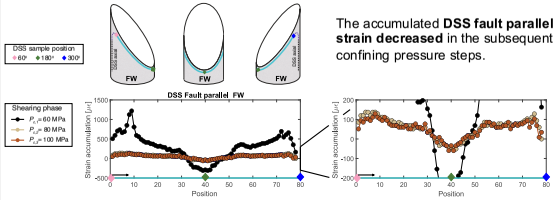

The accumulated **DSS fault parallel strain decreased** in the subsequent confining pressure steps.

Figure 6 . Spatio-temporal evolution of fault parallel strain (DSS fp strain) of FW during the three shearing phases of the peak friction experiment.

Surface Characterization

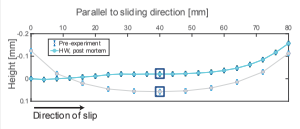

Figure 5. Height measurements with stylus profilometry of the HW fault interface (pre and post experimental).

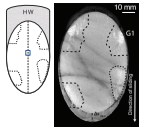

Figure 6. Image of the post-mortem fault surface of the HW.

A The fault has an initial curvature ratio of **h/L= 0.1 %.** This **central asperity** affected the DSS axial strain and **dominated the contact conditions at $P_{c,1}$ (A,B)**.

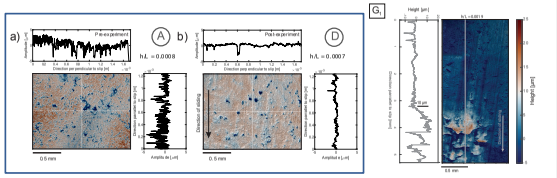

Figure 7. Optical Profilometry images of two sections in the center of the central asperity of the HW (a) pre-experimental (b) post-experimental and (G_1) a gouge location.

The **central asperity smoothened due to wear after the DSE**. Gouge has been deposited closer to the fault periphery. The gouge accommodates strain in the shear bands, resulting in low DSS fault parallel strain.

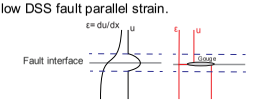

Figure 8. Schematics of the effect of gouge on the strain and slip during the subsequent steps of the experiment.

$(a-b) > 0$ (velocity strengthening (vs)

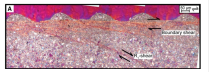

Figure 9. Transmitted light micrograph of a gouge shear band (*by Verberne et al., 2014*).

Conclusions

- Axial DSS measurements showed extensional strain during confinement. Stylus profilometry revealed a central asperity with h/L = 0.1%. This strain heterogeneity due to the asperity was further confirmed by our FEM model. **This asperity dominated the contact conditions and led to dynamic nucleation (DSE).**
- After the DSE, the central asperity was worn and gouge was deposited. The DSS fp strain decreased. **The new contact conditions were dominated by the gouge** and no dynamic nucleation was observed. The **vs gouge**(4) **resulted to (*a-b*) changes** and therefore **aseismic conditions**.

References

1. Selvadurai, P. A., Galvez, P., Mai, P.M., Glaser, S.D., 2023. Modelling frictional precursory phenomena using a wear-based rate- and state dependent friction model in the laboratory. Tectonophysics 847. doi:10.1016/j.tecto.2022.1011 229689
2. Aubry, J., Passelègue, F.X., Escartin, J., Gasc, J., Deldicque, D., Schubnel, A., 2020. Fault Stability Across the Seismogenic Zone. Journal of Geophysical Research: Solid Earth 125. doi:10.1029/2020JB019670
3. Rubin A. and Ampuero J. 2008. Earthquake nucleation on (aging) rate and state faults, Journal of Geophysical Research: Solid Earth 110. doi: 10.1029/2005JB003686
4. Verberne, B.A., Spiers, C.J., Niemeijer, A.R., De Bresser, J.H., De Winter, D.A., Plümper, O., 2014. Frictional Properties and Microstructure of Calcite-Rich Fault Gouges Sheared at Sub-Seismic Sliding Velocities. Pure and Applied Geophysics 171, 2617–2640 doi:10.1007/s00024-013-0760-0

The Life Cycle of an Asperity: Insights from the Laboratory

Sofia Michail[1], P.A. Selvadurai[1], M. Rast[2] , A.F. Salazar Vásquez[1,3], P. Bianchi[1], C. Madonna[4], S. Wiemer[1]

[1]Swiss Seismological Service , ETH Zurich; [2]Geological Institute, ETH Zurich; [3]School of Architecture, Civil Engineering, Landscape Architecture Spatial Planning, Eastern Switzerland University of Applied Sciences, [2,4]Rock Physics and Mechanical Laboratory, Department of Earth Sciences, ETH Zurich

Introduction

Faults in nature exhibit **complex surface characteristics**, such as the presence of contact asperities, which affect the potential for **earthquake nucleation**. A common metric to study frictional stability is the nucleation size *h**, which can change due to spatial heterogeneity(1) and wear. Here we use novel laboratory methods to investigate parameters controlling *h** (2,3) and how they likely changed during our experiment. **Wear** created surface conditions that **eliminated off-fault strain** and **nullified the seismogenic potential of the fault**.

$$h^* \sim \frac{GD_c}{(b-a)\sigma_n}$$

- G : Shear modulus
- $(b-a)$: Rate and state friction parameter(3)
- σ_n : Normal stress

Methodology

We performed a triaxial experiment at sequentially increasing confining pressures ($P_{c,i}$: i = 60, 80, 100 MPa) on a saw-cut Carrara marble sample.

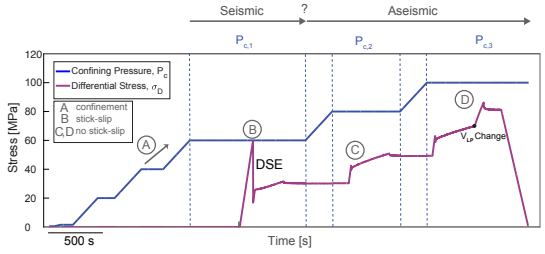

Figure 1. Temporal evolution of the confining pressure P_c and differential stress $\sigma_1-\sigma_3$ during the experiment. The three frictional tests are depicted with $P_{c,1}$, $P_{c,2}$, and $P_{c,3}$ and the stick slip event DSE.

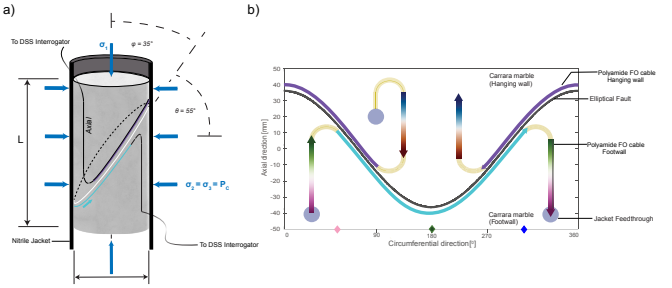

Figure 2. (a) Schematic representation of the saw-cut sample of Carrara marble under triaxial loading. The location of the FO cables attached to the sample's surface is shown as black and purple curves on the hanging wall and as cyan and black curves on the footwall. (b) The distributed strain sensing (DSS) layout is shown on an unwrapped perspective.

Mechanical Data and Numerical Model

$P_{c,1}$: The fault was **seismic** with **nucleation size $h_0^* < L$**

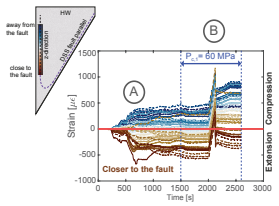

Figure 3. Spatio-temporal evolution of the DSS axial strain of the hanging wall (HW).

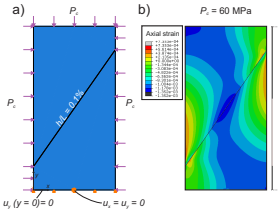

Figure 4. FEM model used to simulate contact stresses in a triaxial with curved interface geometries. (b) Axial stress (LE22 in ABAQUS) through the sample for confining pressure $P_{c,1}$= 60 MPa.

C D

$P_{c,2}$, $P_{c,3}$: Our hypothesis that **increased normal stress σ_n** would lead to **smaller nucleation size *h**** and therefore dynamic nucleation was not confirmed. The **DSS fault parallel strain decreased** in the subsequent confining pressure steps.

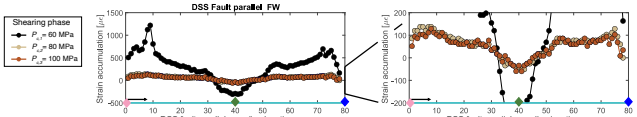

Figure 6 . Spatio-temporal evolution of fault parallel strain of FW during the three shearing phases of the peak friction experiment.

Surface Characterization

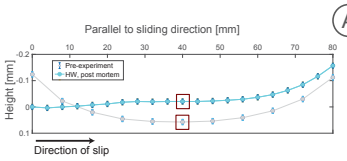

Figure 5. Height measurements with stylus profilometry of the HW fault interface (pre and post experimental).

The fault interface has an initial curvature ratio of ***h/L*= 0.1 %.** This **central asperity** affected the DSS axial strain and **dominated the contact conditions at $P_{c,1}$ (A,B)**.

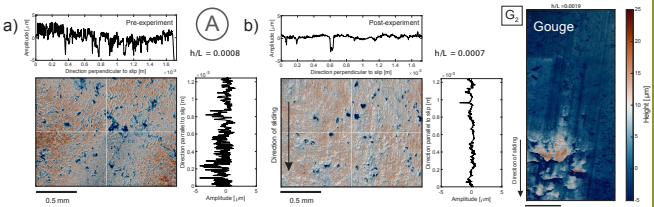

Figure 7. Optical Profilometry images of two sections in the center of the central asperity of the HW (a) pre-experimental (b) post-experimental and (G_2) a gouge location.

The **central asperity smoothened due to wear after the DSE**. Gouge has been deposited closer to the fault periphery. The gouge accommodates strain in the shear bands, resulting in low DSS fault parallel strain.

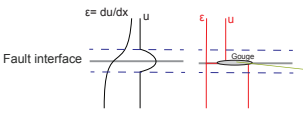

Figure 8. Schematics of the effect of gouge on the strain and slip during the subsequent steps of the experiment.

$(a-b) > 0$ velocity strengthening (vs)

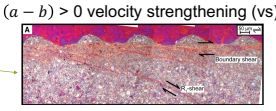

Figure 9. Transmitted light micrograph of a gouge shear band (by Verberne et al., 2014).

Conclusions

- **Axial DSS** measurements showed **extensional strain** during confinement. Stylus profilometry revealed a **central asperity with h/L = 0.1%.** This strain heterogeneity due to the asperity was further confirmed by our **FEM model**. **This asperity dominated the contact conditions and led to dynamic nucleation (DSE).**
- After DSE, the **central asperity was worn** and **gouge was deposited**. The **DSS fault parallel strain decreased**. **The new contact conditions were dominated by the gouge** and no dynamic nucleation was observed. The **vs gouge(4) resulted to *(a-b)* changes** and therefore **aseismic conditions**.

References

1. Selvadurai, P.A., Galvez, P., Mai, P.M., Glaser, S.D., 2023. Modelling frictional precursory phenomena using a wear-based rate- and state-dependent friction model in the laboratory. Tectonophysics 847. doi:10.1016/j.tecto.2022.1011 229689
2. Aubry, J., Passelègue, F.X., Escartín, J., Gasc, J., Deldicque, D., Schubnel, A., 2020. Fault Stability Across the Seismogenic Zone. Journal of Geophysical Research: Solid Earth 125. doi:10.1029/2020JB019670
3. Rubin A. and Ampuero J., 2005. Earthquake nucleation on (aging) rate and state faults, Journal of Geophysical Research: Solid Earth 110. doi: 10.1029/2005JB003686
4. Verberne, B.A., Spiers, C.J., Niemeijer, A.R., De Bresser, J.H., De Winter, D.A., Plümper, O., 2014. Frictional Properties and Microstructure of Calcite-Rich Fault Gouges Sheared at Sub-Seismic Sliding Velocities. Pure and Applied Geophysics 171, 2617–2640. doi:10.1007/s00024-013-0760-0

Partner/Sponsor:

FEAR Modeling Working Group

The aims of the FEAR Modeling Working Group in the past year are:

- Quasi-static and Quasi-dynamic modeling of pre-seismic phase: advanced simulations of the preparatory phase preceding seismic events. This included investigating slow slip episodes under Bedretto-scale conditions.
- Full dynamic modeling of co-seismic ruptures: extensive simulations were performed to model earthquake ruptures during the seismic event, focusing on events up to magnitude $M < 1$.
- Modeling nucleation and rupture propagation: The group investigated the complex processes of earthquake initiation and propagation, considering the evolution of seismicity and the effects of poroelasticity, pre-existing fault structures, and injection protocols.
- Real-time forecasting of injection-induced seismicity: In collaboration with other projects at the SED, the WG developed and tested a framework to model injection-induced seismicity in real-time and to forecast the expected seismicity.
- Collaborative efforts with the Laboratory and Monitoring Working Group: this partnership has enabled the integration of experimental findings with computational models, facilitating a robust comparison and validation process.

Modeling Working Group Highlights

In the past year, the FEAR Modeling Working Group made significant strides in understanding the intricate processes leading to seismic events through a combination of novel laboratory techniques and advanced numerical modeling.

- Development of 3D quasi-static models: we developed a model closely representing the MC fault zone as observed in the field and we performed simulations with the aim of testing hypothesis and help the experimental design of the FEAR experiments.
- Innovative approach to fault rupture dynamics: the prediction that seismic rupture can initiate on velocity-strengthening faults. This finding challenges conventional understanding and opens new avenues for predicting earthquake behavior under diverse geological conditions.
- Critical insights from numerical modeling: Numerical simulations conducted by the group underscored the essential nature of accurately defining poroelastic constants (such as Biot and Skempton coefficients) and frictional properties (both static and dynamic friction) through rigorous laboratory measurements.
- Integration and comparison with laboratory experiments: they focused on deformation localization during triaxial failure tests. This approach provided crucial experimental validation for theoretical models, elucidating how fault structures evolve under stress and contribute to seismic activity.
- Development of a poro-mechanical model: this model facilitated a deeper understanding of how fluid pressure interacts with fault zones, influencing earthquake dynamics. By incorporating fluid dynamics into mechanical models, the group advanced insights into the complex interplay between geological fluids and seismicity.
- Role of permeability barriers in seismic activity: different fluid conditions were found to lead to foreshock-mainshock sequences or earthquake swarms, each with distinct seismic moment and migration velocities (Figure 17).

- Dynamic modeling of pressurized fault patches: by modeling dynamic rupture propagation along fault patches pressurized by injected fluids, they determined the spatial profile of normal stress influenced by pore pressure. This investigation distinguished between self-arresting and run-away ruptures, crucial for understanding maximum event magnitudes.
- Synthetic seismograms for rupture dynamics: this study provided the opportunity to examine how significant rupture deceleration in self-arresting events contrasts with the abrupt cessation of accelerating ruptures, offering insights into the seismic waveforms radiated by induced earthquakes during FEAR experiments in collaboration with the Monitoring Working Group (Figure 18).
- Source parameters estimation: The group implemented the SPAR (Source PARameters estimator) software for application to the network and geometry of the Bedretto stations (i.e., geophones, accelerometers). SPAR permits to retrieve the seismic source parameters (Seismic Moment, Corner frequency, High-frequency decay exponent) and the anelastic attenuation factor (Green function Q-factor) from spectral inversions of the observed ground motion. In Figure 19, the outputs of this software for the M-zero event induced in the VALTER volume at the end of April 2024.
- Real-time analysis and modeling of seismicity: the dashboard platform included comparison of hydraulic and seismic parameters, spatial visualization of induced seismicity, analysis of the frequency-magnitude distribution in real-time, as well as the results of forecasted rate of seismicity and probability of occurrence of a set magnitude. In Figure 20 and 21, some screenshots of the dashboard for frequency-magnitude distribution real-time analysis for the M-zero experiment in April 2024.

Modeling Working Group Next Steps

Next steps for the Modeling WG relies on continuing the implementation and the application of numerical codes to synthetic modeling of FEAR target faults as well as the modeling of the data recorded during the first FEAR experiment consisting of generating a Mw 0 in the VALTER volume.

- Dynamic modeling of the 3D rupture propagation along a pressurized fault patch with spatial heterogeneities of pre-stress and frictional parameters.
- Dynamic simulation of M-zero assuming simple (single fault) dynamic source model and wave propagation in a fractured medium. Study of the effect of the fractured medium on radiated waveforms, in terms of ground motion and peak values (i.e., PGV).
- Dynamic simulation of M-zero assuming rupture propagation on a fault network (complex source).
- Interpretation and modeling of M-zero nucleation (which are the pore pressure conditions that allowed the occurrence of M-zero event?
- Study of Near field versus far-field seismic radiation starting from synthetic models to recorded data.
- Study the high frequency content of observed data (starting from the catalog of seismicity located with hypo-DD) to discriminate among the self-arresting versus run-away ruptures and accounting for potential attenuation effects.
- Computation of focal mechanisms and hybrid MT for observed induced seismicity.
- What is the influence of constitutive law formulation and chosen parameters on rupture modes (crack-like vs pulse-like), rupture velocity, and slip rate history?

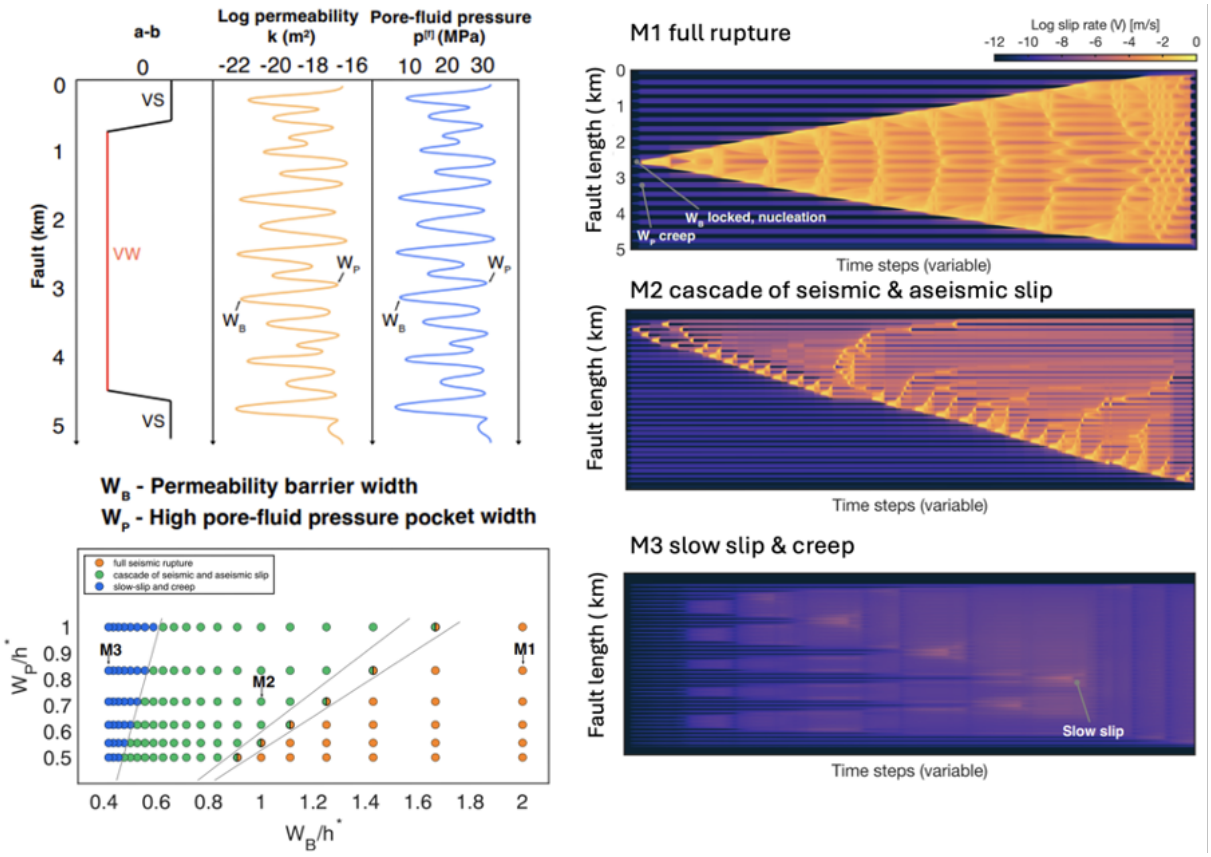

Figure 17: Permeability barrier width Wb, pockets of high pore-fluid pressure width Wp and nucleation size h* are key parameters in controlling the transition from full seismic rupture to cascade of seismic and aseismic slip.

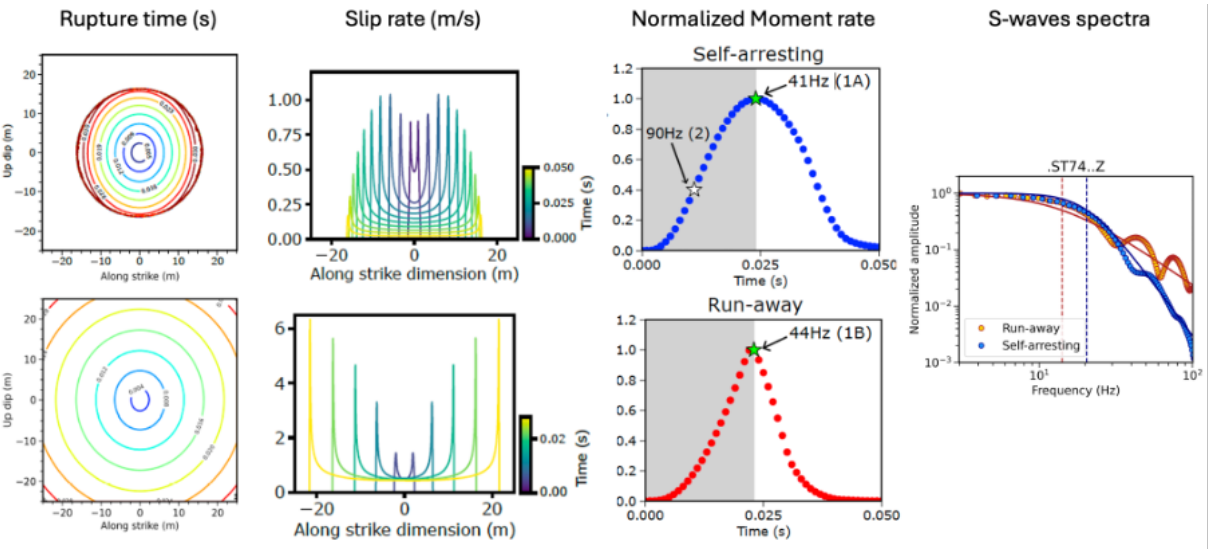

Figure 18: Example of a self-arresting rupture model (top panels) and a run-away model (bottom panels) in terms of rupture time, slip rate and moment rate. On the right panel, the comparison is made in terms of normalized displacement spectra of synthetic S-wave waveforms computed with 3D dynamic rupture simulations: the blue line shows the steeper slope in the high-frequency decay for a self-arresting rupture, while the orange line indicates a lower slope in the high-frequency decay due to larger high-frequency radiation from a runaway earthquake.

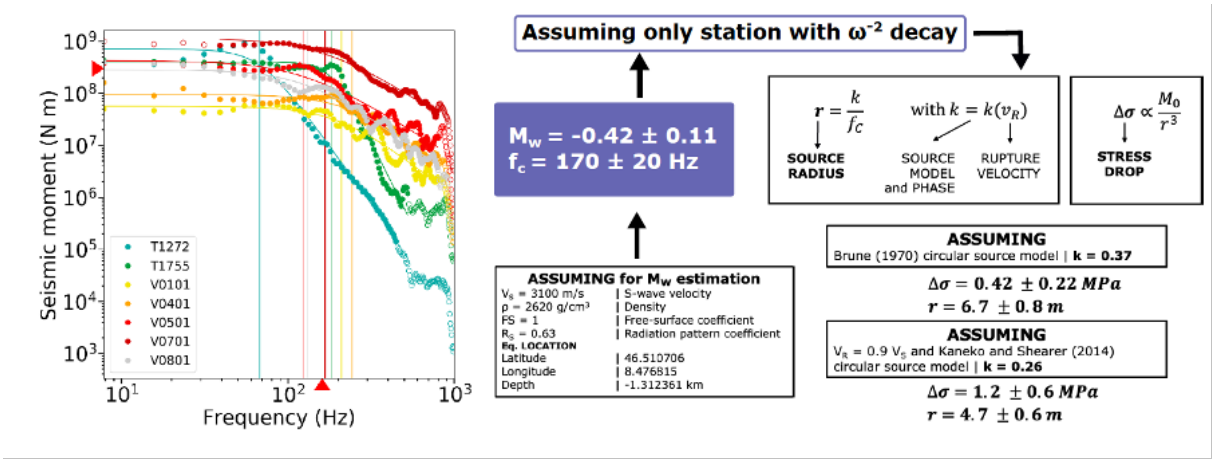

Figure 19: Example of S-waves spectral inversion (from Supino et al 2019 method) done for the M-zero event induced on April 30 in the VALTER volume. Adopted sensors are located a few hundred meters far from the source. Only station T1272 is almost 1.5 km away and shows a significant attenuation effect.

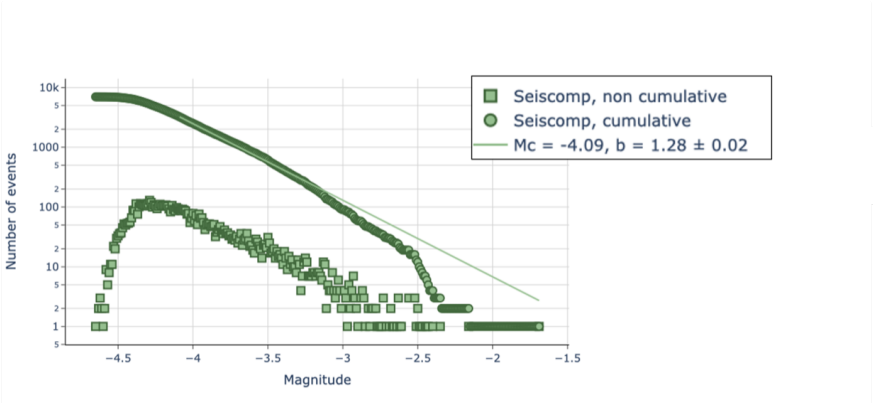

Figure 20: Real-time plot of the frequency-magnitude distribution and fit with Guthenberg-Richter empirical law.

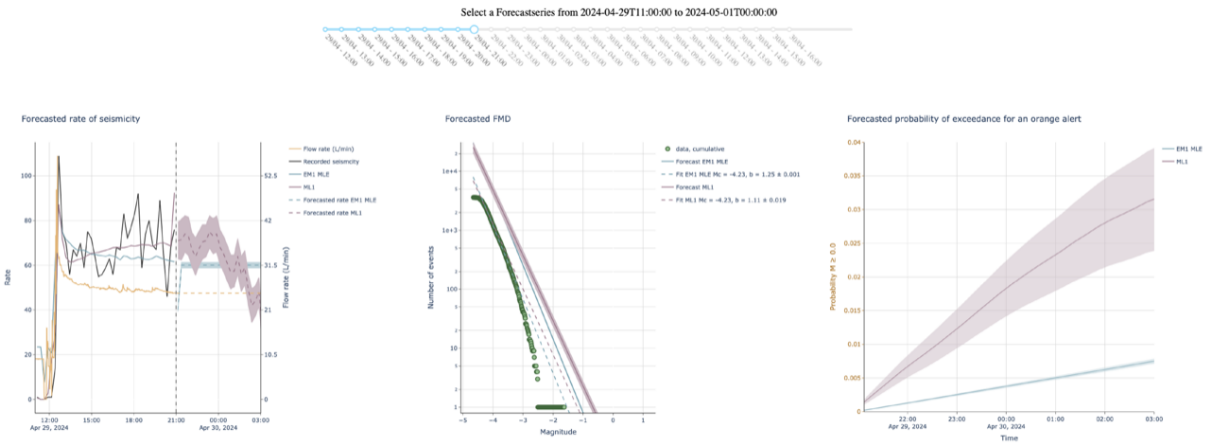

Figure 21: Example of forecast model results, from left to right, fitted and forecasted rate of seismicity, fitted and forecasted frequency-magnitude distribution, and forecasted probability of occurrence for a M-zero event.

- Continued Development of 3D models of injection, modeling slip and pressure in experiments with a focus on the pre-seismic phase or slow slip. Understanding of dilatancy response (if observed).
- Investigate the first order geomechanical response of a fault zone subjected to aseismic and seismic slip through the use of semi-anlytical solutions.
- Improve forecasting models to account for extreme (tail) events and to account for more information from the field (e.g. strain)

Ongoing research of the FEAR Modeling Working Group (presented in the following pages)

Physics-based modeling of FEAR experiment
Jiang, D., Pio Rinaldi, A., Clasen Repollés, V., Jalali, M., Ceccato, A., and FEAR team

---

Exploring the interplay of fault slip, poroelasticity, and permeability barriers
Ye, J., Dal Zilio, L., Giardini, D.

Fracture energy partitioning in a multiscale fracture network for M 1 event
Hendrawan Palgunadi, K., Dal Zilio, L., Tinti, E., Cocco, M., Gabriel, A.A., Martin Mai, P.

Understanding the Regional Stress of the BedrettoLab using Advanced 3D Numerical Modelling
Ufrecht, S., Hamdi, P., Achtziger, P., Amann, F.

Physics-based modeling of FEAR experiment

Danyang Jiang[1], Antonio Pio Rinaldi[1], Victor Clasen Repollés[1], Mohammadreza Jalali[2], Alberto Ceccato[3] and FEAR team
[1]Swiss Seismological Service, ETH Zurich; [2]Engineering Geology and Hydrogeology, RWTH Aachen University;
[3]Structural Geology and Tectonics Group, Geological Institute, Department of Earth Sciences, ETH Zurich

1 Introduction

The FEAR experiment aims to assist scientists in understanding the enigmatic earthquake mechanism. To better comprehend the potential outcomes of the experiment, we have developed a TOUGH-FLAC model to simulate potential scenarios, incorporating all available information at present. The present workflow can be easily rerun with additional measurements expected in the future, providing further insight.

2 Geological structure

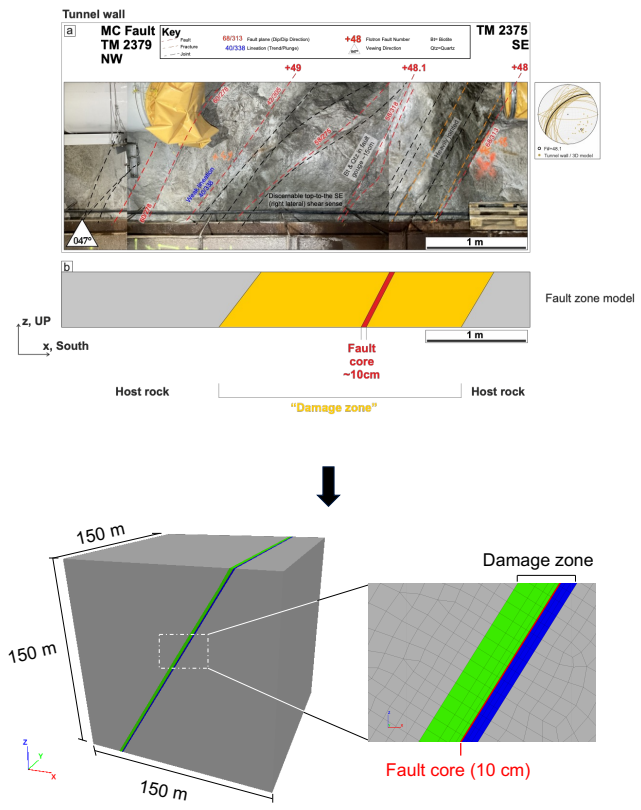

Upper panel shows the geological characterization of the FEAR volume. Bottom panel shows the numerical mesh transferred from geological knowledge.

3 Method

- Two-way sequential coupling simulation by TOUGH-FLAC
- Bilinear strain-softening ubiquitous-joint constitutive model
- Permeability changes
- Initial and boundary conditions are taken from BadBoy

4 Injection protocol

We are injecting fluids at BEF6 according to the protocol shown below.

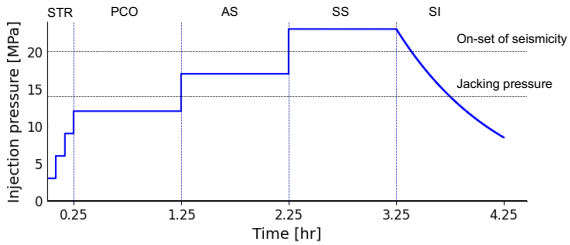

5 Preliminary results

Below is strain increment profile on the fault immediately following the SS phase. The displacement around the injection point shows a stepwise trend corresponding to the injection protocol.

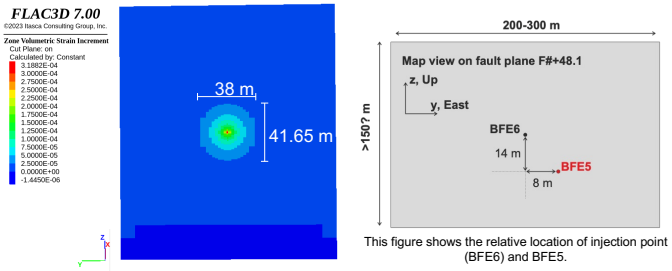

This figure shows the relative location of injection point (BFE6) and BFE5.

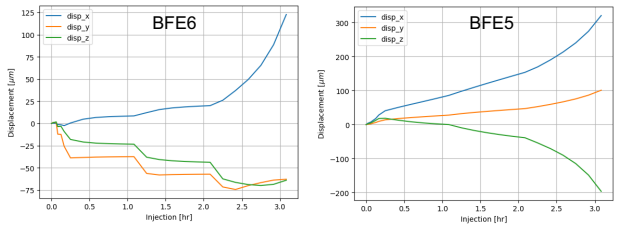

Left panel shows displacement change at injection point. Right panel shows the displacement change at BFE5.

Prior to shutting down the system, the pressurized patch of the fault ~ 47.662 x 62.4 m.

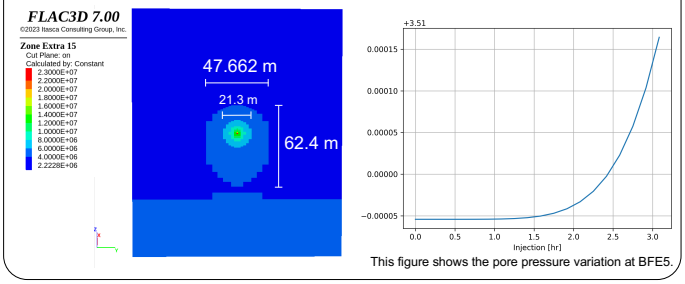

This figure shows the pore pressure variation at BFE5.

Future Work:

1. update the initial conditions and boundary conditions based on the measurements.
2. calibrate the model to get plastic deformation on the faut.

Exploring the interplay of fault slip, poroelasticity, and permeability barriers

Jiayi Ye[1], Luca Dal Zilio[2], Domenico Giardini[1]

Email: jiayi.ye@erdw.ethz.ch

1 Seismology and Geodynamics, Institute of Geophysics, ETH Zürich, Zürich, Switzerland
2 Nanyang Technological University & Earth Observatory of Singapore

Introduction

Observations suggest the importance of fault-zone fluid flow in producing earthquake swarms, foreshocks, and aftershocks. However, modeling the interaction between pore-fluid pressure and fault slip is challenging as they are dynamic and non-linear.

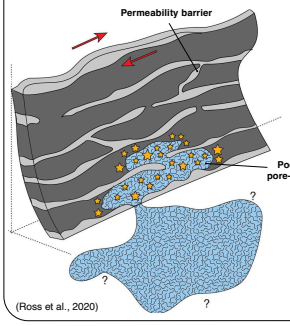

(Ross et al., 2020)

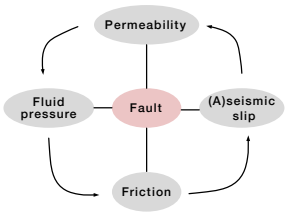

To explore the fully coupling system between fluid flow and fault slip over the earthquake cycle in permeable faults, we developed a 2D anti-plane fault model embedded in a poro-visco-elasto-plastic compressible medium.

Model setup

We use numerical code H-MEC (Hydro-Mechanical Earthquake Cycle), a unified, continuum-based model, which incorporates a staggered finite difference marker-in-cell (SFD-MIC) method (Dal Zilio et al., 2022) and invariant rate-and-state-friction law.

$$\tau_s = f\,\sigma_n = \left[f_0 + a\,ln\left(\frac{V}{V_0}\right) + b\,ln\left(\frac{\Theta V_0}{L}\right)\right](\sigma - p^{[f]})$$

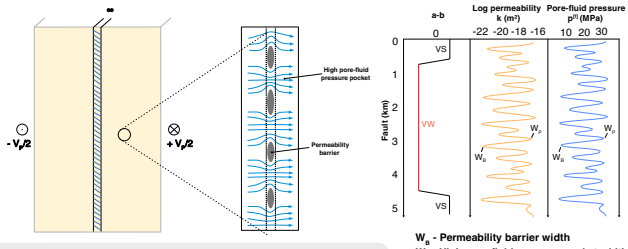

W_B ➡ Lower permeability ➡ Lower fluid pressure ➡ Unstable slip ➡ Seismic
W_P ➡ Higher permeability ➡ Higher fluid pressure ➡ Stable creep ➡ Aseismic

W_B - Permeability barrier width
W_P - High pore-fluid pressure pocket width

Results

Static permeability

Model M1- Full seismic rupture

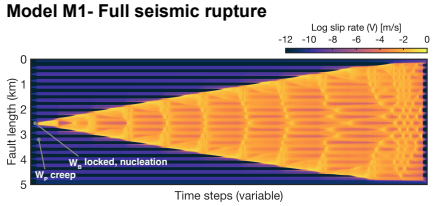

Model M2 - Cascade of seismic & aseismic slip

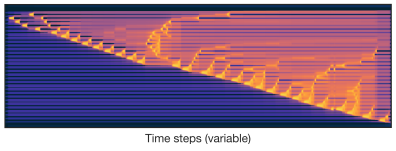

Model M3 - Slow-slip and aseimsic creep

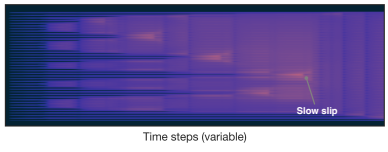

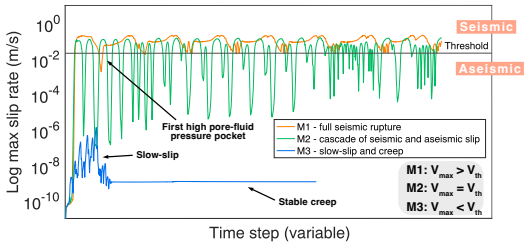

Permeability barrier width W_B, pockets of high pore-fluid pressure width W_P and nucleation size h^* are key parameters in controlling the transition:

- **Full seismic rupture**
- **Cascade of seismic and aseismic slip**
- **Slow-slip and aseismic creep**

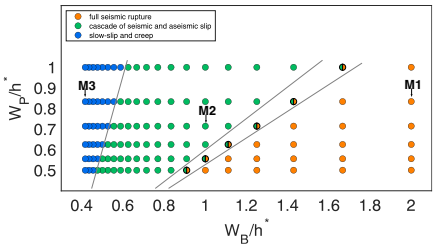

Threshold velocity
(Rubin and Ampuero, 2005)

$$V_{th} = \frac{2\,a\,p_{eff}\,c_s}{\mu}$$

Nucleation size
(Rubin and Ampuero, 2005)

$$h^* = \frac{2\,\mu\,b\,l}{\pi\,(b-a)^2\,p_{eff}}$$

Permeability evolution

Permeability evolution: permeability increases with slip and decreases from healing and sealing processes over time (Zhu et al., 2020):

$$\frac{\partial k^*}{\partial t} = -\frac{V}{L}(k^* - k_{max}) - \frac{1}{T_k}(k^* - k_{min})$$

Model M4 - Healing time T_k = 1 week

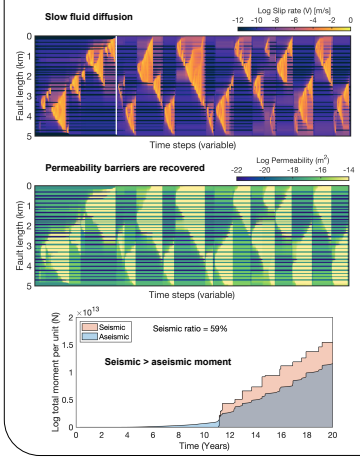

Model M5 - Healing time T_k = 1 year

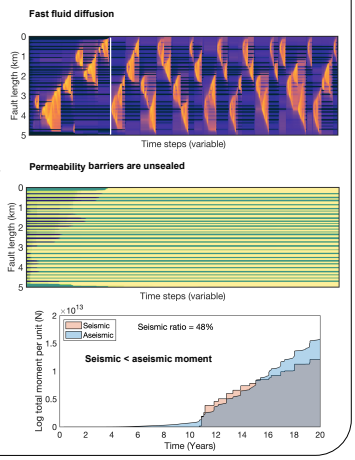

Back-propagating rupture

Model M6

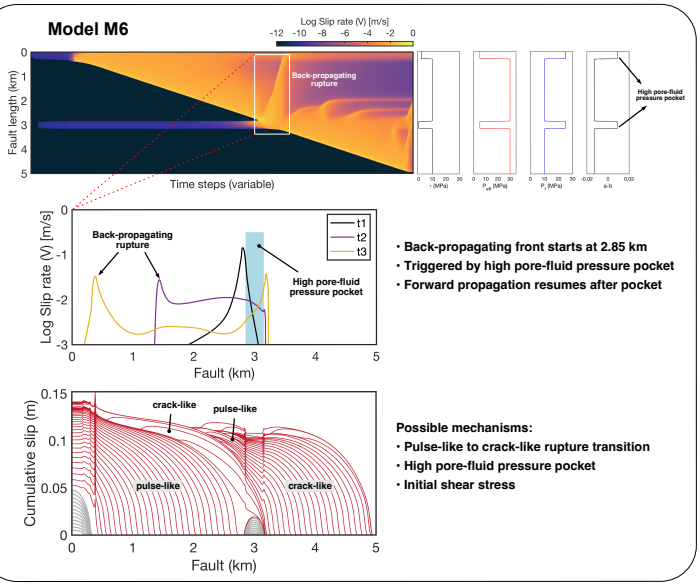

- **Back-propagating front starts at 2.85 km**
- **Triggered by high pore-fluid pressure pocket**
- **Forward propagation resumes after pocket**

Possible mechanisms:

- **Pulse-like to crack-like rupture transition**
- **High pore-fluid pressure pocket**
- **Initial shear stress**

Hydro-mechanical modeling

The representation of dynamic deformation in a continuous medium is given by the following set of fundamental mass and momentum conservation equations:

Total momentum of solid and fluid matrix

$$\nabla \cdot \underline{\boldsymbol{\sigma}} + \boldsymbol{g}\,\rho^{[t]} = \rho^{[t]}\frac{D^{[s]}\boldsymbol{v}^{[s]}}{Dt}$$

Fluid momentum

$$\boldsymbol{v}^{[D]} = -\frac{k^{[\phi]}}{\eta^{[f]}}\left(\nabla p^{[f]} - \rho^{[f]}\left(\boldsymbol{g} - \frac{D^{[f]}\boldsymbol{v}^{[f]}}{Dt}\right)\right)$$

Fully compressible fluid mass

$$\nabla \cdot \boldsymbol{v}^{[D]} = \frac{\alpha}{K^{[d]}}\left(\frac{D^{[s]}p^{[t]}}{Dt} - \frac{1}{B}\frac{D^{[f]}p^{[f]}}{Dt}\right) + \frac{p^{[t]} - p^{[f]}}{\eta^{[\phi]}(1-\phi)}$$

Fully compressible solid mass

$$\nabla \cdot \boldsymbol{v}^{[s]} = -\frac{1}{K^{[d]}}\left(\frac{D^{[s]}p^{[t]}}{Dt} - \alpha\,\frac{D^{[f]}p^{[f]}}{Dt}\right) - \frac{p^{[t]} - p^{[f]}}{\eta^{[\phi]}(1-\phi)}$$

Conclusion

1. Permeability barrier width W_B, pocket of high pore-fluid pressure width W_P, and nucleation size h^* control the nucleation and propagation of seismic and aseismic slip.
2. Rupture of sealed permeability barriers leads to the injection and redistribution of fluid through the fault zone, which control the seismic/aseismic moment release.
3. Rupture propagation to pockets of high pore-fluid pressure induces transition from pulse-like to crack-like rupture, leading to back-propagation rupture.

Reference:
Dal Zilio, Luca, et al. "Hydro-mechanical earthquake cycles in a poro-visco-elasto-plastic fluid-bearing fault structure." Tectonophysics 838 (2022): 229516.
Zhu, Weiqiang, et al. "Fault valving and pore pressure evolution in simulations of earthquake sequences and aseismic slip." Nature communications 11.1 (2020): 4833.
Rubin, Allen M., and J-P. Ampuero. "Earthquake nucleation on (aging) rate and state faults." Journal of Geophysical Research: Solid Earth 110.B11 (2005).
Ross, Zachary E., et al. "3D fault architecture controls the dynamism of earthquake swarms." Science 368.6497 (2020): 1357-1361.

Fracture energy partitioning in a multiscale fracture network for M~1 event

Kadek Hendrawan Palgunadi[1,6*], Luca Dal Zilio[2], Elisa Tinti[3], Massimo Cocco[4] , Alice-Agnes Gabriel[5], Paul Martin Mai[6]

[1]Swiss Seismological Service, ETH Zurich; [2]Nanyang Technological University, Singapore; [3]Dipartimento di Scienze della Terra, La Sapienza Università di Roma, Rome, Italy; [4]Istituto Nazionale di Geofisica e Vulcanologia, Rome, Italy; [5]Scripps Institute of Oceanography, UCSD, USA, Saudi Arabia; [6]Physical Science and Engineering, King Abdullah University of Science and Technology, Saudi Arabia.

*kadek.palgunadi@sed.ethz.ch

1 Introduction

Faults, with their intricate geometry of intersected multiscale segments and fractures, play a crucial role in the spatio-temporal evolution of earthquake rupture processes, both on the main fault and off-fault fractures (Okubo et al., 2019; Gabriel et al., 2023; Palgunadi et al., 2024). The Fault Activation and Earthquake Rupture (FEAR) project, a pioneering initiative under the European Research Council (ERC) Synergy, aims to shed light on these complex processes. Conducted by a consortium of scientists from ETH Zurich, RWTH Aachen University, and INGV, the project utilizes the unique Bedretto Underground Laboratory for Geosciences and Geoenergy (BedrettoLab) situated beneath the Swiss Alps.

In the context of FEAR, we investigate how geometrical fault complexity influences earthquake energy partitioning during rupture, a key factor in understanding earthquake source characteristics (Okubo et al., 2019; Cocco et al., 2023). The presence of off-fault fractures is known to contribute significantly to this energy partitioning, dictating the dynamics of earthquake rupture cascades within multiscale fracture networks. This study presents calculations of energy partitioning across three dynamic rupture cascade scenarios, varying in the orientation and prestress conditions of the main fault and off-fault fractures, directly linking our findings to the core objectives of the FEAR project.

By exploring these scenarios, we aim to contribute to the FEAR project overarching goal of improving earthquake physics. Through hydraulic stimulation experiments in BedrettoLab, FEAR endeavors to initiate small, non-damaging earthquakes, providing a near-field, high-resolution insight into the physics of earthquake processes. This research aligns with FEAR's mission to enhance our understanding of how earthquakes start and stop, advancing our knowledge on earthquake predictability and the safe utilization of geoenergy, by meticulously examining the partitioning of fracture energy in the fault system.

2 Method and Model Overview

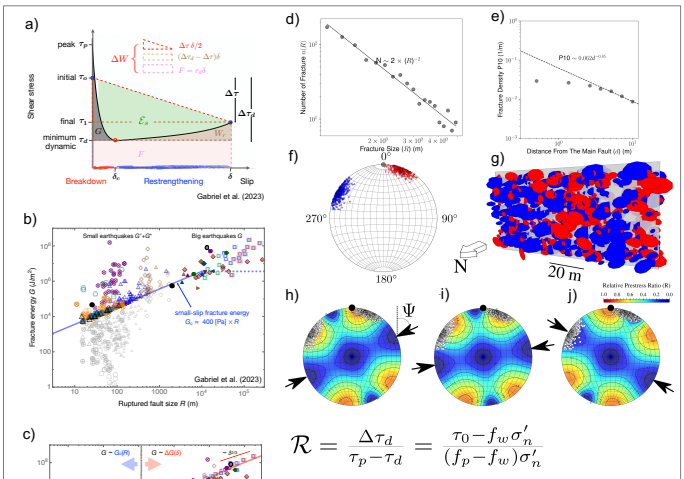

$$\mathcal{R} = \frac{\Delta\tau_d}{\tau_p - \tau_d} = \frac{\tau_0 - f_w\sigma_n'}{(f_p - f_w)\sigma_n'}$$

Figure 1. Assumptions and numerical model used in this study. a) The earthquake energy budget including dynamic weakening and restrengthening. b) Linearly scale-dependent fracture energy, composed of a 'small-slip' fault property and continuously increasing 'large-slip' component. c) same as b) but G vs co-seismic slip. d) Power law distribution of discrete fracture network size. e) same as d) but for fracture density. f) Two fracture populations. g) realization of fracture network with a planar fault. h), i), and j) denotes relative stress ratio for favorably prestressed main fault and fractures (Case 1), only fractures (Case 2), and only the main fault (Case 3), respectively.

3 Numerical Parameters

Parameter	Symbol	Value
Direct effect parameter	a	0.01
Evolution effect parameter	b	0.014
Reference slip velocity	V_0	$10^{-6} m/s$
Steady-state friction coefficient at V_0	f_0	0.6
Weakening slip velocity	V_w	$0.1 m/s$
Fully weakened friction coefficient	f_w	0.1
Initial slip rate	V_{ini}	$10^{-16} m/s$
State evolution distance	L	$3 \times 10^{-7} - 9 \times 10^{-5} m$

Scan to see the movies of the three cases

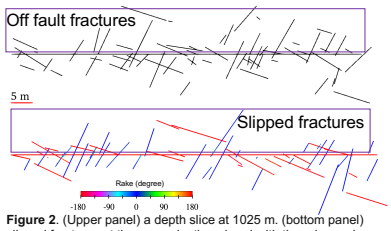

Figure 2. (Upper panel) a depth slice at 1025 m. (bottom panel) slipped fractures at the same depth, colored with the rake angle.

- Employing open-source software SeisSol on supercomputer with average 250k CPUh.
- Using rate and state with fast velocity weakening friction.
- State-evolution distance follow linearly scale fracture size (2 x 10^{-5} x fracture size).
- Assuming fully weakened fractures and main fault.

$$G_{\mathrm{on,off}} = \int_{\Sigma} \left[\int_0^{\delta(\tau_{min})} (\tau(\delta) - \tau_{min}(\delta)) \mathrm{d}\delta \right] \mathrm{d}z$$

- The fracture energy is only calculated on the slipped fractures and main fault (Viesca and Garagash (2015)).

4 Results

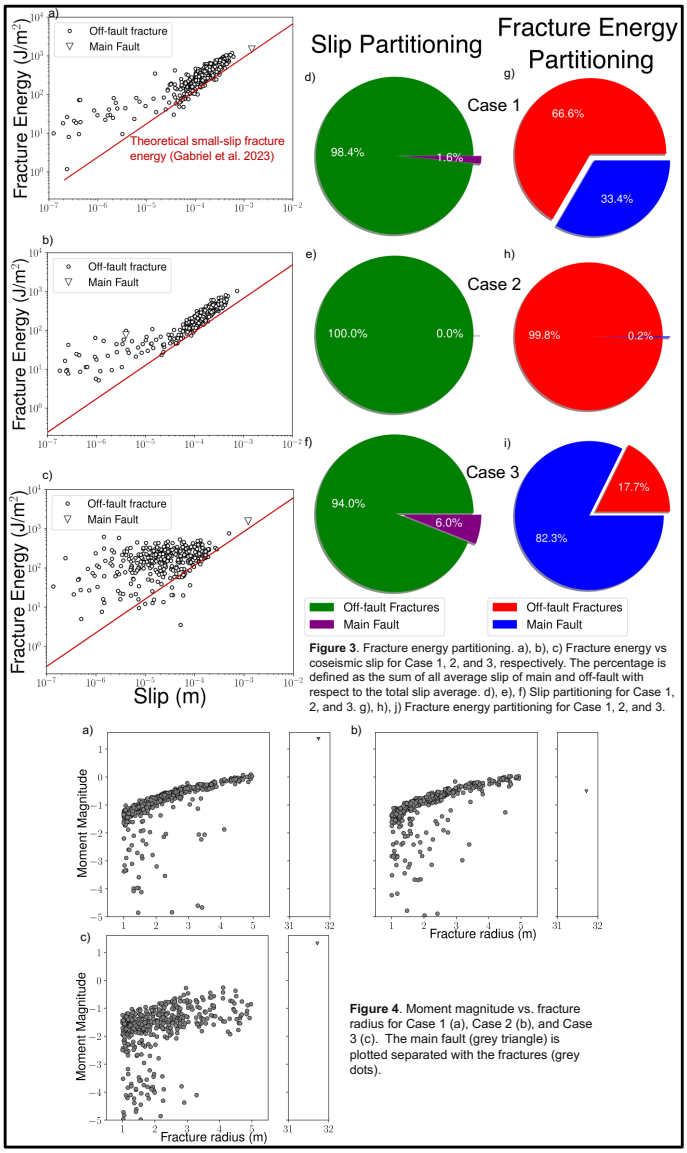

Figure 3. Fracture energy partitioning. a), b), c) Fracture energy vs coseismic slip for Case 1, 2, and 3, respectively. The percentage is defined as the sum of all average slip of main and off-fault with respect to the total slip average. d), e), f) Slip partitioning for Case 1, 2, and 3. g), h), j) Fracture energy partitioning for Case 1, 2, and 3.

Figure 4. Moment magnitude vs. fracture radius for Case 1 (a), Case 2 (b), and Case 3 (c). The main fault (grey triangle) is plotted separated with the fractures (grey dots).

5 Discussions and Conclusion

- Small-scale fracture energy vs. co-seismic slip follows minimum fracture energy approximated from theoretical estimation.
- Fracture energy during rupture cascade activating the main fault (Case 1) is dominated by off-fault fractures.
- In Case 1, although the slip is dominated by more than 98%, the fracture energy of the main fault contributes to more than one-third of the total fracture energy.
- In contrast, the fracture energy for main fault rupture activating the fracture network is dominated by the main fault.
- The fracture energy partitioning may not be correlated with slip partitioning.
- If all surfaces on a fracture slipped, the moment magnitude increases as fracture radius increases.

References

1. Cocco, M., Aretusini, S., Cornelio, C., Nielsen, S.B., Spagnuolo, E., Tinti, E. and Di Toro, G., 2023. Fracture energy and breakdown work during earthquakes. *Annual Review of Earth and Planetary Sciences*, *51*, pp.217-252.
2. Gabriel, A.A., Garagash, D.I., Palgunadi, K.H. and Mai, P.M., 2023. Fault-size dependent fracture energy explains multi-scale seismicity and cascading earthquakes. *arXiv preprint arXiv:2307.15201*.
3. Okubo, K., Bhat, H.S., Rougier, E., Marty, S., Schubnel, A., Lei, Z., Knight, E.E. and Klinger, Y., 2019. Dynamics, radiation, and overall energy budget of earthquake rupture with coseismic off-fault damage. *Journal of Geophysical Research: Solid Earth*, *124*(11), pp.11771-11801.
4. Palgunadi, K.H., Gabriel, A.A., Garagash, D.I., Ulrich, T. and Mai, P.M., 2024. Rupture Dynamics of Cascading Earthquakes in a Multiscale Fracture Network. *Journal of Geophysical Research: Solid Earth (in press)*.
5. Viesca, R.C. and Garagash, D.I., 2015. Ubiquitous weakening of faults due to thermal pressurization. *Nature Geoscience*, *8*(11), pp.875-879.

Partner/Sponsor:

Understanding the Regional Stress of the BedrettoLab using Advanced 3D Numerical Modelling

Simon Ufrecht[1], Pooya Hamdi[1], Peter Achtziger[2], Florian Amann[1]
[1] Chair of Engineering Geology & Hydrogeology, RWTH Aachen, Aachen, Germany
[2] Chair of Engineering Fraunhofer Research Institution for Energy Infrastructures and Geothermal Systems, IEG, Aachen, Germany

Introduction

A numerical stress simulation for the Val Bedretto has been created using the software FLAC3D, based on the in-situ stress measurements at BedrettoLab. The model is 20 km by 17 km,covering the south of the Urseren in addition to the Val Bedretto.
The geometric model is made of an unstructured tetrahedral mesh and was built using DEM from "swissALTI3D" in the software Rhino 6 and the Rhino plugin Griddle. The constructed 3D model is assumed homogenous, elastic and dry and no major structures i.e. faults are modeled. The used rock strength parameters are inferred onto the model region from a nearly complete dataset of Gotthard Base Tunnel region rock published by Loew et al. (2015), but slightly modified for the Rotondo Granite. The model's calculation time renders approximately 270 million years in real time. Besides the BedrettoLab stress measurements, nearly no stress data exists for the Val Bedretto. Regarding the Ticino Alps region, we nearly have no tectonic activity, which impedes working with FPS (Sue et al., 2007; and Labhart, 2005). The main objective of this study is to evaluate the topographical influence of the area on the distribution of stresses around Bedretto Valley.

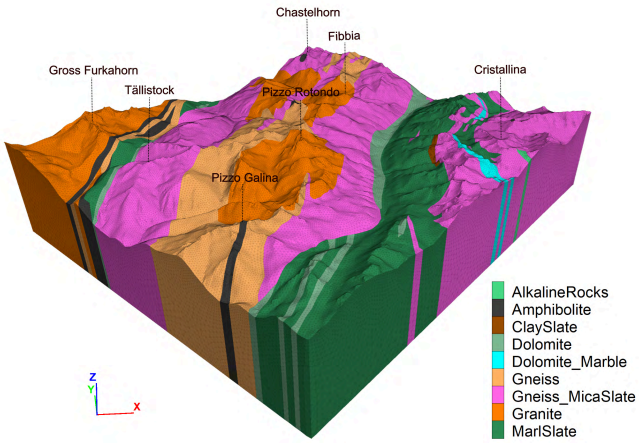

Figure 1: Simplified geotechnical units modeled in FLAC3D Model with annotated peaks. Y-axis points to the northeast

Stress behaviour in the model region and in the Swiss Alps

The model utilizes northwest-southeast compression, with the stress being applied at the northwestern border. This assumption is based on Labhart's characterization of Val Bedretto published in 2005 and equals the first order stress direction of Western Europe as well, mainly caused by the spreading of the North Atlantic Ridge and the collision of the Adriatic and the Eurasian Plate. Momentarily, the Adriatic Microplate is rotated counterclockwise with respect to Europe. As seen in Figure 2, the strike of local horizontal stresses among the Alps follows its curvature, but also changes between the three distinct stress provinces northern Foreland, the Helvetic and Penninic nappes (Kastrup, 2002). There is no wider agreement among the geoscience community regarding the second order stress sources influencing the Alpine stress patterns, as well as the European slab which is subducted below the Adriatic plate (Kastrup, 2002; and Sue et al., 2021). One factor is the Moho's depth, which seems to increase from the northern Alpine foreland to the Alps proper, as seen in Figure 3. The lateral density changes caused by this so-called crustal root could be a reason for extension tectonics to occur in higher parts of the Alps. Additionally, the Alps are uplifted as well, with rates of up to 1.5 mm/a (Kastrup, 2002). Sue et al. 2021 argued a transcurrent stress field in the Central and Western Alps, which is controlled by far-field stress forces mainly caused by the rotation of the Adriatic plate with respect to the European plate, whereas buoyancy forces control extension and compression. The influence of buoyancy forces seems to be largely counterbalanced by the aforementioned rotation of the Adriatic Plate though and extension and uplift are not showing spatial correlation (Sue et al., 2021).

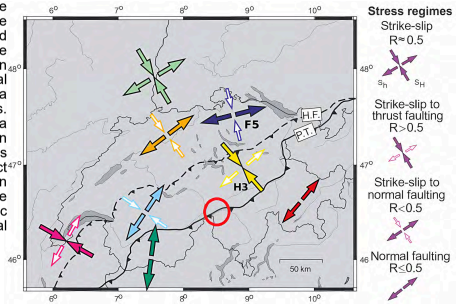

Figure 2: Stress pattern of Swiss Alps, obtained from FPS (Kastrup, 2002). H.F. = Helvetic Front, P.T. = Penninic Thrust. Val Bedretto marked red.

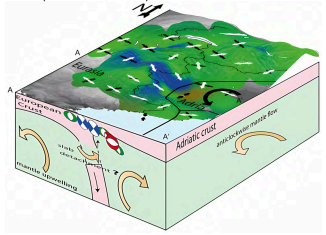

Figure 4: Major tectonic influences on the Swiss Alp's stress field (Sue et al., 2021).

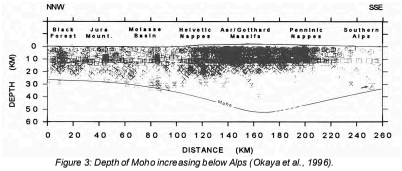

Figure 3: Depth of Moho increasing below Alps (Okaya et al., 1996).

Preliminary Results

The numerical results indicate the transitional state of stress between normal and strike-slip faulting at the Val Bedretto. Rarely, reverse faulting does occur near the surface, agreeing quite well with the in-situ stress measurement data (Ma et al., 2022). At the level of BedrettoLab, the distribution is as follows: 51% strike-slip, 43% normal faulting and 6 % reversed faulting. With increasing depth, the trend changes from a balanced ratio between strike-slip and normal faulting towards strike-slip faulting being dominant at the model's basal boundary. The simulated principal stress direction S1 at BedrettoLab matches the calculated average direction of Smax obtained from the F.E.A.R. borehole BFE_A_05 by 2.6° degrees (Stadler, 2022). Furthermore, the model shows a quasi-linear correlation between overburden / altitude and faulting regime: When comparing the average overburden values at equal level (altitude), normal faulting occurs at high overburden, strike-slip at intermediate overburden and the exact transition between both occurs at an average overburden slightly above the intermediate difference between the normal and strike-slip's average overburden (referred to BedrettoLab altitude).

K-Ratio / Faulting Regime	Dir. Stress [Mpa]	Prin. Stress [Mpa]	Strike/Dip Degrees to N / 0°	S1 Comparison (Stadler)	S1 Comparison (Ma et al.)
Kx	x	S1	S1	BFE-A_05	
Ky	y	S2	S2	SB 2.2 / 2.3	
Faulting	z	S3	S3		6 Boreholes
0.94	25.4	28.6	328.35° / 50.5°	151° ± 23°	
0.54	16.4	24.3	148.91° / 39.5°	77° ± 29°	
Normal	26.9	13.9	58.68° / 0.27°		100° to 110°

Table 1: Stress data at BedrettoLab, compared with borehole Smax direction measurement results (Stadler, 2022; and Ma et al., 2022).

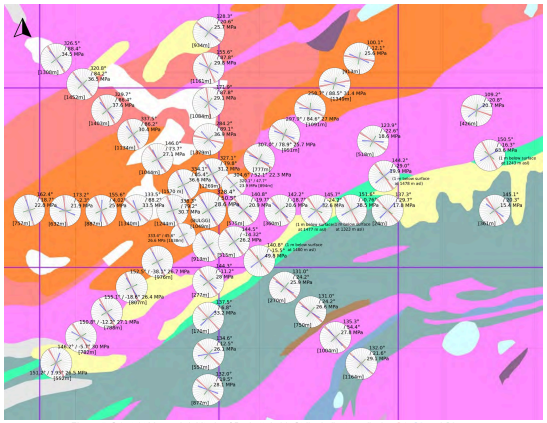

Figure 5: S1 at 1490 m asl. (altitude of BedrettoLab). Strike indicators display S1, S2 and S3. Square brackets show current overburden. Blue outlined quadrant = 5x5 km². Legend in Fig.1.

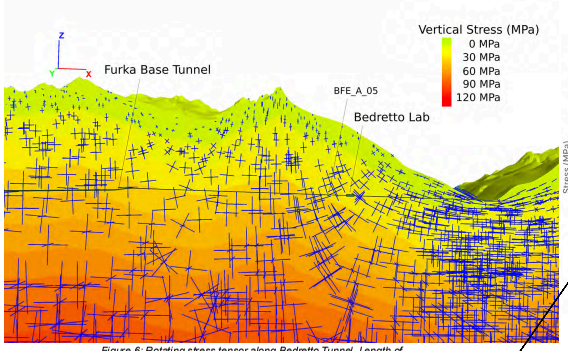

Figure 6: Rotating stress tensor along Bedretto Tunnel. Length of tensor axis corresponds to the amount of compressive stress.

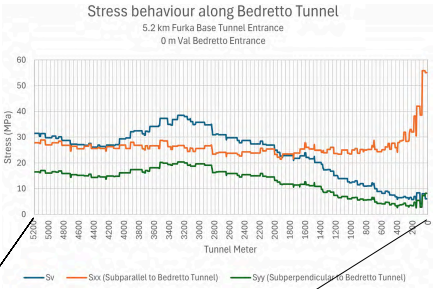

Figure 7: Stress diagram showing directional stresses simulated for the Bedretto Tunnel. BULGG: TM 2000-2100. BFE-A_05: TM 2363.

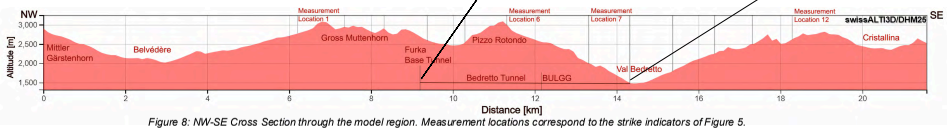

Figure 8: NW-SE Cross Section through the model region. Measurement locations correspond to the strike indicators of Figure 5.

Author's Note: This poster presents parts of the author's upcoming thesis: "Understanding the Regional Stress of the BedrettoLab using Advanced 3D Numerical Modelling." Supervised by Dr. Pooya Hamdi, Dr. Peter Achtziger and Prof. Dr. Florian Amann.

References

- Sue et al. (2007). Extensional neotectonics around the bend of the Central/Western Alps: an overview. International Journey of Earth Science 96 (p.1101-1129), Springer.
- Labhart (2005). Geologischer Atlas der Schweiz – Blatt 1251: Val Bedretto, Bundesamt für Wasser und Geologie.
- Loew et al. (2015). Transient surface deformations caused by the Gotthard Base Tunnel. International Journal of Rock Mechanics & Mining Sciences 75 (p.82-101), Elsevier.
- Kastrup (2002). Seismotectonics and Stress Field Variations in Switzterand. Dissertation at Swiss Federal Institute of Technology Zurich.
- Sue et al. (2021). Present-day geodynamics of the Western Alps: new insights from earthquake mechanisms. Solid Earth 12 (p. 1661-1681), Copernicus Publications.
- Okaya et al. (1996). A lithospheric cross-section through the Swiss Alps-II.Constraints on the mechanical structure of a continent-continent collision zone. International Journey of Geophysics 127 (p.399-414), RAS.
- Stadler (2022). *In situ* stress profiling along Bedretto boreholes via integrated geomechanical approaches. MsC Thesis at ETH Zürich.
- Ma et al. (2022). Multi-disciplinary characterizations of BedrettoLab - an underground research facility. Solid Earth 13 (p. 301-322), Copernicus Publications.

Funding Agency:
BGE BUNDESGESELLSCHAFT FÜR ENDLAGERUNG

Research Partners:
LTH RWTH AACHEN UNIVERSITY
ETH zürich BGE TEC
YORK UNIVERSITY
DALHOUSIE UNIVERSITY

FEAR Monitoring Working Group

The aims of the FEAR Monitoring Working Group this year are:

- The M-zero experiment monitoring and analysis, also described in the Geothermal testbed section. The whole seismicity in the volume is described in the Figure 22.
- FEAR experiment 1 design and built out.

Monitoring Working Group Highlights

- Deep-learning based seismic monitoring: With the densely distributed borehole monitoring network, we can characterize the finite fault system and understand how the mainshock ruptures initiate, propagate and terminate at sub-metre scales. To fully exploit the high-resolution AE data, we are developing deep learning (DL) methods to enhance the automation of microquake detection, location, and focal mechanism analysis. Our segmentation-based U-Net model demonstrated 98% accuracy in P wave classification and 93.1% in S wave classification, and an RNN-based model achieved over 98% accuracy in first-motion polarity classification. Additionally, we implemented uncertainty estimation methods such as dropout, SWAG and model ensembling to calibrate event detection and phase picking. With the continuous recordings of the aftershock sequence of the Mw -0.4 main shock of the M-zero experiment, we applied the trained model throughout the dense network. Although this is work in progress, the results demonstrated substantially higher picking accuracy and detection sensitivity compared to more standard automatic detection methods (Figure 24).
- FEAR 1 build out : The Modeling WG has been working intensely on designing the monitoring system and experiment protocol for the forthcoming FEAR Experiment 1. This involves a multifaceted approach where the group is developing a comprehensive framework to capture and analyze the various data types effectively. Among the main challenges were to reach maximum process resolution across the different observable domains, given the limited number of boreholes. The final experiment design (Figure 23) includes two hybrid SIMFIP probes in the two boreholes (BFE 16 & 17) which cross the MC fault zone, one cemented strain monitoring borehole (BFE 18), which also includes 2 acoustic emission sensors and pressure gauges, and several seismic boreholes. The latter combine AE sensors, AE transmitters, and high frequency borehole accelerometers, and they will complement the already existing and instrumented tetrahedral AE arrays above the roof of the Bedretto tunnel. The AE sensors will be arranged pairwise in order to facilitate beamforming inference. This may be particularly useful if seismicity would occur outside the main monitoring zone of this monitoring system. While BFE 18 is already instrumented and the sensory equipment is up and running, BFE 16 and 17 were instrumented in November 2024. Before that, the open boreholes have been used for a detailed hydrological characterization campaign.

Monitoring Working Group Next Steps

- **FEAR Experiment 2 design:** While working on the FEAR Experiment 1 design, we are starting to tackle the next, bigger experiment: FEAR experiment 2. We already have some preliminary design plans for this experiment, and we are using the experiences we are gaining with the M-zero and FEAR Experiment 1 experiments to optimize and detail our plans for monitoring the processes around the target main shock.
- **AE sensor calibration:** We continue to investigate how we can use calibration techniques to interpret the AE sensor readings in terms of ground motion in physical units. After the full experimental campaign (Jan.-Feb. 2023) at the Merkers salt mine in Thuringia,

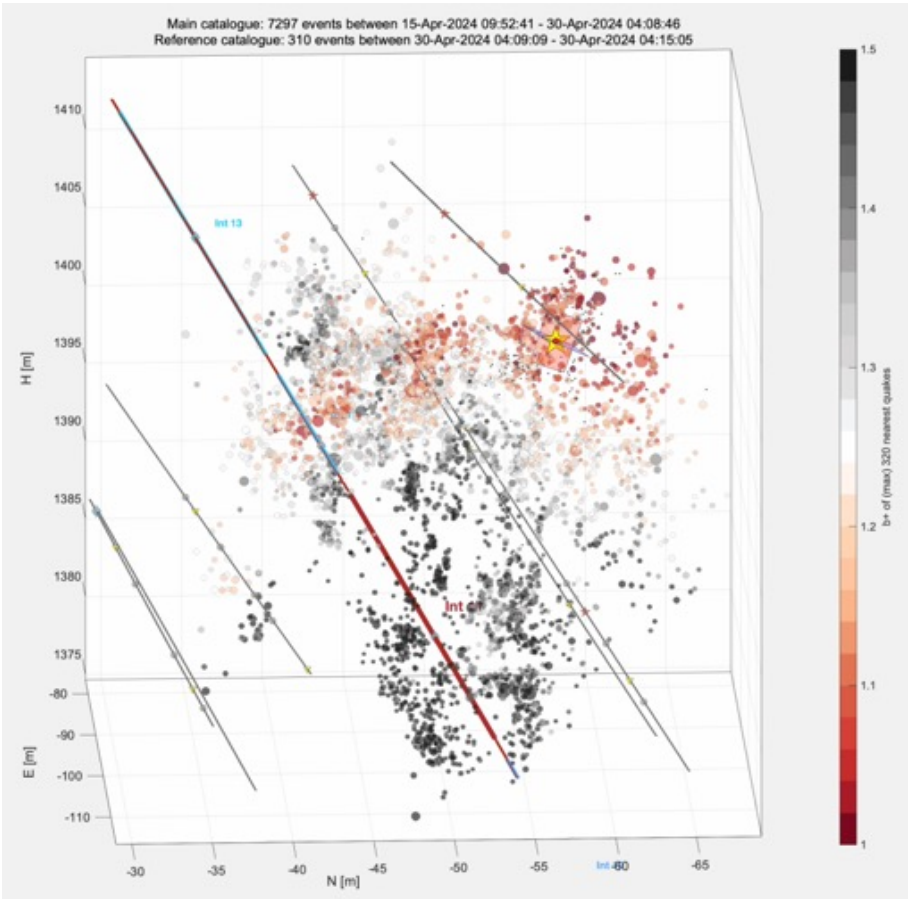

Figure 22: Observed seismicity of the M-zero experiment. Pre-mainshock events are colored by their b-value (after Afanasiev et al, 2019), calculated.

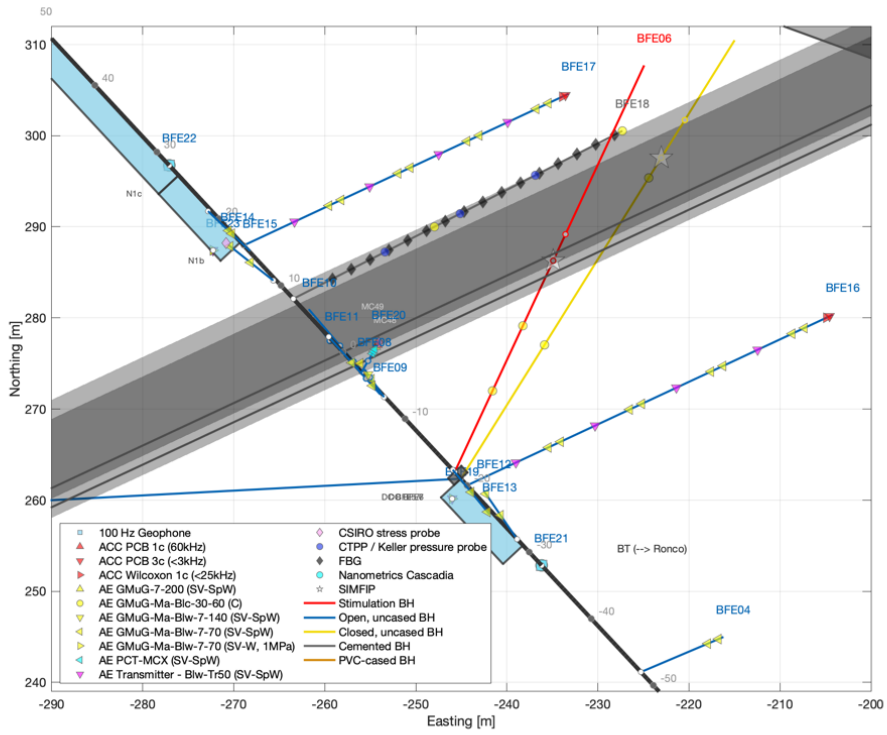

Figure 23: Planned monitoring system for the FEAR Experiment 1.

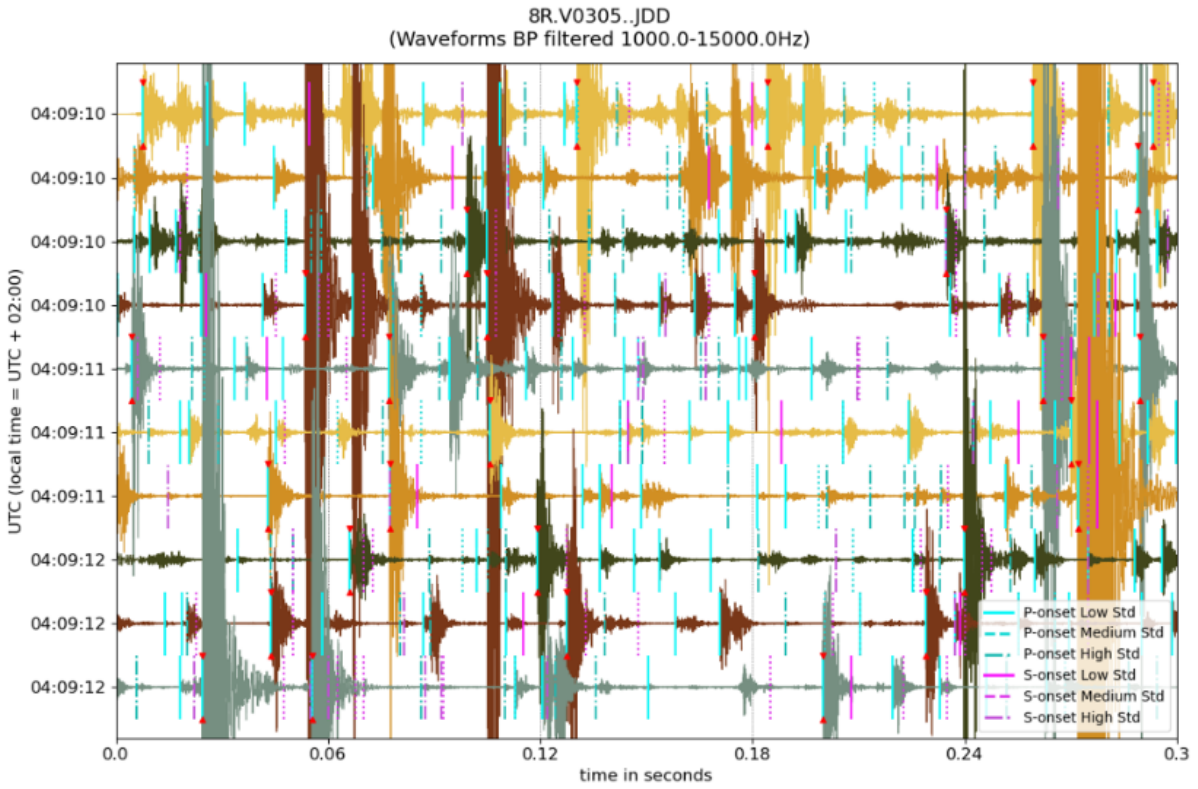

Figure 24: Probabilistic DL phase picker applying onto continuous waveform, 3 seconds example of the M-zero aftershock sequence. Vertical line markers are shown picks by the DL model, mint green for P-wave arrivals and pink for S-wave arrivals. Different dashed lines represent standard deviation across model ensemble. Red triangles are shown events from traditional automatic detectors.

DE, the Salt Mine Experiment (SaMiEx) continued with an extensive data reduction and processing campaign. The goal of the Instrument Response Task Force is to develop a better understanding of the functionality of the acoustic emission (AE) sensors deployed in FEAR or currently deployed in the BedrettoLab. The experiment also served to test some technical constraints (sensor directivity, maximum cable length between sensor and preamplifier, etc.). In parallel to the data reduction, the geometry of the salt column was obtained from the point cloud scan and a digital geometry was used to formalize an elastodynamic model (SALVUS Mondiac). The models were used to calculate Green's functions between all source-receiver pairs in the experiments. For absolute calibration, the modeled ground motions are compared to the measured voltage with basic constraints on the source. Figure 25(a) shows a map view of the numerical ground motions from a pendulum impact simulated in the salt column for a pendulum impact source. Figure 25(b) shows the initial instrument response for selected sensors computed using spectral deconvolution. These were comparable to other instrument responses computed for similar AE sensors at other subsurface laboratories (Villiger et al, 2020; Kwiatek et al, 2011).

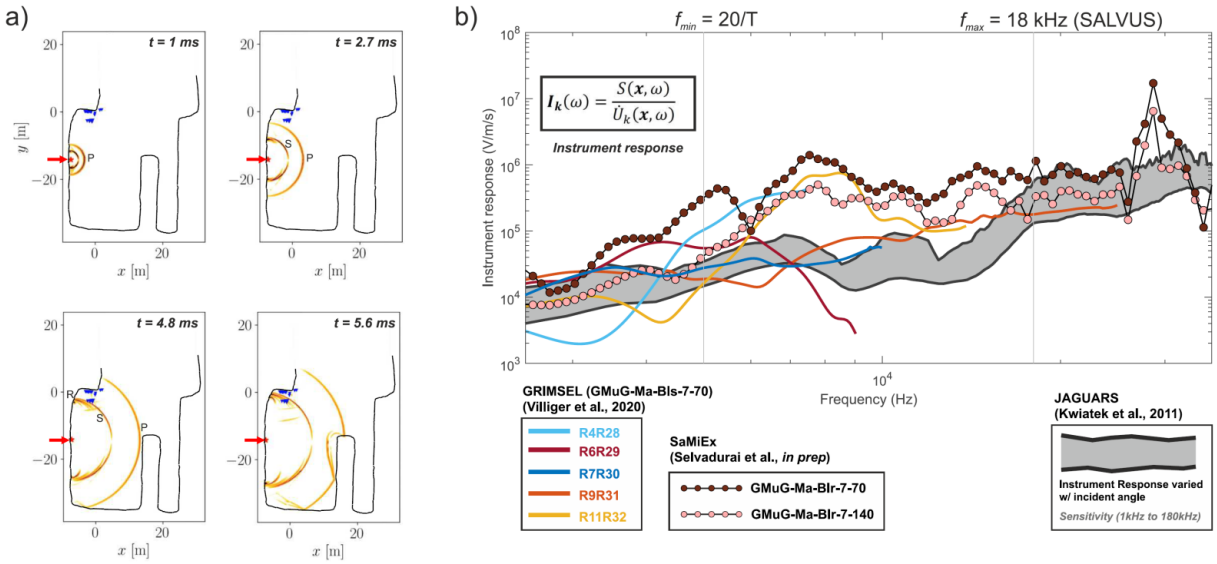

Figure 25: (a) Numerical simulations in SALVUS (Afanasiev et al., 2019) of wavefield produced in salt pillar (map view). (b) Instrument response (dotted lines) for AE sensors in SaMiEx calculated using spectral deconvolution. Comparison are made to Grimsel (Villiger et al, 2019) and JAGUARS (Kwiatek et al, 2011) in other in situ projects.

Ongoing research of the FEAR Monitoring Working Group (presented in the following pages)

FEAR experiment 1 injection strategy
Jalali, R., Rinaldi, A., Jiang, D., Ceccato, A., Pozzi, G., Zappone, A., Schaber, T., Meier, M-A., Amann, F., and the FEAR team

---

Real-time monitoring of seismicity with SeisComP
Mesimeri, M., Scarabello, L., Zimmermann, E., Haag, T., Zylis, E., Villiger, L., Kaestli, P., Meier, M-A., Rinaldi, A., Obermann, A., Hertrich, M., Clinton, J., Giardini, D., and Wiemer, S.

Modeling coupled hydro-mechanical processes during hydraulic stimulation at the Bedretto Lab
Clasen Repollés, V., Jiang, D., Rinaldi, A., Wiemer, S., and the BedrettoLab team

---

Fiber-optics monitoring at the Bedretto Lab
Rinaldi, A., Gholizadeh Doonechaly, N., Clasen Repollés, V., Tuinstra, K., Edme, P.

Joint probability density function of earthquake source parameters from spectral inversion with SPAR method: applications and perspectives for FEAR
Supino, M., Cocco, M., Mosconi, F., Locchi, M-E., Tinti, E.

On the potential of kinematic source inversion for the M1 earthquake using near-field full-waveform data
Wei, G., Mosconi, F., Dal Zilio, L., Tinti, E., Giardini, D.

FEAR EXPERIMENT #1 INJECTION STRATEGY

Reza Jalali[1], Antonio Rinaldi[2], Danyang Jiang[2], Alberto Ceccato[3], Giacomo Pozzi[4], Alba Simona Zappone[2], Tom Schaber[1], Men-Andrin Meier[2], Florian Amann[1, 5], and the FEAR team

[1] Chair of Engineering Geology & Hydrogeology (LIH), RWTH Aachen, Aachen, GERMANY
[2] Swiss Seismological Service (SED), ETH Zürich, Zürich, SWITZERLAND
[3] Department of Earth Sciences, ETH Zürich, Zürich, SWITZERLAND
[4] Istituto Nazionale di Geofisica e Vulcanologia (INGV), Rome, ITALY
[5] Fraunhofer Research Institution for Energy Infrastructures and Geothermal Systems (IEG), Aachen, GERMANY

FEAR Experiment 1 Objectives

- Hydraulic & hydro-mechanical characterization of MC fault including the entire shear zone, fault core and damaged zone
- Induce aseismic (and seismic) slip and determine the microseismic and hydro-mechanical response of the MC fault zone
- Control the pressurized (slip) area via adaptation of various injection/production protocols

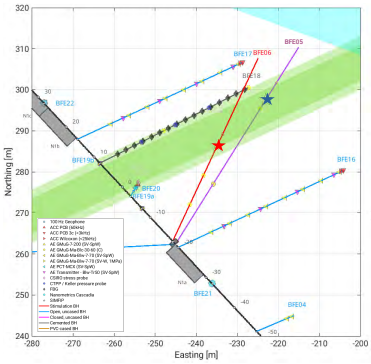

Borehole	Length [m] / Diameter [mm]	Azimuth / Dip	Measurement
BFE 6	50 / 96	68 / 29	ε[SIMFIP], P_{inj}, P_h, Q_{inj}, T, AE
BFE 5	200 / 96	32 / 30	ε[SIMFIP], P_{inj}, P_h, T, AE
BFE 7	90 / 96	248 / 31	ε[DORSSA], P_{inj}, T
BFE 16	45 / 96	65 / -10	AE
BFE 17	45 / 96	65 / -10	AE
BFE 18	42 / 96	60 / 14.8	ε[FBG, DSS], T[DTS], P[CTTP], AE

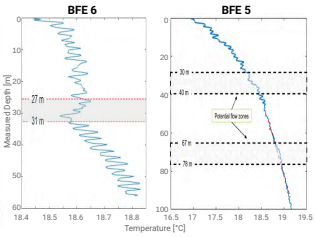

Injection Interval

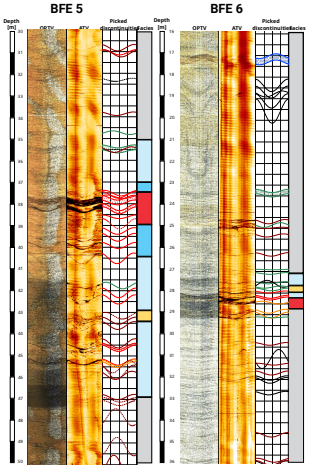

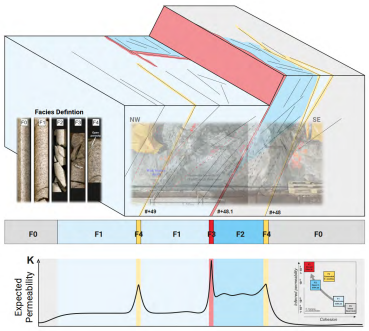

Facies definition

F0: Intact rock with rare (<< 5/m) thin cohesive fractures filled with phyllosilicates

F1: Dense set of oriented cohesive fractures filled with phyllosilicates, exploiting mylonitic fabric

F2: Same as F1 but fractures are not cohesive, host with enhanced matrix porosity

F3: Severely damaged rocks with oriented fractures and presence of fine gouge

F4: Cataclasite cemented by zeolites with high matrix porosity

Injection Protocol

The following injection protocol is conducted for each stimulation:

1. Packer & SIMFIP Installation
2. HM (HTPF) characterization — UNDRAINED
3. Step injection test — UNDRAINED
4. Injection shut-in + monitoring venting
5. HM (HTPF) characterization — DRAINED
6. Step injection test — DRAINED
7. Packer & SIMFIP de-installation

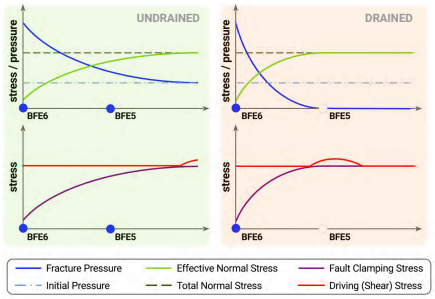

HM (HTPF)Characterization

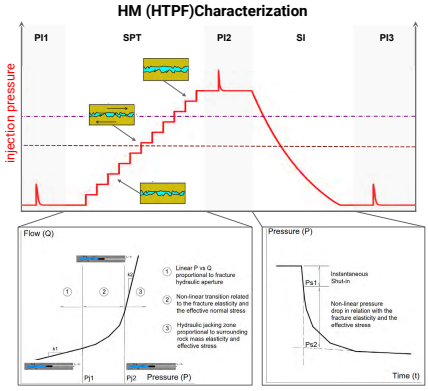

PI1: characterization of the elastic HM response
SPT: estimation of jacking pressure (normal stress)
PI2: characterization of the activated HM response
SI: estimation of instantaneous shut-in pressure (ISIP)
PI3: characterization of permanently induced in HM response

Step Injection Test

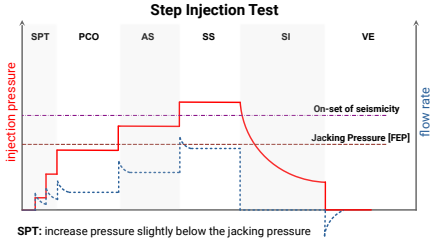

SPT: increase pressure slightly below the jacking pressure
PCO: pre-conditioning via constant pressure injection below the jacking pressure
AS: constant pressure injection below one-set of seismicity → aseismic slip
SS: constant pressure injection above one-set of seismicity → seismic slip
SI: estimation of instantaneous shut-in pressure (ISIP)
SI: estimation of rebounding pressure

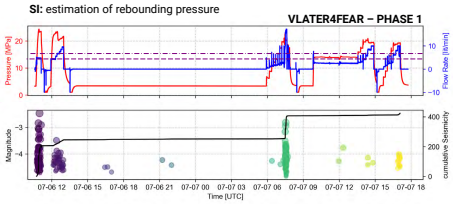

Numerical Simulation

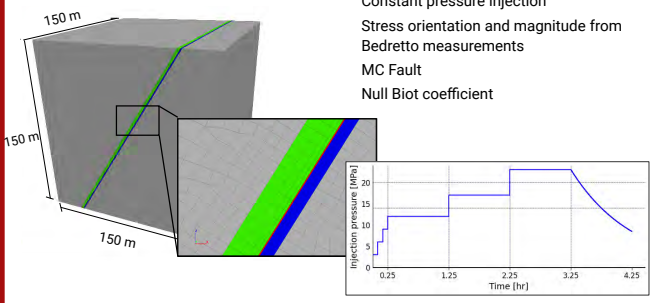

TOUGH3-FLAC3D

- Constant pressure injection
- Stress orientation and magnitude from Bedretto measurements
- MC Fault
- Null Biot coefficient

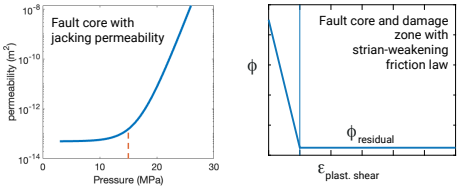

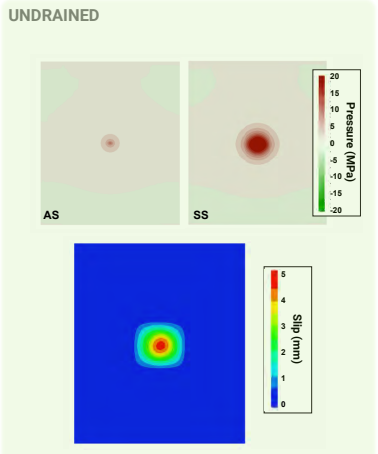

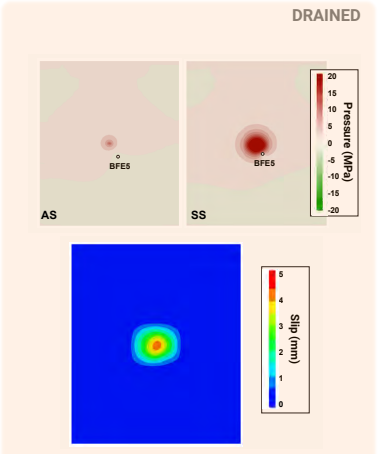

At the end of SS phase the resulting slip pattern is very similar for both drained and undrained conditions, but the magnitude of the slip seems smaller when BFE5 is kept open. The model, however, is not calibrated to produce the same outflow as expected for BFE5 open.

Real-time monitoring of seismicity with SeisComP

Maria Mesimeri[1,2], Luca Scarabello[2], Eric Zimmermann[2], Thomas Haag[2], Emil Zylis[2], Linus Villiger[1], Philipp Kaestli[1], Men-Andrin Meier[3], Antonio Pio Rinaldi[1], Anne Obermann[1], Marian Hertrich[2], John Clinton[1], Domenico Giardini[3], and Stefan Wiemer[1]

[1]Swiss Seismological Service, ETH Zürich, Zürich, Switzerland
[2]Bedretto Underground Laboratory for Geosciences and Geoenergies, ETH Zürich, Zürich, Switzerland
[3]Institute of Geophysics, ETH Zürich, Zürich, Switzerland

1. Natural Event

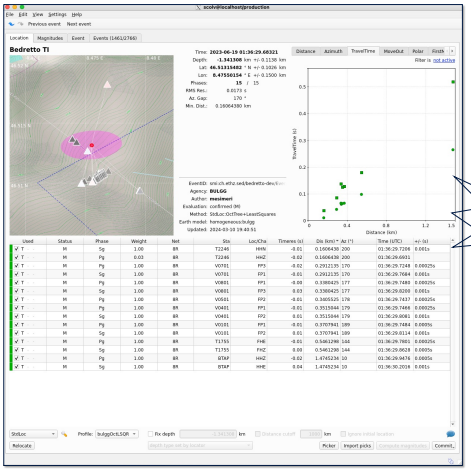

MLc -1.7

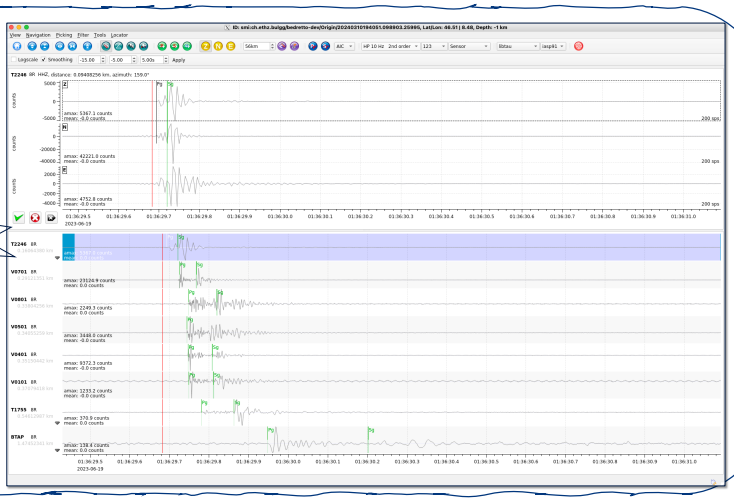

2. Induced Earthquake

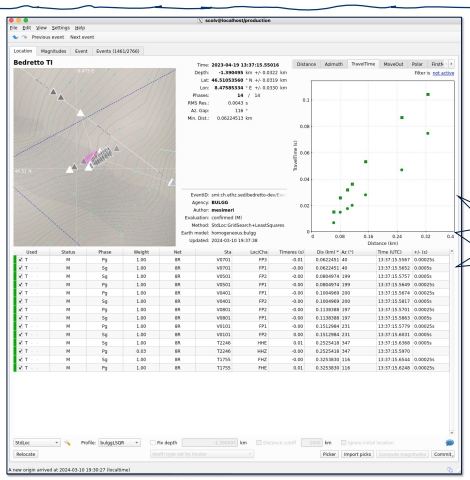

MLc -2.3

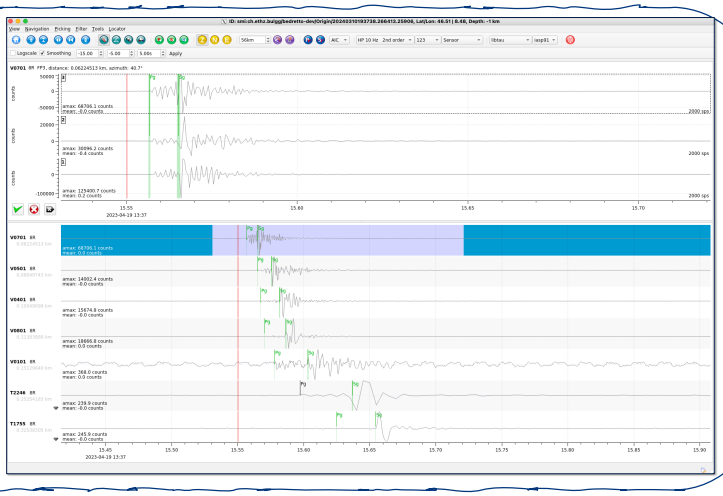

3. Event during tunneling

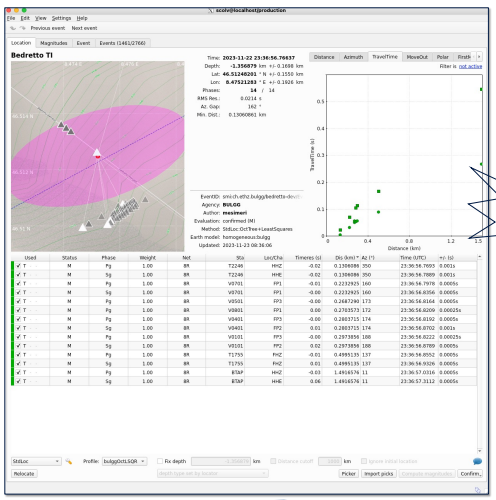

MLc -1.9

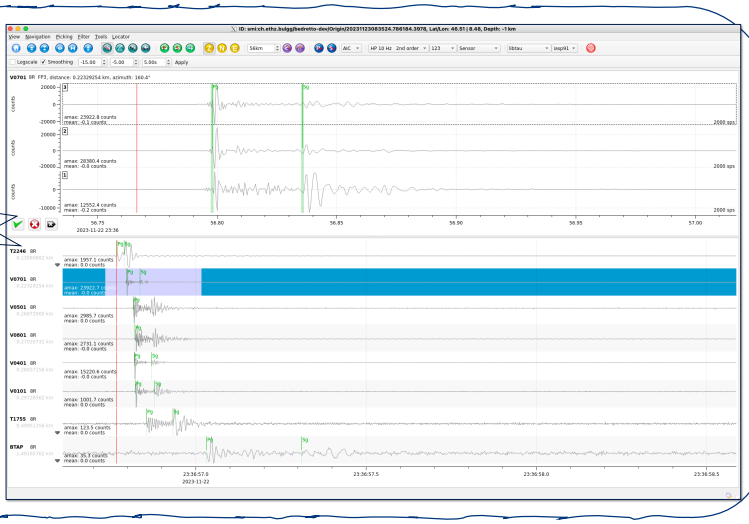

Modeling coupled hydro-mechanical processes during hydraulic stimulation at the Bedretto Lab

victor.clasen@sed.ethz.ch

Victor Clasen Repollés[1], Danyang Jiang[1], Antonio Pio Rinaldi[1], Stefan Wiemer[1], and the BedrettoLab team[2],
[1]Swiss Seismological Service, ETH Zurich;[2]Department of Earth Sciences, ETH Zurich

1 Introduction

Physics-based numerical models are essential tools employed to deepen our understanding of the coupled physical processes occurring during hydraulic stimulations at depth. In this work, we present the development of a TOUGH-FLAC-based model designed to simulate VALTER phase 1 interval 13 injection on March 3rd 2022.

2 Data

- Injection (and production) is restricted solely to the injection interval, neglecting the groundwater fluid flow within the fault zone and thereby reducing the backflow effect by a factor of 5 (Fig. 1a).
- The recorded seismicity (2417 events[1]) aligns with the dominant fault zone (Fig. 1b).

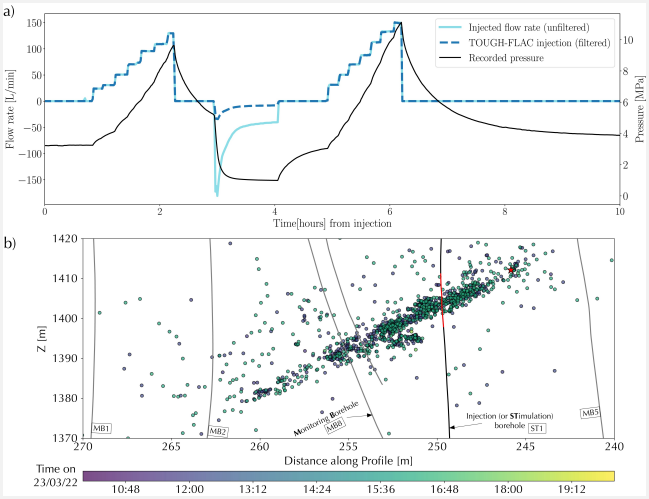

***Figure 1**: a) Injected flow rate (solid light blue), filtered injection used in TOUGH-FLAC (dashed dark blue), and recorded pressure at ST1 interval 13. b) Seismicity cloud aligned with the dominant fault zone crossing interval 13 at ST1 (marked red) and extending along an approximately 40 m-long patch.*

3 Modeling approach

- Two-way sequential TOUGH-FLAC coupled model[2].
- Injected water is restrained to the more transmissive fault core (~4.7m overlap with ST1).
- Isothermal conditions (DTS shows negligible variation).
- The interval is fully saturated with water and impose a linear gradient for P and T (Fig. 2).
- All boundaries are open for fluid flow and impose a no-slip condition.
- A bilinear strain-softening Mohr-Coulomb model assigned for both the fault core and damage zones.

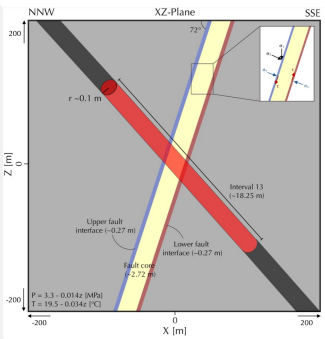

***Figure 2**: Not-to-scale sketch of a XZ-plane cut at the center of the implemented model, showing the more permeable wider fault core (yellow) embedded by two interfaces (damage zones) with lower permeability and porosity. The mesh is constructed such that the fault strikes in y-direction (242.5°N) and dips 72°. The in-situ stress conditions (steady-state) were computed according to: $S_{hmin} \approx 16.7$ MPa < $S_{hmax} \approx 25.4$ MPa (110°N) ≤ $S_v \approx 26.5$ MPa (90°)[3].*

4 Results

We compare our current results (pressure and strain) with observed pressure, DSS and FBG data in Fig. 3, at two monitoring boreholes showing large hydro-mechanical response: a) MB5 (at 95 m depth) and b) MB8 (at 118.76 m depth).

Although the timeseries aligns with the general trend observed at both points in our 3D volume, the current strain is predominantly elastic, and centered around the injection point (Fig. 4). Displacement extends outwards from injection without reactivating the fault.

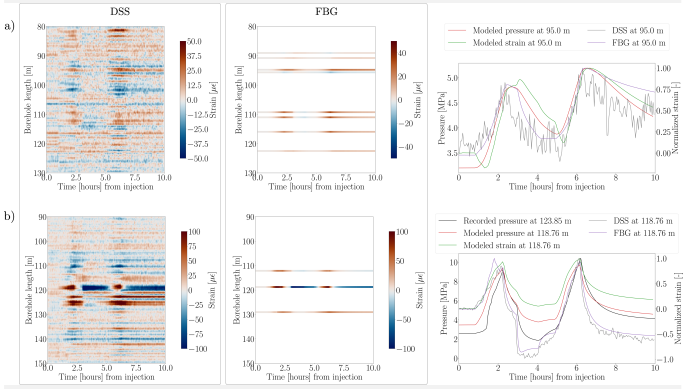

***Figure 3**: Strain waterfall plot for DSS and recordings from FBG sensors for boreholes: a) MB5 (between 80 and 130 m depth along the borehole) and b) MB8 (between 90 and 150 m) and selected timeseries (right panels) at depths with higher observed hydro-mechanical connection along both monitoring boreholes for observations as well as preliminary modeling results.*

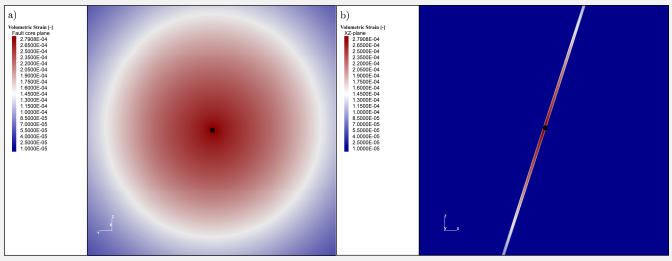

***Figure 4**: 2D plane volumetric strain cuts along: a) the fault core, and b) along the XZ-plane cut at the center of the mesh (0, 0, 0), as in Fig. 2, immediately after shut-in concluding the first injection cycle (~2.5 hours from injection).*

5 Conclusion

- We constructed a detailed 3D model using TOUGH-FLAC coupling with the goal to robustly capture primary observations without adding excessive complexity.
- Further endeavors are needed to induce plastic shear behavior in the joints within the damage zones to trigger reactivation of the fault and match plasticity observed at monitoring points (e.g. 3b right panel).
- Benchmark to design future injection strategies in environments characterized by a larger dominant fault zone.

References

1. Obermann, A. et al. (2024). Seismic response of hectometer-scale fracture systems to hydraulic stimulation in the Bedretto Underground Laboratory, Switzerland. *Submitted to: J. Geophys. Res. – Solid Earth.*
2. Rinaldi, A. P. et al. (2022): TOUGH3-FLAC3D: a modeling approach for parallel computing of fluid flow and geomechanics. *Computational Geosciences*, 26:1563-1580.
3. Bröker, K. and Ma, X. (2022). Estimating the Least Principal Stress in a Granitic Rock Mass: Systematic Mini-Frac Tests and Elaborated Pressure Transient Analysis. *Rock Mechanics and Rock Engineering.*

Fiber-optics monitoring at the Bedretto Lab

Antonio Pio Rinaldi[1], Nima Gholizadeh Doonechaly[2], Victor Clasen Repollés[1], Katinka Tuinstra[1], Pascal Edme[1,2]
[1]Swiss Seismological Service, ETH Zurich; [2]Department of Earth Sciences, ETH Zurich

Introduction

Fiber optics cable can be used to monitor strain and temperature at different frequency. The measurement device (the interrogator) is a high-performance laser and the sensing occurs by analyzing the light backscatter by fiber glass impurities:

Rayleigh: same as pulse light, phase changes if fiber is excited.
Raman: different frequency, amplitude temperature dependent.
Brillouin: frequency shift sensitive to both temperature and strain
Fiber Bragg Gratings: "filter" (exposure pattern) producing a coherent large reflection at a particular wavelength that changes with strain

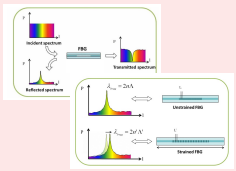

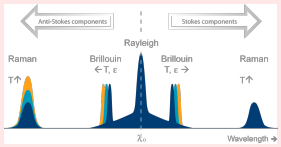

Cables installed at Bedretto/VALTER

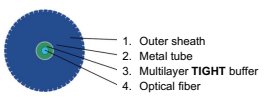

Installed in MB1/MB3/MB4/tunnel, good for DSS/DAS. Very small (only 3.2 mm diameters). Single mode fiber (SMF).

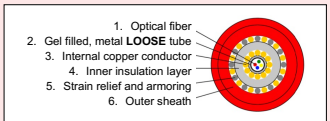

Installed in ST1/ST2, ideal for DTS but good results for DAS. Very noisy for DSS. Two SMF and two multi mode fiber (MMF).

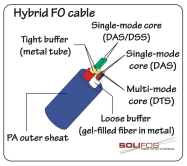

- Hybrid cable, installed in MB5/MB7/MB8.
- Simultaneous monitoring of DTS, DSS, DAS
- Three tubes (two tight buffer, one loose)
- Good results for all distributed sensing
- Combined tight and loose optical fiber

Distributed Temperature Sensing (DTS)



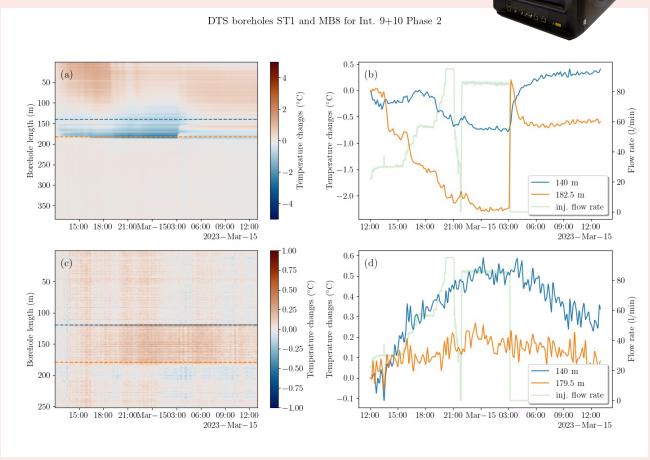

Example of temperature recordings on DTS (Raman) for boreholes ST1 and MB8 during the Interval 9/10 Phase 2A stimulation. a) Waterfall plot in injection borehole ST1. b) Time evolution of temperature changes at depths 140 m (blue) and 182.5 m (orange) in borehole ST1 compared to the injection flow rate (light green). c) Waterfall plot in monitoring borehole MB8. b) Time evolution of temperature changes at depths 140 m (blue) and 179.5 m (orange) in borehole MB8 compared to the injection flow rate (light green).

Distributed Strain Sensing (DSS)



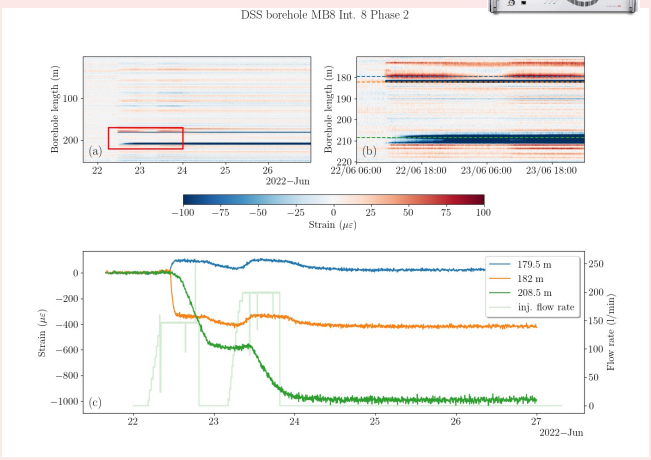

Example of strain recordings on DSS (Brillouin) for borehole MB8 during the Interval 8 Phase 2A stimulation. a) Waterfall plot for DSS along the entire borehole. b) Zoomed waterfall in the region of interest (170 m to 220 m). c) Time evolution of strain changes at depths 179.5 m (blue), 182 m (orange), and 208.5 m (green) compared to the injection flow rate (light green).

Fiber-Bragg Gratings (FBG)



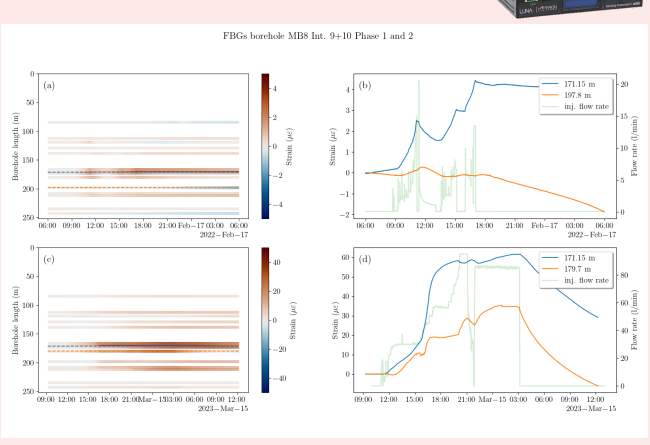

Example of strain recordings on FBG sensors for borehole MB8. a) Contour plot for each FBG during the Interval 9, Phase 1 injection. b) Time evolution of two FBG sensors at about 171.5 m (blue) and 197.8 m (orange) along the borehole compared to the injection flow rate (light green). c) Contour plot for each FBG in borehole MB8 during the Interval 9/10, Phase 2A injection. b) Time evolution of two FBG sensors at about 171.5 m (blue) and 179.7 m (orange) along the borehole compared to the injection flow rate (light green)

Distributed Acoustic Sensing (DAS)



March 2023
ST2 - MB8 - MB5

M_L = -1.4
f = 5000 Hz
dx = 0.8 m
GL = 4 m

July 2023
MB1 – MB8 – MB5

M_L = -1.85
f = 5000 Hz
dx = 0.8 m
GL = 4 m

→ Better coupling, all fiber cemented

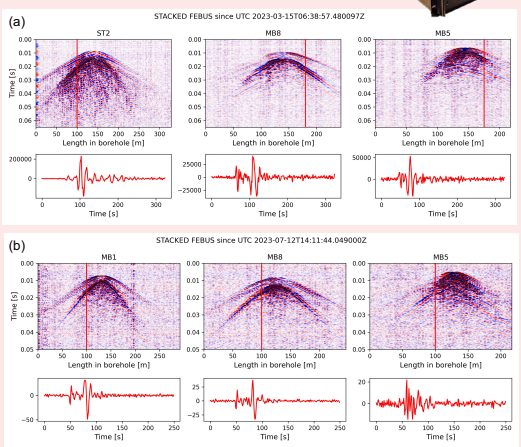

Example of seismic events recorded on DAS (Rayleigh) with waterfall plots (top rows) and example waveform recording for single channels (bottom rows). a) Event during Interval 8 Phase2A stimulation recorded on boreholes ST2 (in water), MB8 (cemented), and MB5 (cemented). b) Event during Interval 11 Phase2B stimulation recorded on cemented boreholes MB1, MB8, and MB5.

Joint probability density function of earthquake source parameters from spectral inversion with SPAR method: applications and perspectives for FEAR

Mariano Supino[1], Massimo Cocco[1], Francesco Mosconi[2], Maria Eugenia Locchi[2], Elisa Tinti[1,2]

mariano.supino@ingv.it | www.supino.eu

1 INGV

2 Sapienza University, Rome

FEAR Annual meeting March 13-15 2024 AACHEN

We present several applications of the probabilistic method SPAR [Supino et al., 2019] to estimate source parameters seismic moment (M_0) and corner frequency (f_c) from different type of data.

SPAR estimates the joint a-posteriori probability density function of source parameters, using the Bayesian framework proposed by Tarantola [2005] and a Markov chain based global optimization technique [1, 3]. Seismic moment estimations are converted to moment magnitudes M_w using the Kanamori [1977] equation.

We show results from:

1. The Community Stress Drop Validation Group by Baltay, Abercrombie et al. .
55 events of the common dataset were inverted, and results compared with SCEC catalog and Trugman [2020] stress drop estimates.

2. A large catalog of ~250,000 events occurred in Italy between 2009 and 2018.
The comparison of M_w and M_L values shows a systematic underestimation of M_L for small magnitude events, as expected [4].

3. A large catalog of ~10,000 low-frequency earthquakes (LFEs) occurred in Shikoku, Japan.
The results show for the first time that LFE source scaling is similar to regular earthquakes, with an almost constant stress drop. However, the latter value (~30 kPa) is much smaller than regular earthquakes.

4. A catalog of raw DAS data from Chile [Strumia et al., 2024].
Source parameters were estimated for the first time from raw DAS data, and compared with catalog values.

5. A preliminary inversion of one event recorded during VALTER experiment (ID 230419, M_L = -1.8).

SPAR: SOURCE PARAMETERS JOINT PDF

We use the probabilistic method of Supino et at. (2019) [1,2,3] to invert single-station S-wave displacement spectra and evaluate the joint PDF $\sigma(\boldsymbol{m})$ of the source parameters $\boldsymbol{m} = (M_0, f_c, \gamma)$.

We integrate the joint PDF to obtain the marginal PDF of each parameter.

The single-station solution and uncertainty are the mean and standard deviation of the parameter marginal PDF.

The final event solution and uncertainty are respectively the weighted average and weighted uncertainty of single-station estimates.

Using marginal PDFs has two major advantages when it comes to uncertainty estimation:

(1) It accounts for between-parameter correlation, as it results from the integration of the joint PDF;
(2) It also accounts for the quantity of information available in the frequency domain (frequency bandwidth), as larger uncertainty are associated to narrower frequency band [1].

A INVERTED OBSERVATION: DISPLACEMENT SPECTRUM

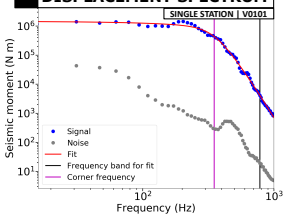

B PROBABILITY DENSITY FUNCTION OF SOURCE PARAMETERS $\boldsymbol{m}$

B.1 Find the a-posteriori joint PDF $\sigma_M(\boldsymbol{m})$ maximum $\boldsymbol{m}^*$ with MC global optimization

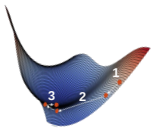

B.2 Evaluate $\sigma_M(\boldsymbol{m})$ around $\boldsymbol{m}^*$ | Tarantola, 2005 [3]

B.3 Evaluate marginal PDFs, mean and variance of source parameters

C EVENT SOLUTION
Inverse-variance weighted average

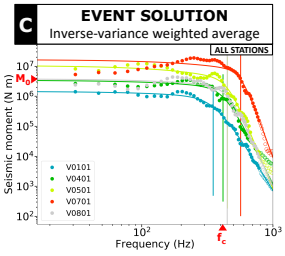

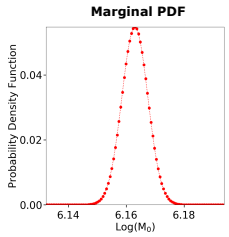

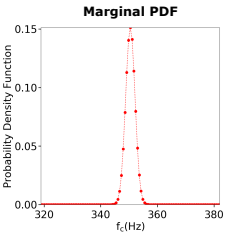

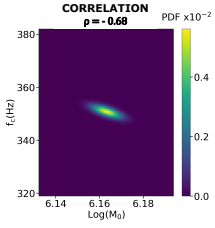

APPLICATIONS

COMMUNITY STRESS DROP VALIDATION GROUP

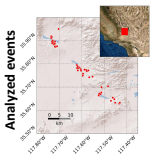

Common dataset
to compare source parameter estimates from **different methodologies**

55 events selected from the Ridgecrest 2019 sequence

Supino and Satriano, in preparation
Abercrombie et al., whole study, in preparation

Good **agreement** between **M_w and M_{CAT}**

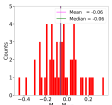

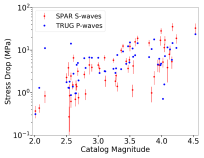

Stress drop similar to Trugman (2020), obtained from P-waves and different methodology

Larger stress drop error for smaller events

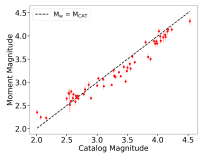

REGULAR EARTHQUAKES | 10-YEAR CATALOG ITALY

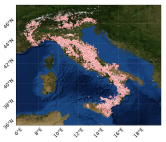

Supino et al., in preparation

2009-2018 catalog **~250,000 events**

S-wave arrival times **manually revised**

M_L homogenous catalog
Di Stefano et al., 2023

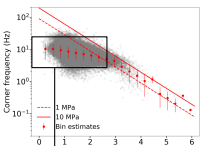

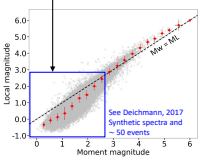

Almost constant stress drop scaling (1-10 Mpa) | **Mw 2.5 - 6**

Almost constant corner frequency f_c ~ 10 Hz | **Mw <~ 2.5**

Apparent lower f_c (higher duration) due to anelastic attenuation low-pass filtering
f_c is the cut-off frequency of the low-pass filter and does not scale with the source [5,6]

Total displacement integral (∝ ampl. x duration) **is conserved after a low-pass filtering**

Q OPERATOR

$$\mathbf{M_0} \propto \int_0^{\infty} u(t)dt \propto \lim_{f \to 0} \tilde{u}(f)$$

Observed signals must exhibit apparent (lower) maximum amplitude to "compensate" apparent higher duration

ML ∝ max. amplitude underestimated [4]

Mw ∝ displacement integral not affected

LOW-FREQUENCY EARTHQUAKES

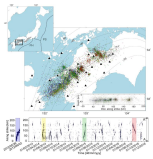

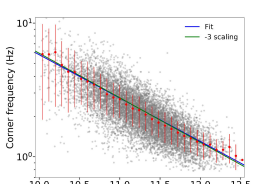

Supino et al., 2020 [3]

LFE catalog in Shikoku

Automated catalog from BTBB
(Poiata et al., 2018)

Manual catalog from JMA

10,000 events

First evidence for **self-similar source scaling** of low-frequency earthquakes

Low stress drop ~ constant value 30 kPa

DAS RAW RECORDS

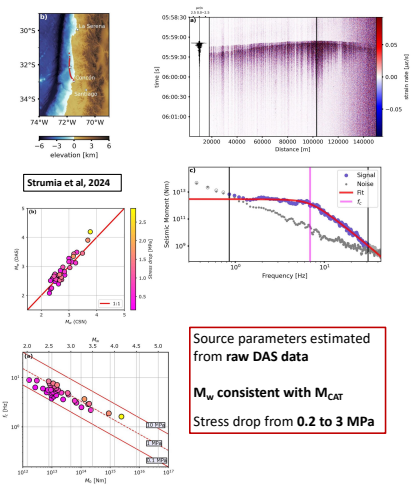

Source parameters estimated from **raw DAS data**

M_w consistent with M_{CAT}

Stress drop from **0.2 to 3 MPa**

FEAR PERSPECTIVES

$\mathbf{M_w = -2.27 \pm 0.10}$ $\mathbf{f_c = 451 \pm 3\ Hz}$

ASSUMING for M_w estimation

V_S = 1530 m/s	S-wave velocity
ρ = 2620 g/cm³	Density
μ = 6 GPa	Shear modulus
FS = 1	Free-surface coefficient
R_S = 0.63	Radiation pattern coefficient

$$r = \frac{k}{f_c} \quad \text{with } k = k(v_R)$$

SOURCE RADIUS | SOURCE MODEL and PHASE | RUPTURE VELOCITY

$$\Delta\sigma \propto \frac{M_0}{r^3}$$ **STRESS DROP**

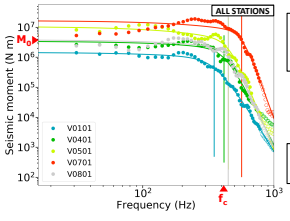

ASSUMING
V_R = 0.9 V_S and Kaneko and Shearer (2014) circular source model | **k = 0.26**

$$\Delta\sigma = 0.32 \pm 0.11\ MPa$$
$$r = 0.88 \pm 0.10\ m$$

ASSUMING
Brune (1970) circular source model | **k = 0.37**

$$\Delta\sigma = 0.11 \pm 0.04\ MPa$$
$$r = 1.25 \pm 0.10\ m$$

REFERENCES

[1] Supino et al. | 2019 | GJI | 10.1093/gji/ggz206
[2] Supino et al. | 2020 | SREP | 10.1038/s41598-020-63584-6
[3] Tarantola | 2005 | Book | 10.1137/1.9780898717921
[4] Deichmann | 2017 | BSSA | 10.1785/0120160318
[5] Abercrombie | 1995 | JGR | 10.1029/95JB02397
[6] Ide et al. | 2001 | GRL | 10.1029/2001GL013106

FEAR Fault Activation and Earthquake Rupture

On the potential of kinematic source inversion for the M1 earthquake using near-field full-waveform data

Guoguang Wei[1,2] Francesco Mosconi[3] Luca Dal Zilio[1,4] Elisa Tinti[3] Domenico Giardini[1]

1 Seismology and Geodynamics, Institute of Geophysics, ETH Zürich, Switzerland
2 Department of Earth and Space Sciences, Southern University of Science and Technology, China
3 Dipartimento di Scienze della Terra, La Sapienza Università di Roma, Italy
4 Earth Observatory of Singapore, Nanyang Technological University, Singapore

1 Introduction

The source of earthquakes involves dynamic shear ruptures, including fractures and frictional slips on fault planes. The seismic event resulting from the reactivated fault in the Bedretto tunnel could be M1 or even smaller, and the off-fault observation data signals are of very high frequency. We investigated the potential of kinematic source inversion using off-fault observation data for the M1 event.

2 Construction of inversion problem

- The fault plane is parameterized into a set of sub-faults (Fig. 1). For a given hypocenter, **the maximum rupture speed across the fault need to be set, which determines the earliest possible time of rupture on each sub-fault**. The source time function (STF) of each sub-fault is expressed with **multiple windows**.

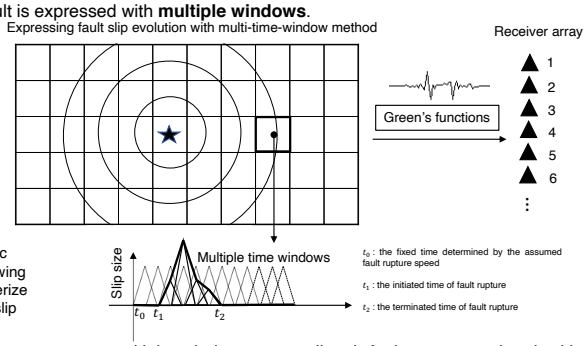

Fig. 1 Schematic illustrations showing how to parameterize spatiotemporal slip distribution.

- Slip amplitudes $\mathbf{m}$ across multiple windows over all sub-faults are correlated with observations $\mathbf{d}$ at receivers via Green's functions[2], which can be organized into a design matrix $\mathbf{G}$, thereby establishing a linear relationship: $\mathbf{d} = \mathbf{Gm}$. Slip parameters $\mathbf{m}$ can be subsequently solved through standard procedures of linear least squares inversion.

- To stable inversion, a spatially Laplacian smoothing regularization and a temporally first derivative smoothing regularization are introduced. The preferred spatial and temporal smoothing strengths are determined by minimizing ABIC (Akaike's Bayesian Information Criterion) values [1].

3 Dynamic rupture model with M_w = 1.32

- The dynamic rupture model is simulated in a homogeneous elastic media with Vs = 1531m/s, Vp = 2620 m/s, and the density of 2620 kg/m^3 . The moment magnitude (M_w) of the simulated rupture model is 1.32. Kinematic parameters for the rupture model are shown below (Figs. 2-4).

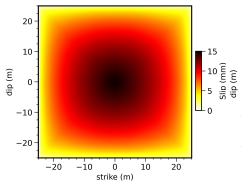

Fig. 2 Fault slip distribution

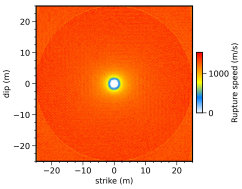

Fig. 3 Rupture speeds

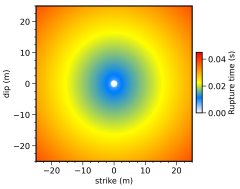

Fig. 4 Rupture time

- The fault plane is dipping by 60° (Fig. 4). There are 7 station arrays at the front of the plane and all stations are located at the depth that is equal to the hypocenter (Fig. 5). The 3-component velocity waveforms are simulated at each station and the length of waveforms is 0.15 s with a maximum available frequency fixed at 400 Hz.

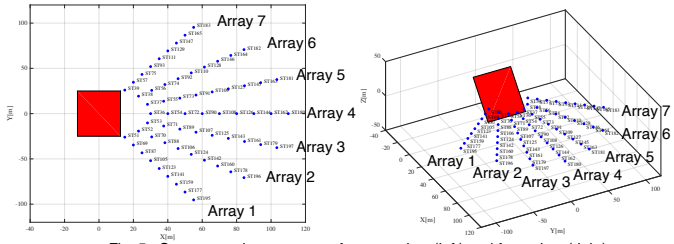

Fig. 5. Source-receiver geometry from top view (left) and front view (right)

4 Kinematic slip model inversion result

The setting of slip model is summarized in Table1. Each sub-fault is represented by a double couple point source for inversion. As adjacent windows are overlapped by half, a sub-fault can therefore allow to have a maximum rupture duration of 0.03s.

Table 1. Setting of slip model parameters

Parameter	Setting	Parameter	Setting
Number of sub-faults	144	Data sampling rate	400 Hz
Sub-fault size	5 m×5 m	Data band filtering	0.00001-200 Hz
The maximum rupture speed	1.5 km/s	Green's function calculation	F-K code[2]
Number of windows	12	Fault rake	[-70°,-110°]
Duration of each window	0.005s	Hypocenter	Fixed at center

A wide range of spatial and temporal smoothing factor are tested in a logarithm space (Fig. 6). The minimum value is marked with the red dot. Fig. 7 shows the slip evolution for the preferred smoothing parameters. The slip propagated in all directions from the hypocenter. The data fit for 7 arrays is shown in Fig. 8. The inverted fault slip model has released moment equal to M_w1.32 (Fig. 9).

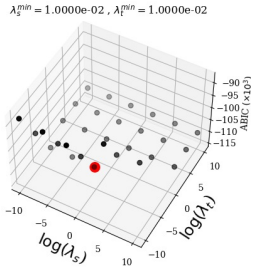

Fig. 6. ABIC values versus different spatial and temporal smoothing parameters.

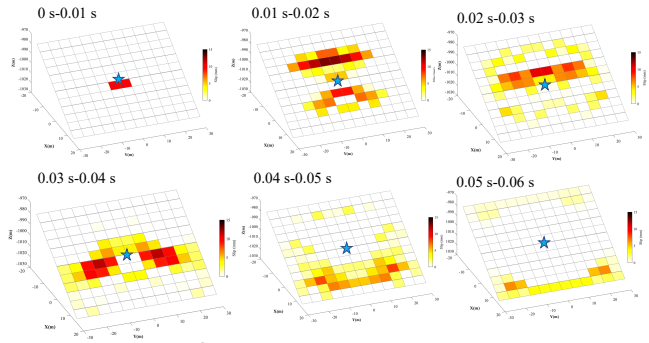

Fig. 7. Snapshots of the rupture evolution at 0.01 s time interval.

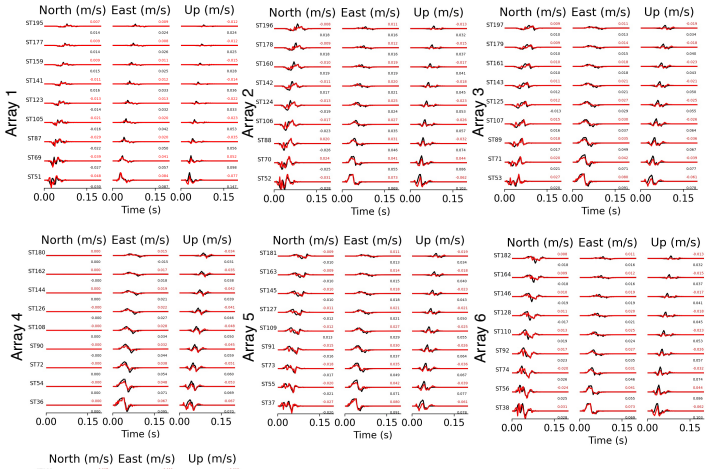

Fig. 8. Observation waveforms (black) vs. modelling waveforms (red). Stations are displayed from bottom to top according to hypocenter distances.

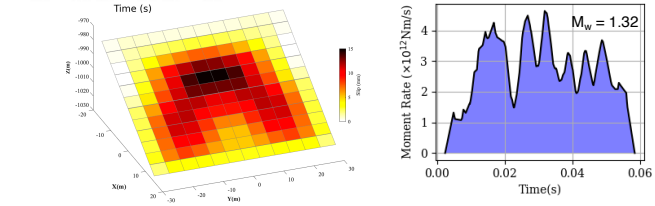

Fig. 9. Left: final fault slip distribution. Right: moment releases over time.

5 Conclusions

- The inverted slip model has the same moment magnitude as the simulated model. Therefore, the total slip amount is correctly estimated.

- However, the fault slip distribution is not satisfactory compared the simulated model. This could be attributed to, 1) The applicability of the Green's function. 2) The fault dips, but the stations are arranged horizontally, causing inconsistencies in their sensitivity to the upper and lower sections of the fault.

Reference

[1] Ide, S., Takeo, M., & Yoshida, Y. (1996). Source Process of the 1995 Kobe Earthquake: Determination of Spatio-Temporal Slip Distribution by Bayesian Modeling. Bulletin of the Seismological Society of America, 86(3), 547-566.
[2] Zhu, L., & Rivera, L. A. (2002). A note on the dynamic and static displacements from a point source in multilayered media. Geophysical Journal International, 148, 619-627

PRECODE: Progressive Excavation Damage Zone Evolution During and Post Mine-By Tunneling

PIs: S. Wiemer (Swiss Seismological Service, ETH Zurich), F. Amann (RWTH Aachen)
Funding: Bundesgesellschaft für Endlagerung (BGE) Germany

The PRECODE project aims to deepen understanding of spatial and temporal development of brittle fracturing in the BedrettoLab. There are significant synergies with the FEAR project. Before and during the Mine-By excavation of the 120-meter FEAR tunnel, the vicinity of the tunnel is densely instrumented with various sensors, including, strain, pore pressure, microseismic, etc to monitor the evolution of the excavation damage zone (EDZ) over a period of 2-3 years. Comprehensive laboratory testing is planned to characterize the brittle fracturing at the micro scale. In addition, advanced numerical modeling will be carried out to evaluate the current modeling capabilities to simulate the EDZ around tunnels. The aims of the PRECODE project include:

- Improving our understanding of short-term rock mass behavior during tunneling with advanced monitoring systems that were not available in previous experiments in crystalline rock (e.g. fiber-optic strain sensors, highly sensitive microseismic sensors, LiDAR scanning, etc.)
- Improving our understanding of the influence of natural repository perturbations (humidity, seismicity, etc) on progressive microcrack development within the EDZ over the long-term
- Determination of changes in excavation damage zone permeability over time (up to 2 years)
- Analysis of the impact of tunnel construction on the potential reactivation of fault zones and the associated changes in their hydraulic properties
- Creation of a hydro-seismo-mechanically coupled reference dataset for numerical simulations, which will be made available to modeling groups
- Assessing the impact of tunneling on dislocations across fault zones and related changes in hydraulic properties

SPINE: Stress Profiling in Enhanced Geothermal Systems

PI: M. Hertrich (ETH Zurich)
Funding: EU Horizon2020 Geothermica Program

The SPINE project is developing a new instrument and test protocols to conduct stress profiling in crystalline rock for a better estimation of stimulation efficiency and induced seismicity related to the creation of subsurface heat exchangers at the laboratory, intermediate field-laboratory, and geothermal project scales. The aims of the project are:

- borehole instrument testing and upgrading at relevant geothermal temperatures and pressures
- field-scale demonstration of stress profiling in the highly controlled environments of two major underground research laboratories, at the Sanford Underground Research Facility (USA) and the BedrettoLab
- laboratory-scale testing of protocols in fully controlled 3D stress regimes
- forward and inverse 3D stress analyses using fully-coupled thermo-hydro-mechanical numerical modeling conducted at different scales

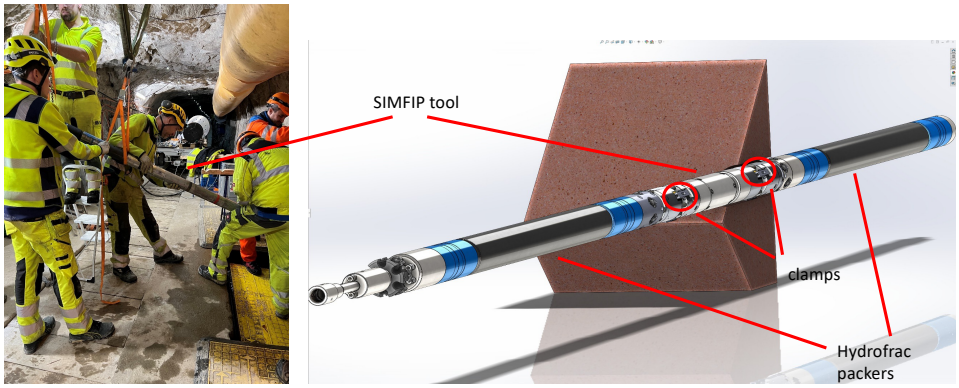

Figure 26: The SIMFIP (Step-Rate Injection Method for Fracture In-situ Properties) probe consists of 6 FBG (Fiber Bragg Grating) strain sensors configured to measure absolute 3D displacement between the clamps in the borehole at micrometer precision.

The SIMFIP tool was used to measure the 3D fracture displacement during small volume injection tests along 11 intervals in borehole BFE 05. The inversion of these data is used to estimate the full stress tensor and its variability along the borehole. Figure 27 shows an example of the acoustic and optical televiewer logging of test interval 1 before and after the SIMFIP experiment. It can clearly be seen that we displaced and enhanced a pre-existing fracture around 81.2 m depth.

Ongoing research of the SPINE Group (presented in the following page)

Investigating S-Wave anisotropy in the Rotondo granite by crosshole seismic surveys
K. Behnen, M. Hertrich, H. Maurer, D. Giardini

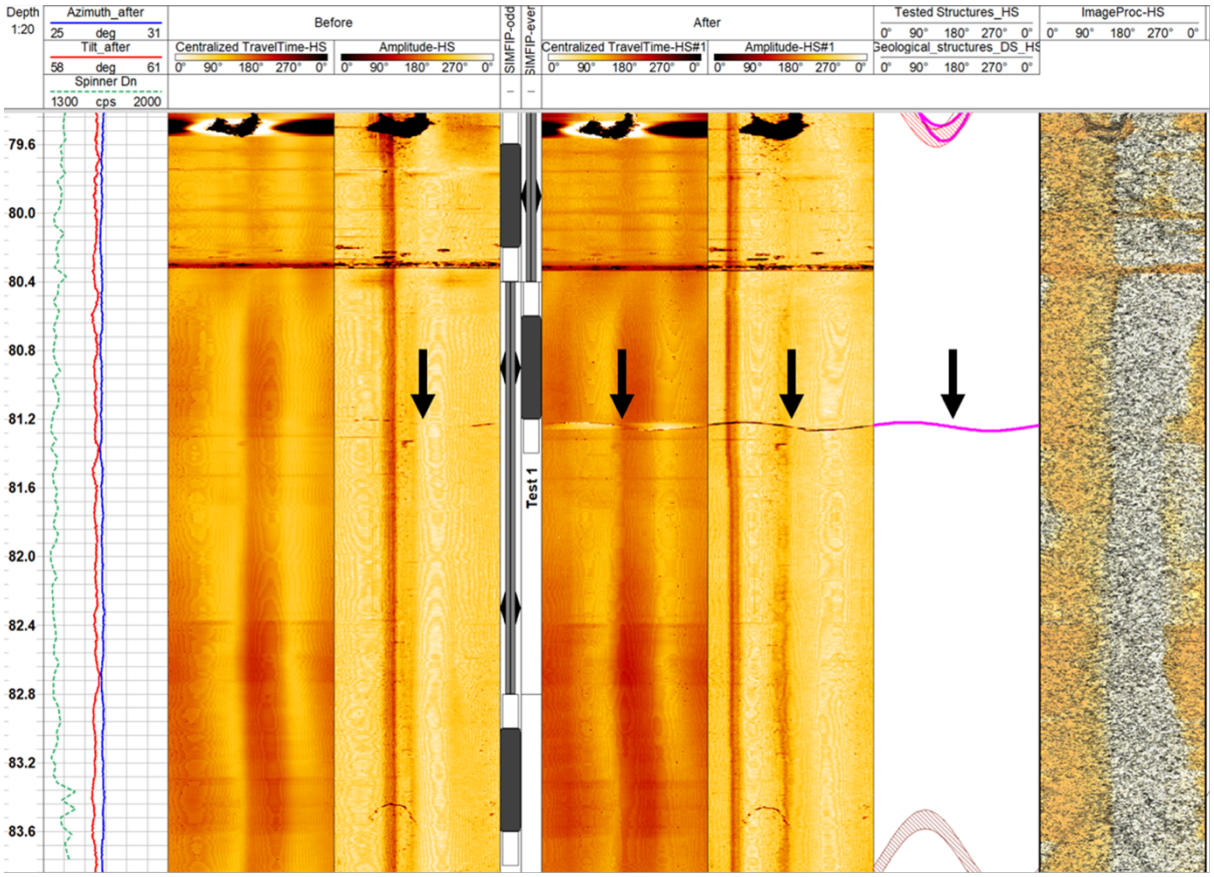

Figure 27: Logging data from SIMFIP test 1 in borehole BFE 05. The acoustic televiewer travel time and amplitude data before and after the experiment are shown, as well as the optical televiewer image and interpreted fracture.

Investigating S-wave anisotropy in the Rotondo granite by crosshole seismic surveys

Kathrin Behnen, Marian Hertrich, Hansruedi Maurer, Domenico Giardini

Bedretto Lab, ETH Zurich, kathrin.behnen@erdw.ethz.ch

Introduction

In our study we use different data sets to analyze the wave propagation in the undisturbed but anisotropic Rotondo Granite. We put special focus on the detection of the different S-Wave types, i.e. shear wave splitting, as evidence of the seismic anisotropy. The traveltimes and traveltime-differences of the S-Waves are used to fully describe the elastic tensor of the medium, assuming a tilted transverse isotropic symmetry (TTI).
Analysis of the full seismic wavefield together with complementary geological and geomechanical observations allows to investigate the main source of the anisotropy.

Measurements

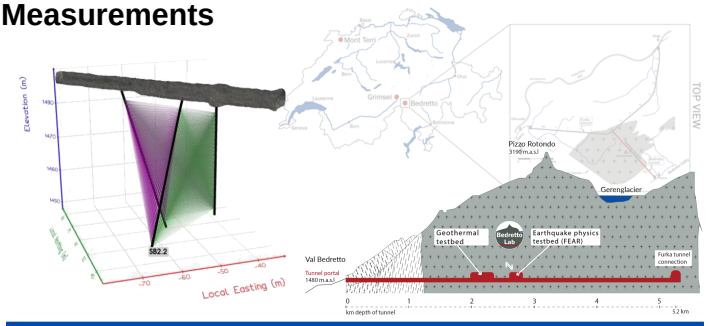

Source	Receiver	Density
P-Wave Sparker	Hydrophones	1m spacing in all planes
P-Wave Sparker	3C Geophones	1m or 2m spacing in all planes
S-Wave Sparker	Hydrophones	Single Shots
Sweeps	Hydrophones	In prep

Data

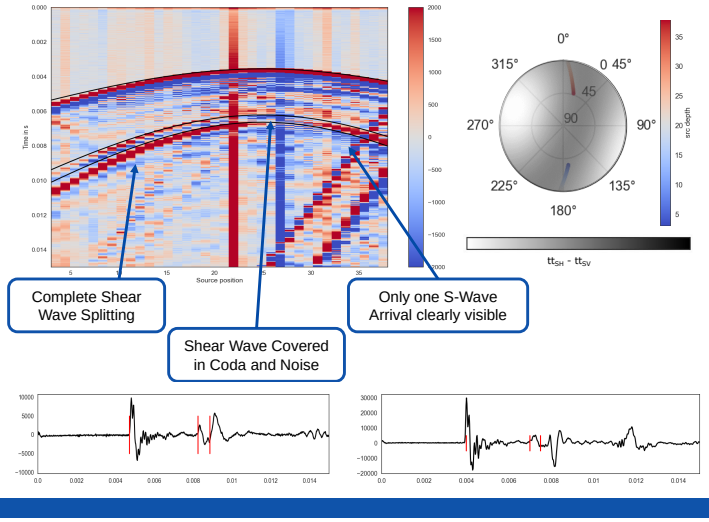

Theory

Assumptions:
- TTI Model with 7 unknowns
- 5 Thomsen parameters or 5 elastic constants + orientation of symmetry axis
- Homogeneous model
- Straight ray paths

$v_P(\theta) = \alpha_0(1 + \delta \sin^2\theta \cos^2\theta + \varepsilon \sin^4\theta)$

$v_{SV}(\theta) = \beta_0(1 + \frac{\alpha_0^2}{\beta_0^2}(\varepsilon - \delta) \sin^2\theta \cos^2\theta)$

$v_{SH}(\theta) = \beta_0(1 + \gamma \sin^2\theta)$

From Thomsen (1986)

Results

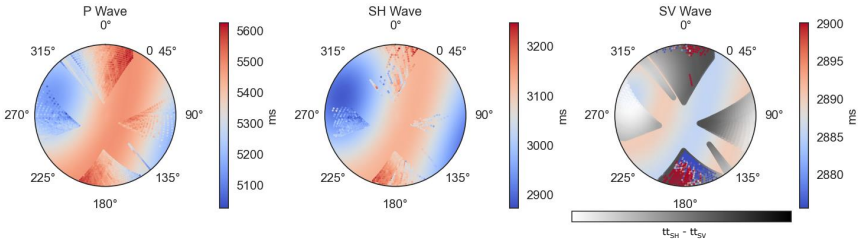

Optimized Parameter:
α_0: 5140 m/s
β_0: 2885 m/s
ε: 0.070
δ: 0.067
γ: 0.088
φ_0: 289.61°
ϑ_n: 18.90°

Observations:
- P- and SH wave show good fit to the model
- SV-Wave show bimodal misfit but shear wave splitting is only detected in the expected part of the volume
- Similar systematic misfit for all three wave types
- Misfit of about 100 m/s → 2 - 3%

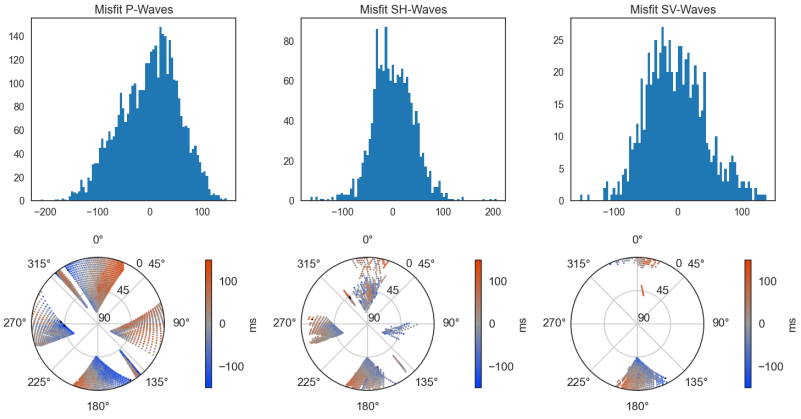

Conclusion

Stress Field

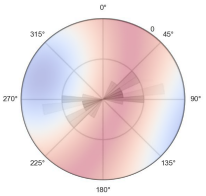

Borehole Trajectories

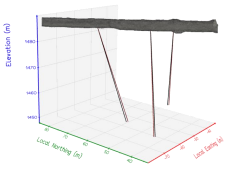

Minerals

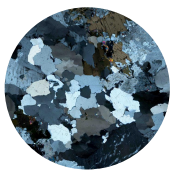

Natural Fractures

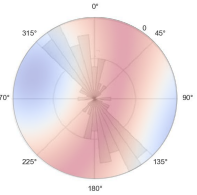

We measure seismic anisotropy of about 10% in the Rotondo Granite. This anisotropy can be modelled by first order with a TTI model using the Thomsen formulation.

The observed systematic misfit for all three wave types is an indicator for a lower symmetry (orthohombric) to better explain the data.
Also an uncertainty in the borehole trajectory can cause such a misfit. This will be verified with geodetic measurements.

As the symmetry plane is approximately aligned to the maximum stress direction, this is likely to be the main source of the anisotropy. While lab measurements show a correlation between seismic anisotropy and applied differential stress, we can put our results in a bigger context of the natural stress field.

Also, a combination with other sources such as microcrack alignment is possible.

Deep Life Observatory (DELOS)

The Deep Life Observatory (DELOS) in the BedrettoLab was established in 2021 to study organisms living at the energy limit of life. A multi-year tunnel-wide characterization of surface and subsurface biogeochemistry revealed high spatial isotopic, ionic and microbiological variability across DELOS (Acciardo et al., in prep). This information provides a biogeochemical baseline that is actively being paired with in-situ experiments throughout the Geothermal and Earthquake Physics testbeds (Brixel et al., in prep).

As part of DELOS, dedicated field instruments and borehole infrastructure have been deployed across the Bedretto tunnel, either near the VALTER volume in the Geothermal testbed or in undeveloped areas (e.g. TM 901, see Figure 28A). In 2023, three new research projects (PHATES, C-FIX and ILLUME) and a transdisciplinary tandem to exchange knowledge and methods of art and geobiology initiated by Monica Ursina Jäger and Lena Bakker (Pro Helvetia-funded project “Unfreezing the Landscape”) were initiated at DELOS.
Over the last year, the Geobiology team, together with the BedrettoLab team and in collaboration with the Geomicrobiology Research Group from Friedrich Schiller University Jena, embarked on a week-long scientific experiment to unravel the unknowns of deep groundwater carbon fixation rates as part of efforts to elucidate deep dark carbon cycling processes. Additionally, research attention was paid to understanding the evolution of life by tracing and cultivating uncharacterized bacteria in the groundwater through rock fractures. Moreover, the Geobiology team was closely involved in monitoring geochemical changes and the alteration of indigenous microbial community structure during the first long-term hydraulic injection experiment in the BedrettoLab.

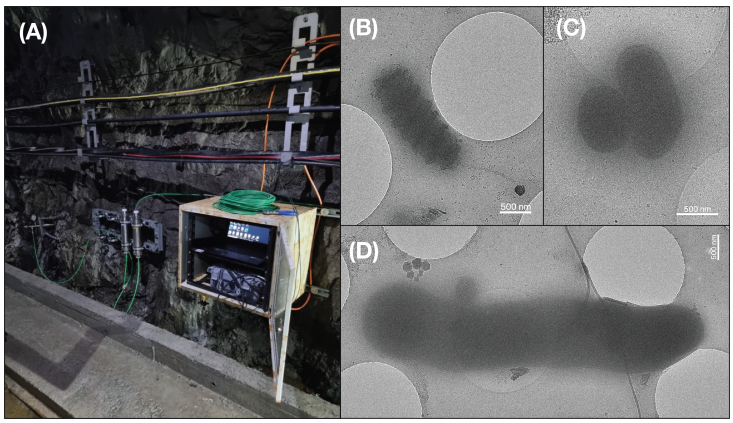

Figure 28: **(A)** Laminar flow "bioreactors" (gray cylinders) are connected to a borehole in the gneiss unit (TM901) as part of an in-situ microbial colonization experiment. Bioreactor outflow water chemistry is monitored using a geochemical monitoring station (white box). **(B-D)** A series of cryogenic transmission electron microscopy images of cell-cell interactions recovered from DELOS. All 3 morphotypes were present in the same sample and display differences in cell shape, size and mode of association.

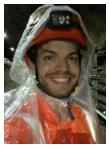

Detection of hydrogen peroxide after hydraulic stimulation of granitic bedrock at the Bedretto Tunnel

Andrew Acciardo[1], Nima Golizadeh[1], Zhe Wang[1], Andre Araujo[1], Maria Mesimeri[1], Luca Scarabello[1], Eric Zimmermann[1], Marian Hertrich[1], Cara Magnabosco[1]

[1]Department of Earth Sciences, ETH Zürich, Switzerland

andrew.acciardo@erdw.ethz.ch

1 Introduction

Seismic activity fractures and crushes rocks, creating surface radicals. When these radicals meet water, they generate reactive oxygen species (ROS), like hydrogen peroxide, which can be lethal to anaerobic subsurface microorganisms. Our laboratory experiments have demonstrated H_2O_2 production from water-rock reactions (Fig. 3), but field evidence is lacking. Therefore, we aim to answer the following questions about H_2O_2 in the subsurface:

-How much seismic activity is required to produce a measurable quantity of H_2O_2?

-Can we observe a relationship between the level of seismic activity and the concentration of H_2O_2?

-What effect does the production of H_2O_2 and other mechanoradical products have on subsurface microorganisms?

2 Study location

- The Bedretto Tunnel, located in Ticino, Switzerland, is home to the Bedretto Laboratory which carries out meso-scale geothermal, geophysical, and geobiological research

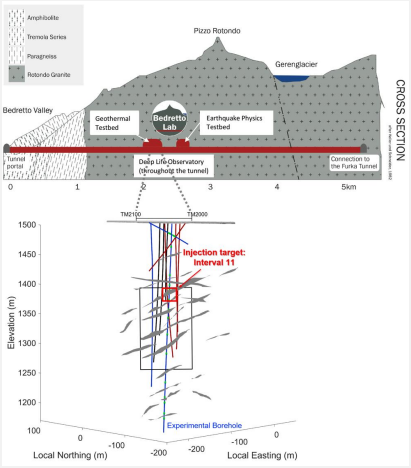

- The boreholes in the laboratory provide an opportunity to test the effects of induced stimulation on the biogeochemistry of the waters that interact with the affected rock

Fig. 1: The Bedretto Tunnel (adapted from Rast et al., 2022) along with a zoomed in section of the Bedretto Laboratory showing the borehole set-up and the interval of the experimental borehole (ST1) that was stimulated

3 Experimental Design

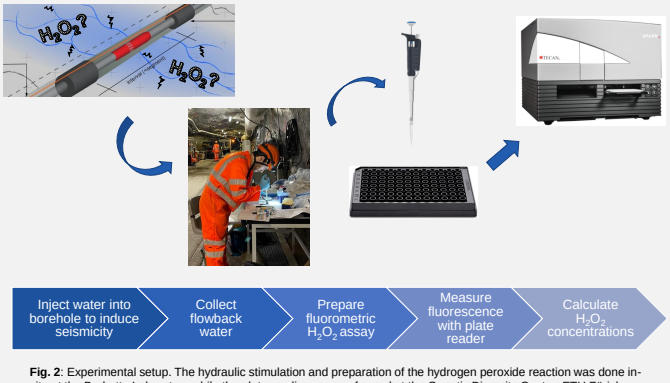

Fig. 2: Experimental setup. The hydraulic stimulation and preparation of the hydrogen peroxide reaction was done in-situ at the Bedretto Laboratory while the plate reading was performed at the Genetic Diversity Centre, ETH Zürich

4 Results

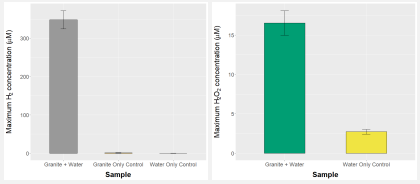

Fig. 3: Laboratory experiments demonstrating the production hydrogen (left) and hydrogen peroxide (right) from water-rock reactions. Crushed granite was placed inside anaerobic vials and anoxic water was added. Hydrogen was measured using gas chromatography and hydrogen peroxide was measured using a UV-vis spectrophotometer

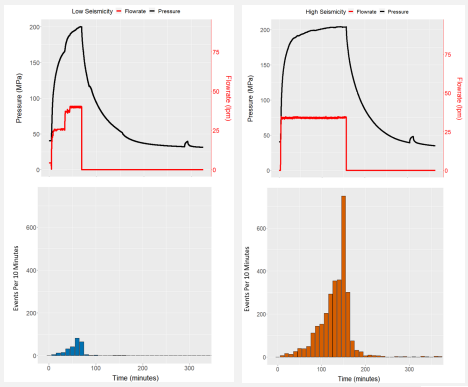

Fig. 4: Stimulation procedure for both experiments. Pressure and flowrate readings were taken with the Geomonitor II software

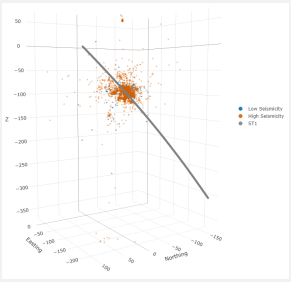

Fig. 5: Seismic events recorded during first stimulation (blue) and second stimulation (orange)

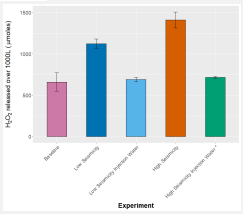

Fig. 6: Hydrogen peroxide released from the first 1000 liters from the borehole during the first (dark blue) and second (orange) stimulations, along with baseline (purple) and injection tank waters (light blue and green). Injection tank water values were based on average concentrations and extrapolated over 1000 liters

5 Conclusions

- Laboratory studies suggest that **mechanoradical production of hydrogen peroxide** from water reacting with fractured rock can occur
- **Hydraulic stimulation** of granitic bedrock produced hundreds to thousands of **measurable seismic events**
- Greater amounts of induced seismicity **corresponded to higher hydrogen peroxide concentrations** in the fluids flowing back from the injection site

6 Outlook

The production of hydrogen peroxide from seismic activity has implications for current subsurface life as well as for early life that inhabited similar ecosystems billions of years ago. These experiments demonstrate that hydrogen peroxide can be detected in fluids following induced seismic activity in granitic bedrock. Further laboratory experiments will aim to determine whether the observed increase in H_2O_2 can be attributed directly to water-rock interactions.

References

1. Ma, X., Hertrich, M., Amann, F., Bröker, K., Gholizadeh Doonechaly, N., Gischig, V., … Giardini, D. (2022). Multi-disciplinary characterizations of the BedrettoLab -- a new underground geoscience research facility. *Solid Earth*, *13*(2), 301–322. doi:10.5194/se-13-301-2022
2. Rast, M., Galli, A., Ruh, J. B., Guillong, M. & Madonna, C. (2022), 'Geology along the Bedretto tunnel: kinematic and geochronological constraints on the evolution of the Gotthard massif (central alps)', Swiss Journal of Geosciences 115(1), 1–31.
3. Stone, J., Edgar, J.O., Gould, J.A. *et al.* Tectonically-driven oxidant production in the hot biosphere. *Nat Commun* **13**, 4529 (2022). https://doi.org/10.1038/s41467-022-32129-y

PHATES: Microbial responses to rapid physical-chemical changes in the continental subsurface

PI: C. Magnabosco (ETH Zurich)
Funding: Swiss National Science Foundation

The continental subsurface holds more bacteria and archaea than any other habitat on Earth yet the origins, eco-evolutionary dynamics and behaviors of these organisms are still largely unknown. As European policies increasingly turn towards CO2 mitigation strategies that form new and innovative interactions with subsurface environments, there is an urgent need to understand how subsurface microorganisms respond to physical-chemical changes in natural and human-altered environments. To address this, the PHATES project will:

- determine how DELOS microbial and viral communities vary over space and time.
- evaluate whether virus-host interactions change when these energy-limited communities are suddenly exposed to oxidative stress generated by natural or anthropogenic activities.
- better understand the evolution of biological and chemical species during enhanced geothermal system experiments.

C-FIX: Carbon fixation in deep crystalline rock

PI: Z. Wang (ETH Zurich)
Funding: ETH Grants

In-situ carbon fixation performed by chemolithoautotrophic microorganisms is an important carbon source to sustain subsurface microorganisms; however, direct quantification of the net primary productivity in deep groundwater is still very scarce, mainly because of the limited access to such deep environments. This project will use Scintillation-based ^{14}C-labelling and Raman-activated microbial cell sorting (RACS) combined with long-read metagenomic sequencing to:

- determine the carbon fixation rates in the deep groundwater and its importance to the total carbon pool
- determine the impact of water mixing on the formation of reactive hot spots and carbon fixation process
- determine the composition and metabolic potential of deep groundwater microbial communities and identifying key carbon-fixing population

ILLUME: Investigations into the diversity of cell-cell associations and non-standard life using metagenomics and cryogenic electron microscopy

PIs: C. Magnabosco, M. Pilhofer & V. Gaisin (ETH Zurich)
Funding: ETH Centre for Origin and Prevalence of Life

The groundwater of DELOS can be viewed as an early Earth analog since they lack of photosynthetically-derived organic carbon and support chemolithotrophic microorganisms that are believed to utilize the same metabolic pathways as some of the earliest cells. By combining cryogenic electron microscopy and metagenomic sequence analysis on DELOS samples, the ILLUME project will provide new insights into the diversity and evolution of cell-cell interactions on early Earth. The main objectives of this study are to:

- characterize the morphology of cell-cell associations in DELOS and determine whether we have identified any new types of cell-cell associations.
- quantify the prevalence of cell-cell associations in DELOS.
- identify environmental and taxonomic drivers of direct cell-cell associations.
- identify potential marker genes and structures of direct cell-cell associations.

Characterizing and understanding Enhanced Geothermal Systems (EGS) - novel tools and applications in a deep underground laboratory

Funding: Swiss National Science Foundation

Investigation of seismic anisotropy in the BedrettoLab

Author: Kathrin Behnen (ETH Zurich)

My project focuses on the investigating of seismic anisotropy across multiple scales—centimeter, decameter, and hectometer—in the controlled environment of the BedrettoLab. Seismic anisotropy, which describes the directional dependency of the seismic wave velocity is linked to the elastic properties of the effective medium. Thus, knowledge about the anisotropy of a medium is crucial to understand the mechanical and structural properties of the rock formation. Working on different scales presents different challenges but also different opportunities for the characterization of the rock.

At the centimeter scale, precise measurements under controlled conditions are conducted to explore how the stress field influences the seismic anisotropy. We carry out repeated seismic velocity measurements on rock samples of the BedrettoLab, changing the stress field after each measurement step. This setup allows the detailed mapping of changes in the anisotropy corresponding to variations in the applied stress conditions.

On the decameter scale, we performed various crosshole seismic surveys in the so-called tripod boreholes, located in the homogeneous background rock. We used different sources and receivers to measure the full spectrum of seismic waves (P-, SV- and SH-waves) in order to determine the anisotropy of the rock. This scale provides the opportunity to compare our results with the well-studied stress field, fracture network, and mineral alignment around the tripod. This allows us to make conclusions on the mechanism, causing the seismic anisotropy in the field. Our results suggest that the anisotropy is mainly controlled by the surrounding stress field, but also an influence of the fracture network cannot be ruled out. Detailed results of this study are provided in Behnen et al. 2024, submitted.

The hectometer scale presents a higher level of complexity due to heterogeneous rock properties but is also more relevant to geothermal applications. The anisotropy can only be described by a full inversion with respect to the different anisotropy parameters. Inverting for seismic anisotropy becomes very challenging and a good ray coverage as well as a-priori knowledge is required to compute a meaningful, well-constrained model. Therefore, we are working on

both, the data collection as well as the code development to obtain a meaningful data set and a powerful inversion tool. The sensitivity as well as the correlation between different anisotropy parameters is also studied with synthetic data, to get a better understanding of the information and the limitations that the model provides.

The acquired knowledge from synthetic data, lab-scale experiments on rock samples and the homogeneous background rock is combined to study the anisotropy on the complexer, heterogeneous hectometer-scale. The project aims to deepen the understanding of seismic anisotropy across different scales and geological settings. It provides valuable insights to improve the description of underground properties which are important for geotechnical and geothermal uses.

Geomechanical modeling of induced seismicity in EGS

Author: Victor Clasen Repollés (ETH Zurich)

Multi-scale performance evaluation of different induced seismicity forecasting models.
For this first work package, I developed two classes of simplified (hybrid) hydromechanical models that are based on 1D radial (or linear) pore-fluid diffusion and fluid injection. The first class (HM0) accounts for linear pore-fluid diffusion from the fluid source, while the second class (HM1) accounts for the non-linear response of the medium due to (both reversible and irreversible) pressure-dependent permeability variations upon fluid injection. Each class is sequentially coupled to two stochastic seismicity models that trigger seismicity if the respective space-time pressure solution reaches a critical value according to the Mohr- Coulomb criterion. However, both seismicity models di=er in the way they simulate seismicity. One model uses an analytical approach based on probability density functions of model parameters to simulate seismicity (CAPS), while the other model simulates seismicity via stochastic seed approach (SEED). I tested the models' real-time forecasting capabilities within a data assimilation scheme (performing pseudo-perspective tests) using datasets from in-situ injection experiments that encompass different spatial scales: Grimsel, Bedretto, FORGE, and Basel. The work "Development of 1-D hybrid hydromechanical models for real-time induced seismicity forecasting", in which we their performance at four different spatial scales is compared also against the performance of well-established statistical models, is currently in the final stages of preparation.

Modeling coupled hydro-mechanical processes during hydraulic stimulation at the BedrettoLab.
For the second work package, I constructed a detailed 3D numerical model (using the fully coupled TOUGH3-FLAC3D simulator - which consists of a two-way sequential coupling of the multiphase and multicomponent fluid flow simulator TOUGH3 and v7.0 of the geomechanical simulator FLAC3D) of VALTER phase 1 interval 13 hydraulic stimulation, which targeted a highly fractured fault damage zone in the reservoir volume (known as the "bad boy"). The goal is to replicate the observations collected during this stimulation, under the assumption that the actual fault is planar and can be represented by two interfaces, to explain the main physical processes leading to reactivation of the fault and to the generation of many seismic events despite injecting at relatively low pressure.

Preliminary results will be published soon in form of a conference paper submitted in March 2024 to the ARMA 2024 Symposium: Clasen Repollés, V., Jiang, D., Rinaldi, A.P., Obermann, A., Bröker, K., Ma, X., Rosskopf, M., Gholizadeh Doonechaly, N., Hertrich, M., Maurer, H., Giardini, D., and Wiemer, S. (2024). Modeling coupled hydro-mechanical processes

during hydraulic stimulation at the Bedretto Underground Laboratory. 58th U.S. Rock Mechanics/Geomechanics Symposium, Golden, Colorado, USA, June 2024

Quantifying Fracture Geometry and Heterogeneity in Rock Reservoirs Using GPR

Author: Daniel Escallon Botero (ETH Zurich)

My research focuses on utilizing remote sensing techniques, specifically Ground Penetrating Radar (GPR), to achieve a 3D geometric understanding of fractures in rock reservoirs. These fractures, which range from large fault zones to sub-millimeter scales, play a critical role in fluid flow within enhanced geothermal reservoirs, making their identification and spatial mapping a top priority. GPR is a powerful, cost-effective, non-destructive, and well-established tool for imaging fractures by analyzing the propagation and scattering of electromagnetic (EM) waves. Due to the high dielectric contrast between the host rock and fracture filling, GPR can detect fracture reflections with sub-millimeter apertures (i.e., thin-bed response), providing detailed insights into the fracture network.

The main objective is to create a model that represents the subsurface geometry and characteristics. However, characterizing fracture curvature remains challenging due to data sparsity and geometric ambiguities. Consequently, most numerical models assume planar fractures to simplify computations. To address this limitation, we present a novel approach for inferring fracture geometry from travel-time data of electromagnetic waves. Our model employs co-kriging interpolation of control points within a 3D surface mesh to effectively simulate fracture curvature, allowing for the modeling of both small-scale heterogeneities and large-scale curvature. We use a deterministic travel-time inversion to precisely position these control points and constrain the fracture geometry. We tested the methodology for a field example to infer the geometry of a large (over 200 m) fracture observed in single-hole GPR field data. The inferred fracture surface closely matches borehole televiewer observations and is also constrained far from the boreholes Escallon, Shakas, and Maurer 2024.

In a second phase, we aim to extract additional information from the GPR profiles (Figure 29). Specifically, when we analyze amplitude changes within the reflector, we assume they result from changes in the filling material or fracture aperture. We designed a controlled experiment where we create centimeter-scale synthetic fractures with heterogeneous apertures to simulate naturally occurring fractures with natural roughness. GPR has proven that the detail extracted from analyzing amplitude changes in the profile is linearly correlated to aperture changes for apertures smaller than a quarter of the wavelength, as predicted by thin-bed equations. This allows us to infer fracture geostatistical information and describe their heterogeneity (Figure 30a and 30b).

In conclusion, our research demonstrates the effectiveness of GPR in characterizing subsurface fracture networks and offers a novel approach to modeling fracture geometry with improved accuracy. The methodologies developed not only enhance our understanding of fracture properties but also provide valuable tools for applications in geothermal reservoir management and other geoscience fields.

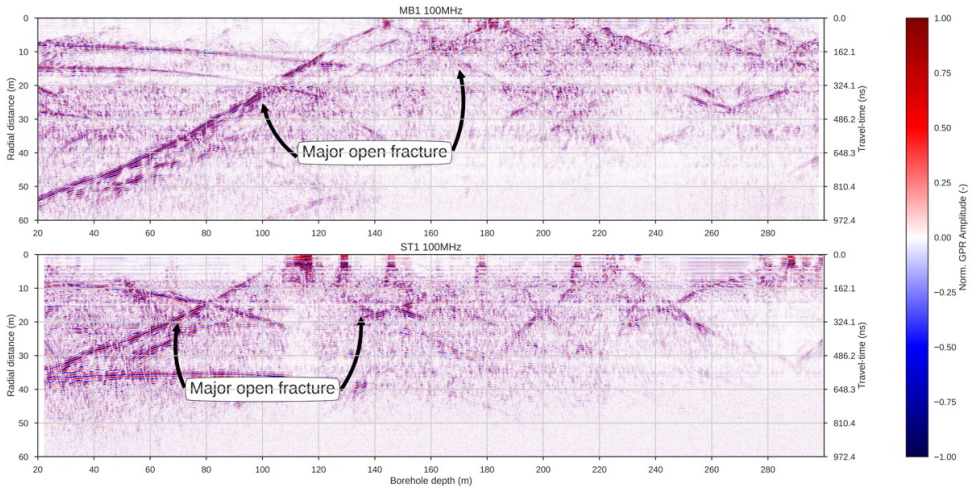

Figure 29: Representative GPR profiles from boreholes MB1 and ST1, highlighting strong reflections from the major open fracture in the volume, spanning approximately 300 m.

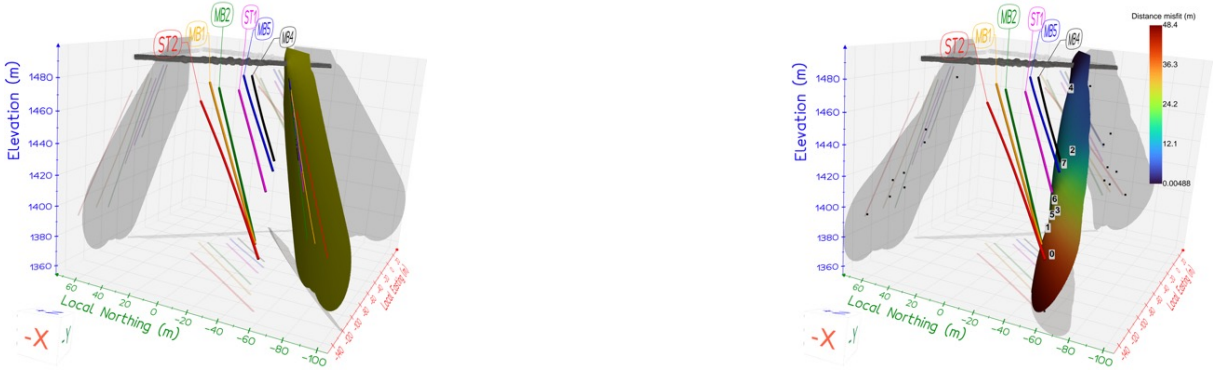

Figure 30: BULGG 3D model, showing the tunnel, boreholes and fault zone. The boreholes are cropped to the source-receiver pairs used in the GPR travel-time picking. On the left: Initial fracture model, extrapolated from tunnel observations. On the right: Inverted geometry where the colored surface represents the relative movement of the geometry, with warmer colors indicating larger distances from the initial geometry of the left side.

Seismicity analysis during hydraulic stimulations

Author: Rosskopf Martina (ETH Zurich)

My project focuses on the analysis of seismicity during the hydraulic stimulations in the Bedrettolab. Different injection experiments were performed in different intervals in a mesoscale volume, where up to 10'000 seismic events during a single stimulation with magnitudes between -4.5 and -1.5 could be observed.

In the first part of my project, I developed parts of the processing workflows to obtain seismic event catalogs from the waveforms recorded by acoustic emission sensors. The processing workflows can be divided into a real-time workflow and a post-processing workflow. The real-time workflow is performed during stimulations. Here it is important to monitor the rock volume and the ongoing processes in order to be able to stop the ongoing injection for risk reasons, e.g. if a large magnitude event occurs. For this purpose, we are mainly interested in the large magnitude events and fast real-time processing, rather than detecting all the smaller events. The DUGseis software (Rosskopf et al. 2024) was used for our processing. Two different pickers (STA/LTA and FBKT picker) were applied to a subset of sensor waveforms. We then located

the events using these picks and estimated a magnitude to get first order catalogs. The first catalog using the STA/LTA picker was slightly faster and gave the first estimate of magnitudes. The second catalog with the FBKT picks more accurate in locations, because the picks were slightly better.

Later, after the stimulations were completed the post-processing workflow was applied. This workflow includes more steps to provide a complete seismic event catalog with high location accuracy. Here we pick the events with the FBKT picker on all sensors and improve the picks with the AIC picker. The events are then located to obtain a first absolute location. In the next step, we perform a relative relocation of all events using HypoDD. Finally, we estimate the magnitudes and manually check the highest magnitudes. All the real-time and post-processing steps have been carefully evaluated to find the best workflow and are described in more detail in a paper currently in preparation. The final event locations align nicely with the pre known fracture network in the volume (seismicity shown in Figure **??**). However, the catalogs show that the distribution and the spatio-temporal evolution of events is highly dependent on the surrounding rock mass. This means, that even neighboring intervals can show completely different behaviors in terms of spatial extent of the event cloud, total number of events and magnitudes.

In addition to the event catalog estimations, I am currently working on focal mechanisms to learn more about the rupture processes of the events. The first results already show that the mechanism can vary not only between intervals but also within a stimulation, when events are located on different faults. In future work, I will extent the study to learn more about the evolution of the mechanisms, for example whether they change with time along a fracture or between injection phases. Moreover, I will investigate how they relate to injection parameters such as injection rate and pressure, and other measurements from pressure and temperature sensors.

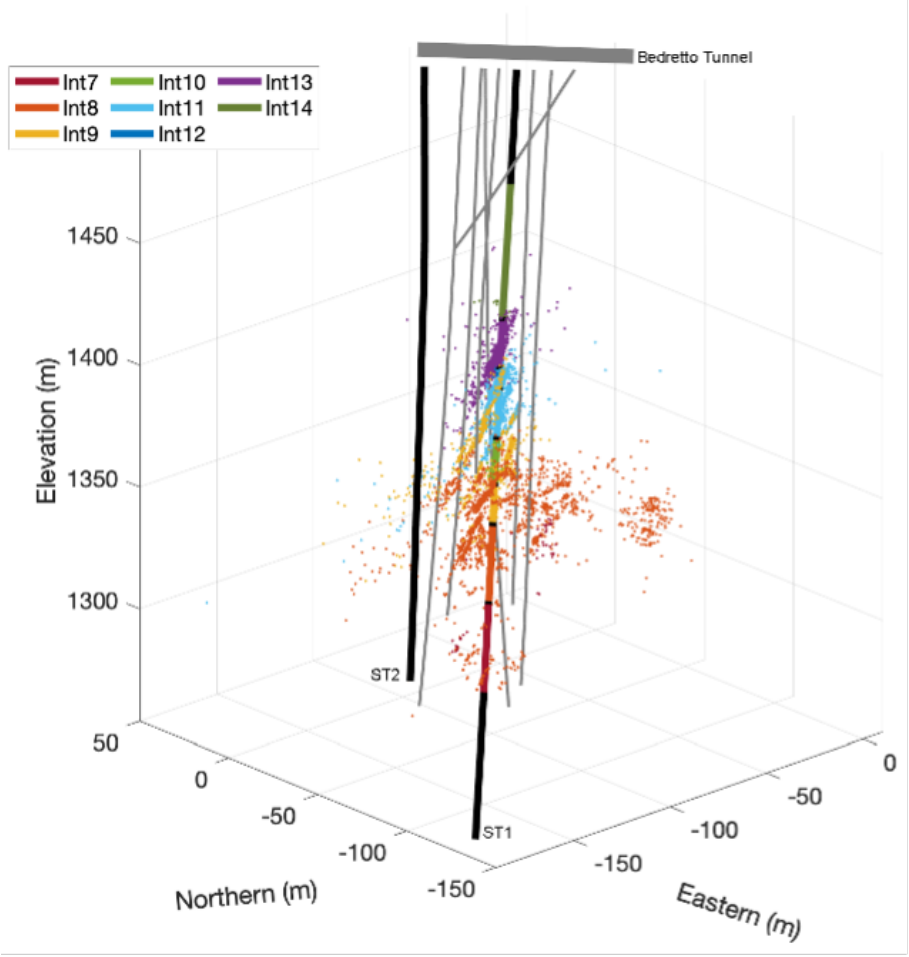

Figure 31: Seismic events recorded during hydraulic stimulations. Each color corresponds to the seismicity in one interval. The grey lines are the monitoring boreholes, the colored line the stimulation borehole and the black line the production borehole (Figure modified after Obermann et al., 2024.

Illuminating hydraulic stimulation processes by advanced seismic techniques

Author: Schwarz Miriam (ETH Zurich)

My PhD is divided into two parts: first, the characterization of the host rock using active seismic measurements; and second, monitoring changes in the host rock during hydraulic simulations.

The first part results in a 3D velocity model. We conducted several active seismic surveys between the VALTER boreholes using the P-wave sparker as source. The data was recorded on hydrophone chains prior to the instrumentation of the boreholes and on the Acoustic Emission sensors (AE) after the instrumentation. All surveys were conducted before hydraulic stimulation experiments were conducted, thus, we can characterize the undisturbed host rock. We were able to compile a comprehensive dataset of 42'843 manual P-picks with a picking uncertainty between 0.1 - 0.2 ms. Source receiver distances vary between 10 m and 186.5 m. The signals recorded on the hydrophone chain have larger amplitudes. However, the frequency content is comparable, with the energy of the first-arriving wave between 1 kHz and 10 kHz.

For simplicity, crosshole tomography applications are often performed in 2D planes. Seismic waves travel through heterogeneous media along complex paths, which causes inherent limitations of the 2D tomography. Especially in case of a complex subsurface 3D investigation should be applied. In case of the VALTER volume we benefit from the large amount of eight boreholes that are suitable for a 3D tomography. However, 3D investigations suffer from a poorer ray coverage. We solve this issue by using "Fat rays" instead of the classical high-frequency approximation of a ray. The frequency dependent Fat ray is taking the first Fresnel zone into account and is obtained by summing the source and receiver traveltime fields which results in the banana-shaped Fat ray (Woodward 1992. With the use of the Fat ray concept we could improve the subsurface image. In the paper that we prepare currently, we compare our results with other measurements in the boreholes such as borehole logging and GPR measurements (Escallon, Shakas, and Maurer 2024).

The second part of my PhD is dedicated to the hydraulic stimulation experiments. We conducted a series of experiments in the VALTER volume in Phase 1 for the hydraulic characterization of the different stimulation intervals. In a second Phase we revisited a couple of interesting intervals with different research interests. During these experiments we conducted repeated active seismic measurements to monitor the velocity changes of the subsurface. With these measurements we want to relate the changes to pressure changes. The interpretation of the data in the context of induced seismicity might help us to shed light on the physical processes resulting in induced seismicity.

Publications 2023-2024

Achtziger-Zupančič, Peter et al. (2024). “Selection and Characterisation of the Target Fault for Fluid-Induced Activation and Earthquake Rupture Experiments”. In: *EGUsphere* 2024, pp. 1–38.

Aretusini, S et al. (2023). “Heterogeneity-driven localization and weakening in scaly clays from a fossil accretionary prism”. In: *Journal of Geophysical Research: Solid Earth* 128.9, e2023JB027332.

Behnen, Kathrin et al. (2024). “Investigation of Seismic Anisotropy in the Undisturbed Rotondo Granite”. In: *EGUsphere* 2024, pp. 1–20.

Bianchi, Patrick et al. (2024). “Pre-Failure Strain Localization in Siliclastic Rocks: A Comparative Study of Laboratory and Numerical Approaches”. In: *Rock Mechanics and Rock Engineering*, pp. 1–25.

Bröker, K et al. (2023). “Hydro-Geomechanical Observations During Multistage Hydraulic Stimulation at the Bedretto Underground Laboratory, Switzerland”. In: *ARMA US Rock Mechanics/Geomechanics Symposium*. ARMA, ARMA–2023.

Bröker, Kai et al. (2024). “Constraining the stress field and its variability at the BedrettoLab: Elaborated hydraulic fracture trace analysis”. In: *International Journal of Rock Mechanics and Mining Sciences* 178, p. 105739.

Chen, Han et al. (2024). “3-D coseismic displacement mapping of the 2015 Mw7. 8 Gorkha earthquake using multi-viewed InSAR”. In: *Tectonophysics*, p. 230254.

Cocco, Massimo et al. (2023). “Fracture energy and breakdown work during earthquakes”. In: *Annual Review of Earth and Planetary Sciences* 51, pp. 217–252.

Dal Zilio, Luca and Jean-Paul Ampuero (2023). “Earthquake doublet in Turkey and Syria”. In: *Communications Earth & Environment* 4.1, p. 71.

Dal Zilio, Luca, Domenico Giardini, et al. (2023). “Harnessing the potential of digital twins in seismology”. In: *Nature Reviews Earth & Environment* 4.8, pp. 510–512.

Doonechaly, Nima Gholizadeh et al. (2024). “Insights from Subsurface Monitoring for Engineering of the Stimulation Pattern in Fractured Reservoirs”. In.

Erickson, Brittany A et al. (2023). “Incorporating full elastodynamic effects and dipping fault geometries in community code verification exercises for simulations of earthquake sequences and aseismic slip (SEAS)”. In: *Bulletin of the Seismological Society of America* 113.2, pp. 499–523.

Escallon, Daniel, Alexis Shakas, and Hansruedi Maurer (2024). “Modelling and inferring fracture curvature from borehole GPR data: A case study from the Bedretto Laboratory, Switzerland”. In: *Near Surface Geophysics* 22.2, pp. 235–254.

Gholizadeh Doonechaly, Nima et al. (2024). “Multiphysics monitoring of cementation operation: implications for wellbore integrity and hydrogeological characterization”. In: *Environmental Earth Sciences* 83.5, pp. 1–15.

Gualandi, Adriano et al. (2023). “Deterministic and stochastic chaos characterize laboratory earthquakes”. In: *Earth and Planetary Science Letters* 604, p. 117995.

Halter, Théo, Nima Gholizadeh Doonechaly, et al. (2024). “Thermal Energy Storage and Recovery in Fractured Granite Reservoirs: Numerical Modeling and Efficiency Analysis”. In.

Halter, Théo, Nima Gholizadeh Doonechaly, et al. (2024). “Exploring the Feasibility of Energy Extraction from the Bedretto Tunnel in Switzerland”. In: *Energies* 17.15, p. 3669.

Huang, Kai et al. (2024). “The 2023 Mw 6.8 Morocco Earthquake: A Lower Crust Event Triggered by Mantle Upwelling?” In: *Geophysical Research Letters* 51.12, e2024GL109052.

Kammer, David S et al. (2024). “Earthquake energy dissipation in a fracture mechanics framework”. In: *Nature communications* 15.1, p. 4736.

MOSCONI, Francesco et al. (2024). “Modeling the 3D dynamic rupture of microearthquakes induced by fluid injection”. In: *Authorea Preprints*.

Osten, Julian et al. (2024). “A multi-method investigation of the permeability structure of brittle fault zones with ductile precursors in crystalline rock”. In: *Grundwasser* 29.1, pp. 49–61.

Plenkers, Katrin et al. (2023). “Multi-disciplinary monitoring networks for mesoscale underground experiments: advances in the bedretto reservoir project”. In: *Sensors* 23.6, p. 3315.

Rosskopf, M et al. (2024). “DUGseis: A Python package for real-time and post-processing of picoseismicity”. In: *Submitted to: Journal for Open Source Software*.

Selvadurai, Paul Antony et al. (2023). “Modeling frictional precursory phenomena using a wear-based rate-and state-dependent friction model in the laboratory”. In: *Tectonophysics* 847, p. 229689.

Vaezi, Iman et al. (2024). “Numerical modeling of hydraulic stimulation of fractured crystalline rock at the bedretto underground laboratory for geosciences and geoenergies”. In: *International Journal of Rock Mechanics and Mining Sciences* 176, p. 105689.

Volpe, Giuseppe et al. (2023). “Laboratory simulation of fault reactivation by fluid injection and implications for induced seismicity at the BedrettoLab, Swiss Alps”. In: *Tectonophysics* 862, p. 229987.

Wang, Xiaoyu et al. (2023). “Non-Precursory Accelerating Aseismic Slip During Rupture Nucleation”. In: *Journal of Geophysical Research: Solid Earth* 128.6, e2022JB026066.

Wei, Guoguang et al. (2023). “Complex strike-slip faulting during the 2021 Mw7. 4 Maduo earthquake”. In: *Communications Earth & Environment* 4.1, p. 319.

Woodward, Marta Jo (1992). “Wave-equation tomography”. In: *Geophysics* 57.1, pp. 15–26.

Wu, Rui, Paul Selvadurai, et al. (2024). *Time-lapse Acousto-Mechanical Response to Moisture-Induced Reduction of Fracture Stiffness in Granite*. Tech. rep. Copernicus Meetings.

Wu, Rui, Paul A Selvadurai, et al. (2023). “Laboratory Acousto-Mechanical Study Into Moisture-Induced Reduction of Fracture Stiffness in Granite”. In: *Geophysical Research Letters* 50.23, e2023GL105725.

Wu, Rui, Paul Antony Selvadurai, et al. (2023). “Laboratory acousto-mechanical study into moisture-induced changes of elastic properties in intact granite”. In: *International Journal of Rock Mechanics and Mining Sciences* 170, p. 105511.

Zhang, Shihuai et al. (2023). “Fault zone spatial stress variations in a granitic rock mass: Revealed by breakouts within an array of boreholes”. In: *Journal of Geophysical Research: Solid Earth* 128.8, e2023JB026477.

Zhang, Yingfeng et al. (2024). “Strain partitioning and fault kinematics in the northern Qilian Shan (NE Tibet) determined from Bayesian inference of geodetic data”. In: *Geophysical Research Letters* 51.9, e2023GL107324.

References

- Achtziger-Zupančič P, Ceccato A, Zappone AS, Pozzi G, Shakas A, Amann F, Behr WM, Escallon Botero D, Giardini D, Hertrich M, Jalali M, Selection and characterization of the target fault for fluid-induced activation and earthquake rupture experiments, Solid Earth 15.8 (2024): 1087-1112.
- Michael Afanasiev, Christian Boehm, Martin van Driel, Lion Krischer, Max Rietmann, Dave A May, Matthew G Knepley, Andreas Fichtner, Modular and flexible spectral-element waveform modelling in two and three dimensions, Geophysical Journal International, Volume 216, Issue 3, March 2019, Pages 1675–1692, https://doi.org/10.1093/gji/ggy469
- Amann, F., Gischig, V., Evans, K., Doetsch, J., Jalali, M., Valley, B., Krietsch, H., Dutler, N., Villiger, L., Brixel, B., Klepikova, M., Kittilä, A., Madonna, C., Wiemer, S., Saar, M., Loew, S., Driesner, T., Maurer, H. & Giardini, D. (2018) The seismo-hydromechanical behavior during deep geothermal reservoir stimulations: open questions tackled in a decameter-scale in-situ stimulation experiment. Solid Earth, 9, 115-137, https://doi.org.10.5194.se-9-115-2018.
- Araujo, A. (2023). Impact of cataclastic radical-induced hydrogen and hydrogen peroxide production on subsurface microbial dynamics in the Bedretto tunnel. BSC thesis, ETH.
- Aretusini S., Cascajero A. N., Cornelio C., Echevarria X. B., Spagnuolo E., Tapetado A., Vazquez C., Di Toro G., Cocco M. Mechanical energy dissipation during seismic dynamic weakening in calcite-bearing faults" under review on Journal of Geophysical Research - Solid Earth.
- Arnet, M. (2021). Deep Alpine Fluids: Origin, pathways and dynamic remobilisation in response to hydraulic stimulations at the Bedretto Underground Laboratory for Geoenergies (BULGG). MSc thesis, ETH
- Bossart, P., Bernier, F. Birkholzer, J., Bruggeman, C., Connolly, P., Dewonck, S., Fukaya, M., Herfort, M., Jensen, M., Matray, J.-M., Mayor, J.C., Moeri, A., Oyama, T., Schuster, K., Shigeta, N., Vietor, T. Wieczorek, K. (2017) Mont Terri rock laboratory, 20 years of research: introduction, site characteristics, and overview of experiments. Swiss Journal of Geosciences, 110(1), 3-22. https://doi.org/10.1007/s00015-016-0236-1.
- Dieterich, J. H. (1992), Earthquake nucleation on faults with rate- and state-dependent friction, Tectonophysics, 211, 115–134.
- Guglielmi Y, Cappa F, Avouac JP, Henry P, Elsworth D. (2015) Seismicity triggered by fluid injection-induced aseismic slip. Science. Jun 12;348(6240):1224-6. doi: 10.1126/science.aab0476. Epub 2015 Jun 11. PMID: 26068845.
- Keller, F. & Schneider, T. R. (1982) Geologie und Geotechnik, Schweizer Ing. Archit. 24, 512-520.
- Kressig, N. (2022). Testing the microbial response to hydraulic stimuation: Incubation experiments with fluids from the Bedretto Underground Laboratory for Geosciences and Geoenergies. MSc thesis, ETH

- G. Kwiatek, K. Plenkers, G. Dresen, JAGUARS Research Group; Source Parameters of Picoseismicity Recorded at Mponeng Deep Gold Mine, South Africa: Implications for Scaling Relations. Bulletin of the Seismological Society of America 2011;; 101 (6): 2592–2608. doi: https://doi.org/10.1785/0120110094

- Ma, X., Hertrich, M., Amann, F., Bröker, K., Gholizadeh Doonechaly, N., Gischig, V., Hochreutener, R., Kästli, P., Krietsch, H., Marti, M., Nägeli, B., Nejati, M., Obermann, A., Plenkers, K., Rinaldi, A.P., Shakas, A., Villiger, L., Wenning, Q., Zappone, A., Bethmann, F., Castilla, R., Serberto, F., Meier, P., Driesner, T., Löw, S., Maurer, H., Saar, M.O., Wiemer, S. & Giardini, D. (2022) Multi-disciplinary characterizations of the BedrettoLab - a new underground geoscience research facility. Solid Earth, 13, 301–322, https://doi.org/10.5194/se-13-301-2022.

- Moein, M.J.A., Langenbruch, C., Schultz, R. et al. The physical mechanisms of induced earthquakes. Nat Rev Earth Environ 4, 847–863 (2023). https://doi.org/10.1038/s43017-023-00497-8

- Anne Obermann, Martina Rosskopf, Virginie Durand, Katrin Plenkers, Kai Bröker, Antonio Pio Rinaldi, Nima Gholizadeh Doonechaly, Valentin Gischig, Alba Zappone et al., Seismic Response of Hectometer-Scale Fracture Systems to Hydraulic Stimulation in the Bedretto Underground Laboratory, Switzerland, AGU Publications.

- Villiger, L., Gischig, V. S., Doetsch, J., Krietsch, H., Dutler, N. O., Jalali, M., Valley, B., Selvadurai, P. A., Mignan, A., Plenkers, K., Giardini, D., Amann, F., and Wiemer, S.: Influence of reservoir geology on seismic response during decameter-scale hydraulic stimulations in crystalline rock, Solid Earth, 11, 627–655, https://doi.org/10.5194/se-11-627-2020, 2020.

- Volpe, G., Pozzi, G., Collettini, C., Spagnuolo, E., Achtziger-Zupančič, P., Zappone, A., Aldega, L., Meier, M. A., Giardini, D., & Cocco, M. (2023). Laboratory simulation of fault reactivation by fluid injection and implications for induced seismicity at the BedrettoLab, Swiss Alps. Tectonophysics, 862, 229987. https://doi.org/10.1016/J.TECTO.2023.229987